Order Number 9307669

Effects of deconfinement on J/psi formation

Ryan, William Howard, Ph.D.

The University of Arizona, 1992

U·M·I

300 N. Zeeb Rd.
Ann Arbor, MI 48106

EFFECTS OF DECONFINEMENT ON J/PSI FORMATION

by

William Howard Ryan

A Dissertation Submitted to the Faculty of the

DEPARTMENT OF PHYSICS

In Partial Fulfillment of the Requirements
For the Degree of

DOCTOR OF PHILOSOPHY

In the Graduate College

THE UNIVERSITY OF ARIZONA

1 9 9 2

THE UNIVERSITY OF ARIZONA
GRADUATE COLLEGE

As members of the Final Examination Committee, we certify that we have read the dissertation prepared by William Howard Ryan

entitled EFFECTS OF DECONFINEMENT ON J/PSI FORMATION

and recommend that it be accepted as fulfilling the dissertation requirement for the Degree of Doctor of Philosophy

Robert L. Thews	Nov 12, 1992 Date
Michael D. Scadron	Nov 12, 1992 Date
John O. Stoner	Nov. 12, 1992 Date
Peter Carruthers	Nov 12, 1992 Date
Laurence McIntyre	Nov 12, 1992 Date

Final approval and acceptance of this dissertation is contingent upon the candidate's submission of the final copy of the dissertation to the Graduate College.

I hereby certify that I have read this dissertation prepared under my direction and recommend that it be accepted as fulfilling the dissertation requirement.

Dissertation Director Robert L. Thews — Nov 30, 1992 Date

STATEMENT BY AUTHOR

This dissertation has been submitted in partial fulfillment of requirements for an advanced degree at The University of Arizona and is deposited in the University Library to be made available to borrowers under rules of the library.

Brief quotations from this dissertation are allowable without special permission, provided that accurate acknowledgment of source is made. Requests for permission for extended quotation from or reproduction of this manuscript in whole or in part may be granted by the head of the major department or the Dean of the Graduate College when in his or her judgment the proposed use of the material is in the interests of scholarship. In all other instances, however, permission must be obtained from the author.

SIGNED: William Howard Ryan

ACKNOWLEDGEMENTS

There have been many professors who have provided important guidance throughout my academic career. However, I must especially thank my advisor, Dr. Robert Thews, and Dr. Michael Scadron for their instruction and advise in my studies of high energy physics. I must also thank Dr. Thews for suggesting the problem that eventually became my dissertation.

I would also like to thank my parents for encouraging me to continue my education and for their support through this time. Most of all, I would like to thank my wife, Eileen, for her support, help, and encouragement through our years in graduate school.

TABLE OF CONTENTS

TABLE OF CONTENTS–*Continued*

TABLE OF CONTENTS–*Continued*

LIST OF FIGURES

LIST OF FIGURES–*Continued*

LIST OF FIGURES–*Continued*

LIST OF FIGURES–*Continued*

LIST OF TABLES

ABSTRACT

We present an analysis of the formation of charmonium resonances of heavy quark pairs immersed in a deconfined environment for a finite time interval. This is intended to model the J/ψ suppression due to the possible formation of a color screening quark gluon plasma in heavy ion collisions. In particular, we examine how the the χ_c and J/ψ states are affected in a quantum mechanical suppression model. We then investigate how the momentum dependence of the fraction of J/ψ's that come from radiative χ_c decays or that are directly created can affect the momentum dependence of the resulting J/ψ suppression. We examine under what circumstances could this suppression momentum dependence be enhanced. This is of interest since previous quantum mechanical analyses have failed to model the strong momentum dependence observed in heavy ion collisions.

CHAPTER 1

INTRODUCTION

Quarks are usually bound together, or "confined", into a colorless state. However, at extremely high temperatures or densities, there may exist a deconfined phase in which quarks and gluons behave as quasi-free particles. This is the so-called quark gluon plasma. If such a state of matter does indeed exist, it would have certainly have been formed in the very early universe and possibly in the interiors of neutron stars. However, these are somewhat inaccessible to experimental study. It is also possible that an energetic collision of two heavy nuclei might create a large enough hot region to form a quark gluon plasma. Recently, much effort has been devoted to the feasibility of this and the possible signatures of the plasma's formation (for reviews, see [1, 2]).

One signature predicted was the suppression of J/ψ formation [3]. The J/ψ consists of a heavy quark-antiquark pair bound in a confining potential. When immersed in a deconfining medium, the quarks would be free to follow separate trajectories. If, at the time of hadronization, the pair has separated far enough, they would be more likely to recombine with a light quark than with each other or another thermally suppressed heavy quark. Thus, we would see an enhancement of open charmed mesons at the expense of J/ψ's. It was subsequently reported, by the NA 38 Collaboration [4], that such a suppression is actually seen. They found that, in highly relativistic collisions involving sulfur and oxygen beams on a uranium target, J/ψ production was significantly decreased in events with higher transverse energy (E_T). Interpreting higher E_T with more central, violent collisions, one might conclude that the suppression was due to the formation of a quark gluon plasma in

these events. However, very quickly, more conventional nuclear absorption models were proposed [5, 6, 7].

One distinct feature of the NA 38 data was that the suppression disappeared for J/ψ's with larger transverse momenta (p_T). This was also explained within the context of quark gluon plasma formation [8]. Since the plasma obviously occupies a finite space-time region, J/ψ's with larger p_T would escape the plasma faster, spending less time in the deconfining environment. Also, time dilation in the J/ψ's rest frame would produce the same effect. This strong momentum dependence provided crucial support for plasma suppression because nuclear absorption models were less successful in explaining this. Suppression models based on nuclear absorption required introducing the additional effect of initial state parton scattering to explain the observed momentum dependence [9, 10, 11].

The somewhat successful explanation of the momentum dependence was based on the idea of a finite formation time for the J/ψ. If the time spent in the deconfining environment, which is small for higher p_T pairs, is smaller than the formation time, then the J/ψ will still be created. This description was basically classical. However, it was pointed out that the formation of the J/ψ was essentially a quantum mechanical problem and that the "J/ψ formation time" had no real meaning [12, 13]. Subsequent studies incorporating this into a plasma model predicted that the distinct momentum dependence would be washed out in this more correct quantum treatment [14, 15].

In this paper we will investigate further the effects of deconfinement on J/ψ formation. Specifically, we will examine the effects on different production mechanisms and show that the momentum dependence may be stronger than previously thought in the quantum mechanical model. In Chapter 2, we will review the "normal" J/ψ production in NN collisions and what assumptions must be introduced to model AA collisions. In Chapter 3, we will discuss classical arguments

for J/ψ suppression. In Chapter 4, we examine one-dimensional, quantum mechanical suppression models, both relativistic and non-relativistic, and show that, for sufficiently wide (spatially) bound states, a non-relativistic approach is applicable. In Chapter 5, we develop a full three-dimensional suppression model and examine the effect on different production mechanisms. We will be particularly interested to see if there are any conditions in which the observed p_T-dependence of the J/ψ suppression is replicated in a quantum mechanical model. Chapter 6 is our conclusion.

CHAPTER 2

J/ψ FORMATION IN NN AND HEAVY ION COLLISIONS

At this time, there is no universally accepted complete theoretical picture of the formation of heavy quark resonances in hadronic collisions. Therefore, before discussing the suppression of the J/ψ resonance, we must review the model that we shall use to explain "normal" J/ψ formation. The goal of this chapter is to provide this background picture for J/ψ production on which we will later consider plasma suppression effects. This will be based heavily on the work in References [14, 16, 17]. In Section 2.1, we will review the parton model formulation for calculating cross sections for ${\alpha_s}^2$ and ${\alpha_s}^3$ QCD processes. In Section 2.2, we present a rather detailed description of J/ψ formation originating from intermediate χ_c production. This is done to illustrate how the hard QCD process, which is responsible for the production of a $c\bar{c}$ pair, is merged with a non-relativistic model of the charmonium bound state. We then present the results for ${\alpha_s}^3$ J/ψ production, which we believe to be dominate at high-p_T. Our "definition" of the J/ψ in terms of non-relativistic charmonium bound states is given in Section 2.3. In Section 2.4, we discuss the assumptions, excluding QGP formation, that are involved in extending our model to collisions of nuclei. We then review the points raised in this chapter that are pertinent to modeling J/ψ suppression in Section 2.5.

2.1 Parton Model Formalism

Before discussing the individual subprocesses that contribute to J/ψ production, we first outline the parton formalism [18, 19] for heavy quark resonance production

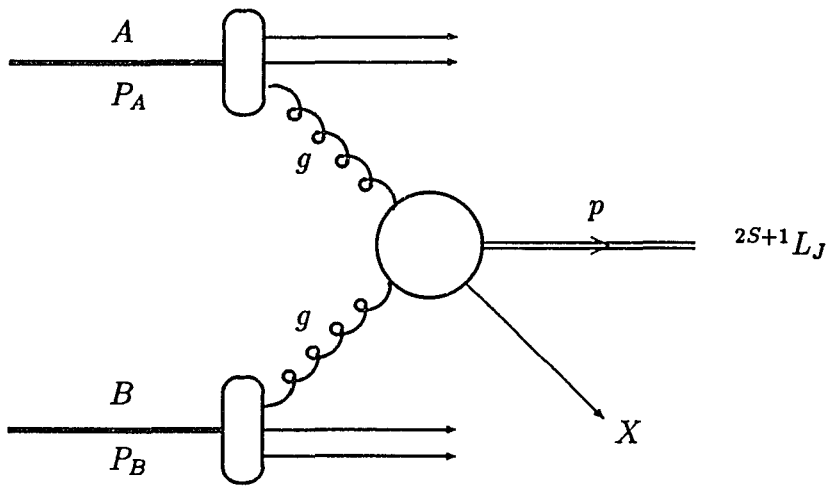

Figure 2.1: Hadroproduction of heavy quark resonance.

[16] in hadronic collisions. We consider the generic process shown in Figure 2.1, where A and B represent the two colliding hadrons. In the standard parton model, we assume that each hadron consists of many non-interacting pointlike particles that carry some momentum fraction, x_i, of the parent hadron. In the figure, the two partons with momenta, $p_a = x_a P_A$ and $p_b = x_b P_B$, interact producing the resonance, denoted by $^{2S+1}L_J$, plus anything else, that we collectively refer to as X. Denoting the invariant differential cross section for the subprocess as $E\,d^3\sigma/dp^3(ab \to {}^{2S+1}L_J X)$, we write the inclusive hadronic cross section as [18]

$$E\frac{d^3\sigma}{dp^3}(AB \to {}^{2S+1}L_J X) = \int dx_a\, dx_b\, f_a^A(x_a)\, f_b^B(x_b) \left[E\frac{d^3\sigma}{dp^3}(ab \to {}^{2S+1}L_J X)\right], \tag{2.1}$$

where $f_{a(b)}^{A(B)}(x_{a(b)})$ is the probability of finding a parton of species, $a(b)$, with momentum fraction, $x_{a(b)}$, in the hadronic species, $A(B)$. Here, we have taken the hadronic cross section to be an incoherent sum of the cross sections for all subprocesses, weighted by the probability of finding the initial partons with the appropriate momenta.

The lowest order QCD subprocess to produce a charmonium resonance

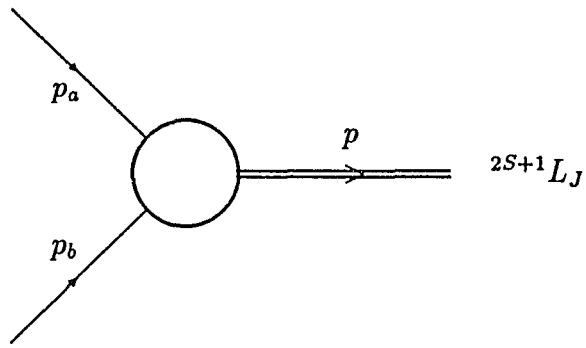

Figure 2.2: ${\alpha_s}^2$ partonic process.

is ${\alpha_s}^2$ gluon fusion. We depict a generic ${\alpha_s}^2$ process in Figure 2.2 and write the associated cross section in the form [19],

$$E\frac{d^3\sigma}{dp^3}(ab \rightarrow^{2S+1} L_J) = \frac{\pi|\mathcal{M}(ab \rightarrow^{2S+1} L_J)|^2}{2\hat{s}}\delta^4(p_a + p_b - p) \ , \qquad (2.2)$$

where $\mathcal{M}$ is the invariant matrix element. The Mandelstam variable, $\hat{s}$, has the standard definition [1], $\hat{s} \equiv (p_a + p_b)^2$, and we have considered the limit, $m_a, m_b \rightarrow 0$. Inserting Equation 2.2 into Equation 2.1, we find the contribution to the inclusive cross section from this ${\alpha_s}^2$ process to be

$$E\frac{d^3\sigma}{dp^3}(AB \rightarrow^{2S+1} L_J) = \sum_{a,b} f_a^A(x_1)\, f_b^B(x_2)\, \hat{\sigma}_0(ab \rightarrow^{2S+1} L_J)\, \tau\, \delta({p_T}^2) \ , \qquad (2.3)$$

where $x_{\frac{1}{2}} \equiv \sqrt{x_F^2 + 4\tau} \pm x_F$ with $\tau \equiv M^2/s$ and $x_F \equiv 2p_z/\sqrt{s}$. Here, M is the mass of the resonance. We have also employed the notation [2] $\hat{\sigma}_0(ab \rightarrow^{2S+1} L_J) \equiv \pi/\hat{s}^2|\mathcal{M}(ab \rightarrow^{2S+1} L_J)|^2$. We note that, if the partons have no initial transverse momentum, which is a standard parton model assumption, the ${\alpha_s}^2$ process can only

[1] We use the standard notation that carets refer to Mandelstam variables defined with respect to the parton momenta.

[2] This notation originates from writing the total partonic cross section in the form $\hat{\sigma} = \pi/\hat{s}^2|\mathcal{M}|^2\delta(1 - M^2/\hat{s}) \equiv \hat{\sigma}_0\delta(1 - M^2/\hat{s})$.

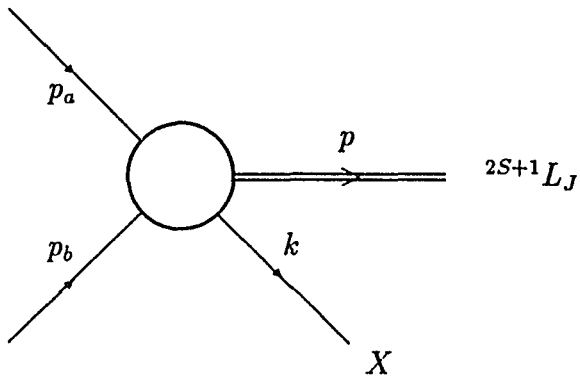

Figure 2.3: $\alpha_s{}^3$ partonic processes.

create a zero p_T resonance. This is usually modified by smearing the above cross section with some initial transverse momentum distribution to simulate partonic fermi motion within the hadron.

The next higher order contributions will come from $\alpha_s{}^3$ processes of the type shown in Figure 2.3. Beginning with the basic cross section [19],

$$E\frac{d^3\sigma}{dp^3}(ab \to {}^{2S+1}L_J X) = \frac{|\mathcal{M}(ab \to {}^{2S+1}L_J X)|^2}{16(2\pi)^2(k_1 \cdot k_2)}\,\delta^4(p_a + p_b - p - k)\,\frac{d^3k}{E_k}\,, \quad (2.4)$$

we integrate over all momenta, k, to write the subprocess cross section as

$$\begin{aligned} E\frac{d^3\sigma}{dp^3}(ab \to {}^{2S+1}L_J X) &= \frac{\hat{s}}{\pi}\left[\frac{|\mathcal{M}(ab \to {}^{2S+1}L_J X)|^2}{16\pi\hat{s}^2}\right]\delta(\hat{s}+\hat{t}+\hat{u}-M^2) \\ &= \frac{\hat{s}}{\pi}\frac{d\hat{\sigma}}{d\hat{t}}\,\delta(\hat{s}+\hat{t}+\hat{u}-M^2)\,. \end{aligned} \quad (2.5)$$

Inserting this into Equation 2.1, we write

$$\begin{aligned} E\frac{d^3\sigma}{dp^3}(AB \to {}^{2S+1}L_J X) &= \sum_{a,b}\int dx_a\,dx_b\,f_a^A(x_a)\,f_b^B(x_b) \\ &\times \left[\frac{\hat{s}}{\pi}\frac{d\hat{\sigma}}{d\hat{t}}(ab \to {}^{2S+1}L_J X)\right]\delta(\hat{s}+\hat{t}+\hat{u}-M^2) \end{aligned} \quad (2.6)$$

for the inclusive $\alpha_s{}^3$ cross section.

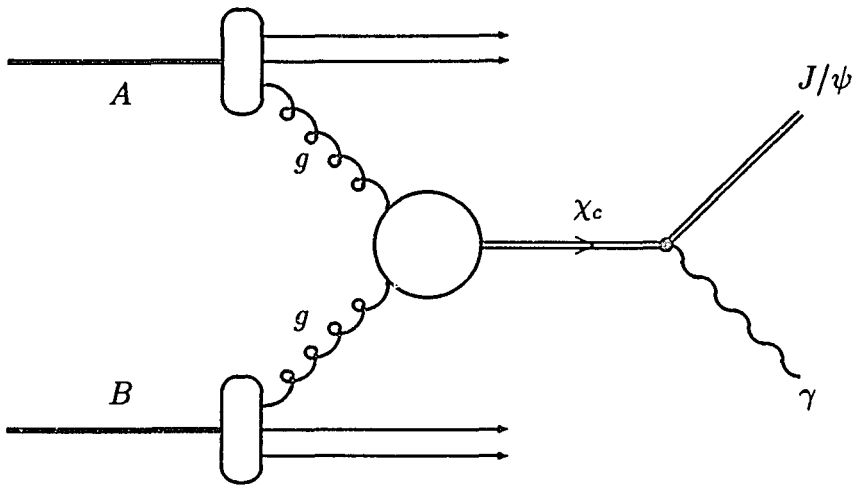

Figure 2.4: Hadroproduction of a J/ψ from an intermediate χ_c state.

2.2 Partonic Cross Sections

The lowest order process contributing to J/ψ hadroproduction is through the formation of an intermediate $c\bar{c}$ state [17, 14]. This is depicted in Figure 2.4. Here, two gluons interact, producing a χ_c pair that is bound in the χ_c ($L = 1, S = 0$) state. This then decays electromagnetically into the J/ψ and a photon. In this section, we will first calculate the invariant matrix element for this process that is required in the parton model formalism. Though the goal of this chapter was to provide a review, we find it instructive to examine this lowest order process in more detail. This will demonstrate the methods and assumptions used in fusing the relativistic QCD pair production formalism with a non-relativistic definition of the heavy quark bound state. We will then simply present the results for the higher order processes.

We begin by calculating the matrix element for the gluon fusion process shown in Figure 2.5. We do this by defining an *effective* Hamiltonian that is related

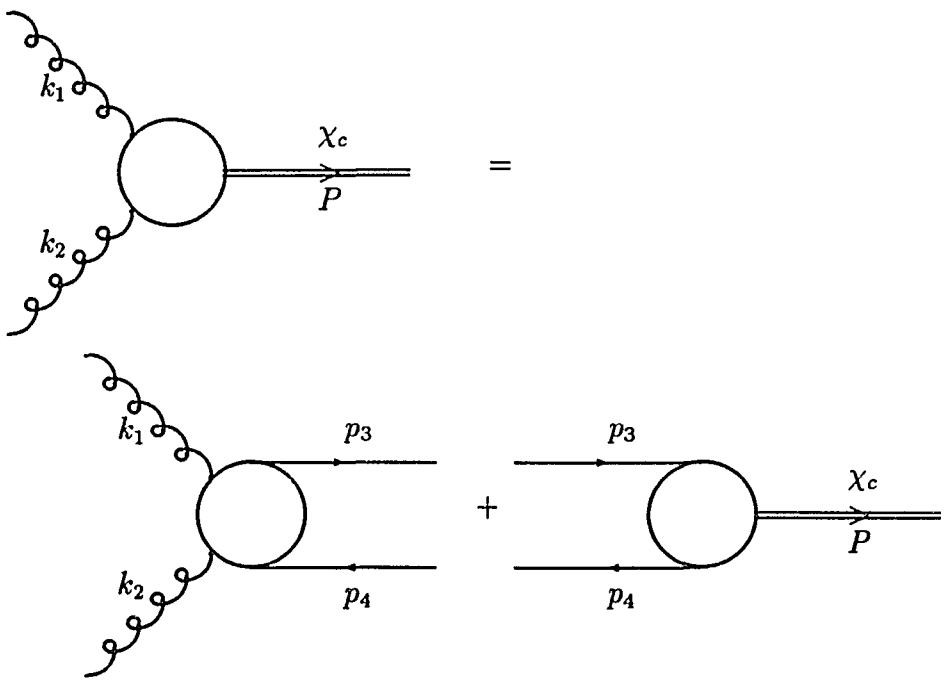

Figure 2.5: Formation of arbritrary heavy quark resonance from gluon fusion. Note that we have also explicitly separated the perturbative QCD process and the formation of the bound state.

to the invariant matrix element through the S-matrix definition[3] [20, 21]

$$\begin{aligned} S_{gg\to^{2S+1}L_J} &\equiv \frac{-i(2\pi)^4\delta^4(k_1+k_2-P)\mathcal{M}(gg\to^{2S+1}L_J)}{\sqrt{(2k_1)(2k_2)(2E_P)}} \\ &= -i(2\pi)\delta(E_1+E_2-E_P) < \psi_{JM}|H_{eff}|gg > , \end{aligned} \tag{2.7}$$

where $|\psi_{JM}>$ is the final charmonium wavefunction. We insert a complete set of $c\bar{c}$ states to write the effective Hamiltonian as

$$< \psi_{JM}|H_{eff}|gg >= \frac{1}{(2\pi)^6}\sum_{spins}\int d^3P\, d^3q < \psi_{JM}|Pq >< Pq|H_{eff}|gg > , \tag{2.8}$$

where $< Pq|\psi_{JM} >$ is the Fourier transform of the charmonium wavefunction and $< Pq|H_{eff}|gg >$ is related to the QCD matrix element as

$$< Pq|H_{eff}|gg >= (2\pi)^3\delta^3(P-k_1-k_2)\frac{\mathcal{M}_{gg\to c\bar{c}}(P,q)}{\sqrt{(2k_1)(2k_2)(2E_3)(2E_4)}}. \tag{2.9}$$

Here, we have defined center of mass and relative momenta as $P = \frac{1}{2}(p_3+p_4)$ and $q = (p_3-p_4)$, respectively. We write the momentum space charmonium wavefunction in the form

$$< Pq|\psi_{JM} >= (2\pi)^3\delta^3(P_\psi - P)\tilde{\phi}_L(q)Y_{LM_L}(\Omega_{\mathbf{q}}) , \tag{2.10}$$

where we have assumed that the center of mass wavefunction is represented by a plane wave of momentum P_ψ. This, along with Equations 2.7, 2.8 and 2.9, allow us to write $\mathcal{M}(gg\to^{2S+1}L_J)$ as

$$\mathcal{M}(gg\to^{2S+1}L_J) = \frac{\sqrt{2E_\psi}}{(2\pi)^3}\int \frac{d^3q}{\sqrt{(2E_3)(2E_4)}}\tilde{\phi}_L(q)Y_{LM_L}(\Omega_{\mathbf{q}})\,\mathcal{M}_{gg\to c\bar{c}}(P_\psi,q) , \tag{2.11}$$

where we have performed the trivial P integration.

So far, we have neglected the spin structure of this interaction. We examine this by first decomposing the $|\psi_{JM}>$ state as

$$|JM >= \sum_{M_LM_S}|LM_LSM_S >< LM_LSM_S|JM > , \tag{2.12}$$

[3]Note that this is not the *invariant* S-matrix defined in Reference [21]

where L and S are the orbital angular momentum and spin of the charmonium state, which are fixed. We further decompose the $|SM_S>$ state, assuming is consists of spin-$\frac{1}{2}$ states, to write it as

$$|SM_S>=\sum_{m_3 m_4}|\frac{1}{2}m_3\frac{1}{2}m_4><\frac{1}{2}m_3\frac{1}{2}m_4|SM_S> \ . \tag{2.13}$$

Inserting Equation 2.13 into Equation 2.12, we get

$$|JM>=\sum_{M_L M_S m_3 m_4}<LM_L SM_S|JM><\frac{1}{2}m_3\frac{1}{2}m_4|SM_S>|LM_L\frac{1}{2}m_3\frac{1}{2}m_4> \ . \tag{2.14}$$

We have now written the final charmonium spin state as the sum over states of a pair of spin-$\frac{1}{2}$ (anti)quarks with orbital angular momentum, L, weighted by the appropriate Clebsch-Gordon coefficients. We may now write the invariant matrix element as

$$\begin{aligned}\mathcal{M}(gg\rightarrow{}^{2S+1}L_J)=&\frac{\sqrt{2E_\psi}}{(2\pi)^3}\sum_{M_L M_S m_3 m_4}<SM_S|\frac{1}{2}m_3\frac{1}{2}m_4><JM|LM_L SM_S> \\ &\times\int\frac{d^3q}{\sqrt{(2E_3)(2E_4)}}\tilde{\phi}^*_L(q)Y^*_{LM}(\Omega_{\mathbf{q}})\mathcal{M}_{gg\rightarrow c\bar{c}}(P_\psi,q,m_3,m_4) \ ,\end{aligned} \tag{2.15}$$

where we have now taken into account the full spin structure.

We must now calculate the perturbative QCD matrix element for the gluon fusion interaction depicted in Figure 2.6. We will only consider gluon fusion processes capable of producing a color singlet $c\bar{c}$ pair, required for the final bound state. Therefore, we have not included diagrams of the form shown in Figure 2.7. We note that other models exist where this requirement is not imposed [22]. There, it is assumed that "color bleaching" occurs through soft gluon interactions in the final state. The matrix elements for the diagrams shown in Figure 2.6 are written as (excluding color) [20]

$$\begin{aligned}\mathcal{M}^a &= -ig^2\bar{u}(p_3)\ \not{\epsilon}(1)\left[\frac{i(\not{p}_3-\not{p}_1+m)}{t-m^2}\right]\not{\epsilon}(2)v(p_4) \\ \mathcal{M}^b &= -ig^2\bar{u}(p_3)\ \not{\epsilon}(2)\left[\frac{i(\not{p}_3-\not{p}_2+m)}{u-m^2}\right]\not{\epsilon}(1)v(p_4) \ .\end{aligned} \tag{2.16}$$

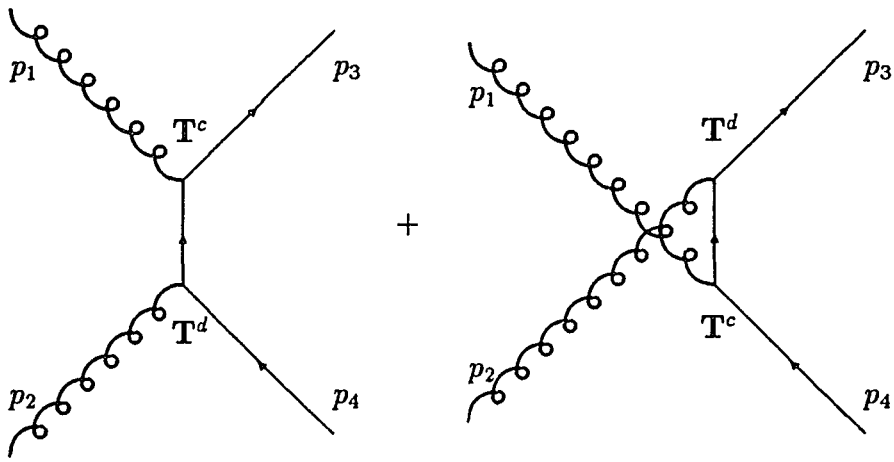

Figure 2.6: Heavy quark pair production through $\alpha_s{}^2$ gluon fusion.

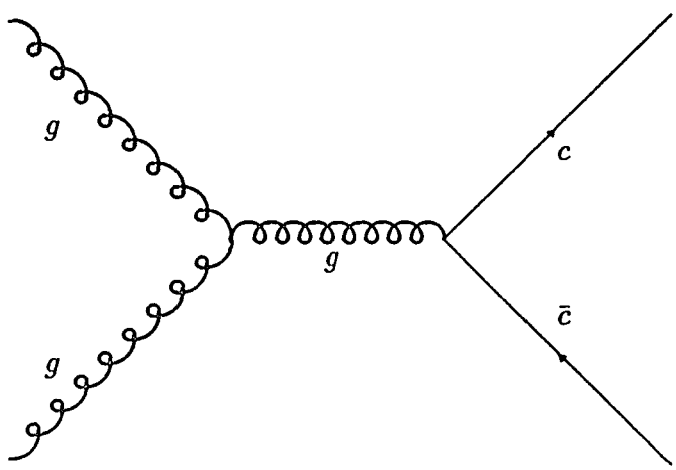

Figure 2.7: Non-color singlet heavy quark pair production through gluon fusion.

Here, the gluon polarizations are taken to satisfy $p_i \cdot \epsilon(i) = 0$. To calculate the color matrix element, we write the color singlet wavefunction, $1/\sqrt{2}(R\bar{R} + G\bar{G} + B\bar{B})$, in the matrix notation, $\eta_j^{\mathcal{T}}(3)\eta_i(4) = 1/\sqrt{3}\delta_{ij}$. The color matrix element then becomes

$$\begin{aligned} \eta_j^{\mathcal{T}}(3)\mathbf{T}_{ki}^c\mathbf{T}_{jk}^d\eta_i(4) &= \frac{1}{\sqrt{3}}\delta_{ij}\mathbf{T}_{ki}^c\mathbf{T}_{jk}^d \\ &= \frac{1}{\sqrt{3}}Tr(\mathbf{T}^c\mathbf{T}^d) \\ &= \frac{1}{2\sqrt{3}}\delta^{ab}\,, \end{aligned} \tag{2.17}$$

where $\mathbf{T}^c$ are the eight SU(3) color matrices as described in Reference [20]. Since the result is symmetric with respect to $c \leftrightarrow d$, the color matrix element is identical for $\mathcal{M}^a$ and $\mathcal{M}^b$. We therefore may now write

$$\begin{aligned} \mathcal{M}_{gg\to c\bar{c}} &= C[\mathcal{M}^a + \mathcal{M}^b] \\ &= \left(\frac{-ig^2\delta^{cd}}{2\sqrt{3}}\right)\bar{u}(p_3)\mathcal{A}v(p_4)\,, \end{aligned} \tag{2.18}$$

with

$$\mathcal{A} = \not{\epsilon}(1)\frac{(\not{p}_3 - \not{p}_1 + m)}{t - m^2}\not{\epsilon}(2) + \not{\epsilon}(2)\frac{(\not{p}_3 - \not{p}_2 + m)}{u - m^2}\not{\epsilon}(1)\,, \tag{2.19}$$

for the complete $\alpha_s{}^2$ gluon fusion matrix element.

Anticipating that we will project this amplitude onto a non-relativistic bound state, we "de-boost" the Dirac spinors, writing them in the form [21]

$$\bar{u}(p_3) = (\phi^\dagger(3), 0)\frac{\not{p}_3 + m}{\sqrt{E_3 + m}} \tag{2.20}$$

and

$$v(p_4) = \frac{-\not{p}_4 + m}{\sqrt{E_4 + m}}\begin{pmatrix} 0 \\ \chi(4) \end{pmatrix}\,, \tag{2.21}$$

where ϕ and $\chi = i\sigma_2\phi$ are the two-component spinors for the quark and antiquark. We then evaluate $\mathcal{M}_{gg\to c\bar{c}}$ in the center of mass frame as

$$\mathcal{M}_{gg\to c\bar{c}}(0, \mathbf{q}, m_3, m_4) = \left(\frac{-ig^2\delta^{cd}}{2\sqrt{3}}\right)\phi^\dagger(3)\{2E[(\epsilon_1 \cdot \mathbf{q})(\epsilon_2 \cdot \boldsymbol{\sigma}) + (\epsilon_2 \cdot \mathbf{q})(\epsilon_1 \cdot \boldsymbol{\sigma})]D_+$$

$$-4N^2[(\epsilon_1\cdot\mathbf{q})(\epsilon_2\cdot\mathbf{q})(\mathbf{q}\cdot\boldsymbol{\sigma})D_+ - 2N^2[(\mathbf{k}\cdot\mathbf{q})(\epsilon_1\cdot\epsilon_2)(\mathbf{q}\cdot\boldsymbol{\sigma})]D_-$$
$$+2E[(\mathbf{k}\cdot\boldsymbol{\sigma})(\epsilon_1\cdot\epsilon_2)]D_- - i2m[\mathbf{k}\cdot(\epsilon_1\cdot\epsilon_2)]D_+\}\chi(4)\,, \qquad (2.22)$$

where $N = 1/\sqrt{E+m}$ and $D_\pm = 1/(t-m^2) \pm 1/(u-m^2)$. The kinematics are defined such that $p_{\frac{1}{2}} = k_0(1,\pm\hat{\mathbf{k}})$ and $p_{\frac{3}{4}} = (E,\pm\mathbf{q})$, with $k_0 = E$. The gluon polarization four-vectors have been written as $\epsilon_\mu(i) = (0,\epsilon_i)$. Since the non-relativistic nature of $\tilde{\phi}_L(q)$ weights the integral in Equation 2.15 for $q \ll m$, we will find it useful to expand Equation 2.22 in powers of q/m as

$$\mathcal{M}_{gg\to c\bar{c}}(\mathbf{q},m_3,m_4) = \left(\frac{g^2\delta^{cd}}{2\pi}\right)\phi^\dagger(3)\left[\mathcal{A}^{(0)} + \mathcal{A}^{(1)} + \cdots\right]\chi(4)\,, \qquad (2.23)$$

where

$$\mathcal{A}^{(0)} = 2\hat{\mathbf{k}}\cdot(\epsilon_1\times\epsilon_3) \qquad (2.24)$$

and

$$\mathcal{A}^{(1)} = \frac{2iq}{m}[(\epsilon_1\cdot\hat{\mathbf{q}})(\epsilon_2\cdot\boldsymbol{\sigma}) + (\epsilon_2\cdot\hat{\mathbf{q}})(\epsilon_1\cdot\boldsymbol{\sigma}) + (\hat{\mathbf{k}}\cdot\hat{\mathbf{q}})(\hat{\mathbf{k}}\cdot\boldsymbol{\sigma})(\epsilon_1\cdot\epsilon_2)] \qquad (2.25)$$

are the lowest order ($O(0)$ and $O(q/m)$) contributions. Note that we have dropped the explicit $P_\psi = 0$ label in $\mathcal{M}_{gg\to c\bar{c}}$ with the assumption that we are in the center of mass frame.

We now proceed with the calculation of $\mathcal{M}(gg \to {}^{2S+1}L_J)$. Though we will be primarily interested in the results for the $\chi_c(L=S=1)$ states, we continue with our illustrative calculation by considering a simpler case, that of the $\eta_c(L=S=0)$. Using the appropriate Clebsch-Gordon coefficients for $L=S=0$ in Equation 2.15, we write $\mathcal{M}(gg\to\eta_c)$ as

$$\mathcal{M}(gg\to\eta_c) = \frac{\sqrt{2M_{\eta_c}}}{(2\pi)^3}\int\frac{d^3q}{\sqrt{(2E_3)(2E_4)}}\{\tilde{\phi}_0^*(q)Y_{00}^*(\Omega_\mathbf{q})$$
$$\times\frac{1}{\sqrt{2}}[\mathcal{M}_{gg\to c\bar{c}}(\mathbf{q},\tfrac{1}{2},-\tfrac{1}{2}) - \mathcal{M}_{gg\to c\bar{c}}(\mathbf{q},-\tfrac{1}{2},\tfrac{1}{2})]\}\,. \qquad (2.26)$$

As noted before, $\tilde{\phi}_0(q)$ weights this integral in the region $q \ll m$. We therefore evaluate this integral by expanding the rest of the integrand in powers of (q/m),

neglecting terms of order $(q/m)^2$. Inserting Equation 2.23 into 2.26 above, taking $E_3 \approx E_4 \approx m$, and setting $M_{\eta_c} \approx 2m$, we write

$$\mathcal{M}(gg \to \eta_c) = \left(\frac{g^2\delta^{cd}}{2\sqrt{3}}\right)\sqrt{\frac{8\pi}{m}}\frac{1}{(2\pi)^3}[2\hat{\mathbf{k}}\cdot(\epsilon_1 \times \epsilon_2)]\left[\int_0^\infty dq\, q^2 \tilde{\phi}_0^*(q)\right] . \qquad (2.27)$$

Here, only the $\mathcal{A}^{(0)}$ term contributes due to the spherical symmetry of the η_c state. Also, we have employed the result, $\mathcal{M}^{(0)}(\mathbf{q}, \frac{1}{2}, -\frac{1}{2}) = -\mathcal{M}^{(0)}(\mathbf{q}, -\frac{1}{2}, \frac{1}{2})$. Since the coordinate and momentum space wavefunctions are related as

$$\phi_L(r) = \frac{4\pi}{(2\pi)^3}\int_0^\infty dq\, q^2 j_L(qr)\tilde{\phi}_L(q) , \qquad (2.28)$$

we may use

$$\int_0^\infty dq\, q^2 \tilde{\phi}_0^*(q) = 2\pi^2\, \phi_0^*(0) \qquad (2.29)$$

to write

$$\mathcal{M}(gg \to \eta_c) = \left(\frac{g^2\delta^{cd}}{2\sqrt{3}}\right)\sqrt{\frac{2}{\pi m}}\phi_0^*(0)[\hat{\mathbf{k}}\cdot(\epsilon_1 \times \epsilon_2)] . \qquad (2.30)$$

We then average over the eight colors and two polarizations of the initial gluons to write

$$|\mathcal{M}(gg \to \eta_c)|^2 = \frac{\pi {\alpha_s}^2}{6m}|\phi_0(0)|^2 \qquad (2.31)$$

for the spin averaged matrix element, where $\alpha_s = g^2/4\pi$. This may finally be inserted into the parton model formalism of the previous section to calculate the invariant cross sections.

To calculate the matrix element for the χ_c state, we will find it helpful to employ a notation similar to that in Reference [14] and rewrite Equation 2.15 in the form

$$\mathcal{M}(gg \to \chi_{JM}) = \sqrt{2M_\chi}\sum_{M_L M_S} < JM|1M_L 1M_S > I_{M_L M_S} , \qquad (2.32)$$

where we have defined

$$I_{M_L M_S} \equiv \frac{1}{(2\pi)^3}\int \frac{d^3q}{\sqrt{(2E_3)(2E_4)}}\tilde{\phi}_1^*(q)Y_{1M_L}^*(\Omega_{\mathbf{q}})$$
$$\left[\sum_{m_3 m_4} < 1M_L|\frac{1}{2}m_3\frac{1}{2}m_4 > \mathcal{M}_{gg\to c\bar{c}}(q, m_3, m_4)\right] . \qquad (2.33)$$

Employing the same non-relativistic approximations as before and defining the gluon polarizations in the spherical form, $\epsilon_{\lambda_i} = \sum_q (-1)^q \delta_{-q\lambda_i} \hat{e}_{-q}$, we find

$$I_{\pm 1 \pm 1} = \left(\frac{g^2 \delta^{cd}}{2\sqrt{3}}\right)\left(\frac{2i}{m^2}\right)\sqrt{\frac{3}{2\pi}}\phi_1'^*(0)(\delta_{\pm 1 \lambda_1}\delta_{\pm 1 \lambda_2}) \tag{2.34}$$

and

$$I_{00} = -I_{\pm 1 \mp 1} = \left(\frac{g^2 \delta^{cd}}{2\sqrt{3}}\right)\left(\frac{i}{m^2}\right)\sqrt{\frac{3}{2\pi}}\phi_1'^*(0)[\epsilon_1 \cdot \epsilon_2]\,, \tag{2.35}$$

with all others vanishing. In this case, the angular integration has projected out the $\mathcal{A}^{(1)}$ term defined in Equation 2.25. Also, we have used the result

$$\int_0^\infty dq q^3 \tilde{\phi}_1(q) = 6\pi^2 \phi_1'(0)\,. \tag{2.36}$$

We insert the $I_{M_L M_S}$'s and the appropriate Clebsch-Gordon coefficients into Equation 2.32 to find the non-vanishing matrix elements to be

$$\begin{aligned} \mathcal{M}(gg \to \chi_{00}) &= \sqrt{2M_\chi}\frac{1}{\sqrt{3}}(I_{+1-1} - I_{00} + I_{-1+1}) \\ &= -3i\left(\frac{g^2\delta^{cd}}{2\sqrt{3}}\right)\sqrt{\frac{2}{\pi m^3}}\phi_1'^*(0)[\epsilon_1 \cdot \epsilon_2] \end{aligned} \tag{2.37}$$

and

$$\begin{aligned} \mathcal{M}(gg \to \chi_{2\pm 2}) &= \sqrt{2M_\chi}\, I_{\pm 1 \pm 1} \\ &= 4i\left(\frac{g^2\delta^{cd}}{2\sqrt{3}}\right)\sqrt{\frac{3}{2\pi m^3}}\phi_1'^*(0)(\delta_{\pm 1\lambda_1}\delta_{\pm 1\lambda_2})\,, \end{aligned} \tag{2.38}$$

where we have again used $M_R \approx 2m$. The spin-color averaged matrix elements are then found to be

$$|\mathcal{M}(gg \to \chi_0)|^2 = \frac{3}{2}\pi\frac{{\alpha_s}^2}{m^3}|\phi_1'(0)|^2 \tag{2.39}$$

and

$$|\mathcal{M}(gg \to \chi_2)|^2 = 2\pi\frac{{\alpha_s}^2}{m^3}|\phi_1'(0)|^2\,. \tag{2.40}$$

Again, this is inserted into the parton formalism.

To produce J/ψ's with higher transverse momenta, we must consider processes of order ${\alpha_s}^3$. This has been studied in great detail in Reference [16]. Here, we shall simply discuss the results pertinent to our analysis.

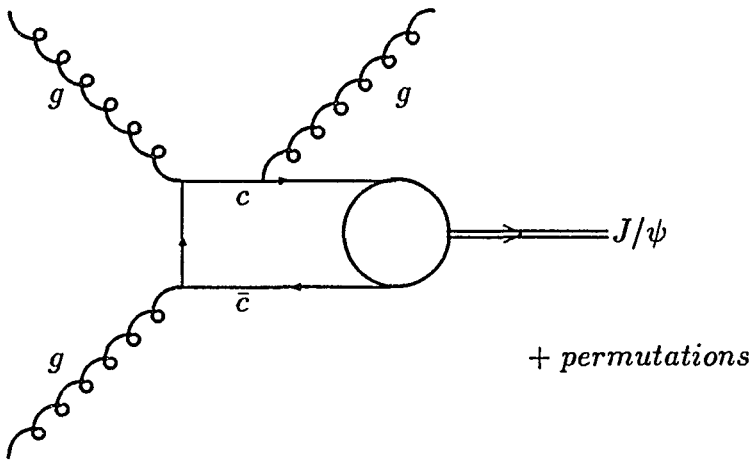

Figure 2.8: $\alpha_s{}^3$ direct J/ψ production.

In Figure 2.8, we show the $\alpha_s{}^3$ mechanism responsible for direct J/ψ production. Employing the same approximation concerning the bound state wavefunction as in the $\alpha_s{}^2$ case, the partonic differential cross section is found to be [16]

$$\begin{aligned}\frac{d\sigma}{d\hat{t}}(gg \to J/\psi g) &= \frac{5\pi\alpha_s{}^3|\phi_0(0)|^2}{9M_\psi \hat{s}^2}\frac{M_\psi^2}{(\hat{s}-M_\psi^2)(\hat{t}-M_\psi^2)(\hat{u}-M_\psi^2)} \\ &\times \{[\hat{s}^2(\hat{s}-M_\psi^2)]+[\hat{s}\to\hat{t}]+[\hat{s}\to\hat{u}]\}\,. \qquad (2.41)\end{aligned}$$

To account for indirect J/ψ's at large p_T, the $\alpha_s{}^3$ cross sections for the χ_c must also be included. We refer the reader to the Appendix A of Reference [16] and References [34, 35] for their rather lengthly explicit expressions. We note, however, that they are written as a hard QCD partonic cross section times the *derivative* of the wave function at the origin. Inserting these into Equation 2.6 and performing the appropriate integrations will yield the hadronic differential cross sections.

The $\alpha_s{}^2$ and $\alpha_s{}^3$ were combined and compared to differential cross sections measured at the CERN-ISR in Reference [16]. The authors *assumed* that the $\alpha_s{}^2$ process dominates at low p_T. A Gaussian smearing function of the form $f(p_T) \sim \exp[-p_T{}^2/4a^2]$, with $a = 0.48\,GeV$, was used to simulate primordial transverse

momentum. The low and high p_T results were the joined at $p_T \sim 2\,GeV$. It was found that at least half of the high p_T J/ψ's also resulted from χ_c decay. Of interest to us is the suggestion that the fraction of indirect J/ψ's is close to one at zero p_T with a decreasing influence at higher p_T.

2.3 "Definition" of Charmonium States

In our discussions in the previous sections, we have assumed that the charmonium bound states are described by some non-relativistic wavefunction. We will now examine specific forms for these wavefunctions. In particular, we will examine the harmonic oscillator model employed in Reference [14] and the QCD motivated Cornell model [23]. This is not meant to be a complete review of the application of non-relativistic quantum mechanics to charmonium spectroscopy. Such reviews can be found in References [24, 25, 26]. Again, our goal here is to provide the background picture on which we will discuss charmonium suppression.

The harmonic oscillator potential, $V(r) = 1/2\,\mu\omega_\psi^2 r^2$ with μ being the reduced mass, provides a simple model for the charmonium system. For a central potential, the non-relativistic Schrödinger equation,

$$\left[\frac{1}{2\mu}\nabla^2 + V(r)\right]\Psi(\mathbf{r}) = E\Psi(\mathbf{r}), \tag{2.42}$$

may be separated, allowing us to write solutions in the form

$$\Psi_{nlm}(\mathbf{r}) = R_{nl}(r)Y_{lm}(\Omega)\,. \tag{2.43}$$

For the harmonic oscillator, the radial functions are [27]

$$R_{nl}(r) = N_{nl}(\beta)\,(\beta r)^l \exp\left[-\frac{\beta^2 r^2}{2}\right] L^{l+1/2}_{(n/2-l/2-1)}(\beta^2 r^2)\,, \tag{2.44}$$

where $L_n^\alpha(x)$ are the associated Laguerre polynomials [28]. The normalization is given by

$$N_{nl}(\beta) = \beta^{\frac{3}{2}}\left[\frac{2(n/2-l/2-1)!}{\Gamma(n/2+l/2+1)}\right]^{\frac{1}{2}}\,. \tag{2.45}$$

	Calculated	Observed [29]
$\psi(1S)$	3.31	3.068 ± 0.002
$\chi_c(1P)$	3.52	3.531 ± 0.010
$\psi'(2S)$	3.73	3.633 ± 0.002

Table 2.1: Charmonium masses (in GeV) in the harmonic oscillator model.

We have also defined $\beta^2 = \mu\omega_\psi$.

The energy levels in this model are given by

$$E_n = \left(n + \frac{1}{2}\right)\omega_\psi \tag{2.46}$$

where

$$n = 2k + l + 1 \qquad k = 0, 1, 2 \ldots . \tag{2.47}$$

We define the radial quantum number, $n_r = k + 1$, in accordance with the spectroscopic notation $(n_r L)$, employed in [24, 25]. The resulting charmonium masses, given by $M_n = 2m_c + E_n$, are shown in Table 2.1 along with the observed (spin averaged) masses. Here, we have used the parameters, $m_c = 1.5\,GeV$ and $\omega_\psi = 0.207\,GeV$, employed in Reference [14]. We see that the charmonium masses are reproduced to within $\sim 8\%$. It is possible to adjust ω_ψ and μ to better match the observed masses. However, in Chapter 4, we shall be interested in the one dimensional case for which these parameters yield $M_\psi = 2m_c + 1/2\omega_\psi = 3.1\,GeV$.

To determine whether we have truly created a non-relativistic model for the J/ψ we calculate $< p^2 >$ for the ground state as

$$< p^2 >= |N_{10}|^2 \int_0^\infty \exp\left[-\frac{p^2}{\beta^2}\right] p^4 dp = \frac{3}{2}\beta^2 \,, \tag{2.48}$$

where $\beta^2 = \mu\omega_\psi$. This implies $< v^2 >=< p^2 > /m^2 \approx 0.1$. With this, one could assume that we have successfully modeled (to within 5-10 %) the charmonium

system as a non-relativistic harmonic oscillator. However, this model gives the ratio of the wavefunctions at the origin of the ψ' and ψ states as

$$\frac{|\Psi_{2S}(0)|^2}{|\Psi_{1S}(0)|^2} = \frac{3}{2} . \tag{2.49}$$

This quantity is related to the leptonic decay widths by

$$\frac{\Gamma(\psi' \rightarrow e^+e^-)}{\Gamma(\psi \rightarrow e^+e^-)} = \left(\frac{M_\psi^2}{M_{\psi'}^2}\right) \frac{|\Psi_{2S}(0)|^2}{|\Psi_{1S}(0)|^2} . \tag{2.50}$$

The observed [29] $\Gamma_e(\psi')/\Gamma_e(\psi) = 0.45 \pm 0.06$ implies a wavefunction ratio of $\sim 0.55 - 0.72$. Therefore, though the non-relativistic harmonic oscillator crudely reproduces the charmonium spectrum, it does not yield the correct $\Gamma_e(\psi')/\Gamma_e(\psi)$.

To construct a more realistic model, we examine the nature of the QCD interaction that we assume is the interquark binding force. At short distances, we expect a Coulomb-like interaction. At long distances, we assume a confining force that we take to be constant. This gives rise to the Cornell form [23],

$$V(r) = -\frac{k}{r} + ar , \tag{2.51}$$

of the interquark potential. A recent analysis [29] fit the combined charmonium-bottomonium spectra with the parameters $k = 0.471$, $a = 0.192\,GeV^2$, $m_c = 1.320\,GeV$, and $m_b = 4.746\,GeV$. We shall employ these parameters to model the charmonium system and examine the results.

To write solutions of the Schrödinger equation with the Cornell potential, we follow the example of Reference [29] and employ the Rayleigh-Ritz-Galerkin method [29, 30]. The details of the solutions are given in Appendix B. The solutions are expanded in terms of some orthonormal basis which we take to be the set of harmonic oscillator eigenfunctions written in the form[4] [31]

$$\Omega_{il}^m(\beta, \mathbf{r}) = N_{il}(\beta) \exp\left[-\frac{\beta^2 r^2}{2}\right] L_{i-1}^{l+1/2}(\beta^2 r^2)(\beta r)^l Y_{lm}(\Omega) , \tag{2.52}$$

[4]Note that the index, i, is different than in our previous discussion of harmonic oscillator solutions. The present notation is more convenient for expansion purposes.

	Calculated	Observed [29]
$\psi(1S)$	3.07	3.068 ± 0.002
$\chi_c(1P)$	3.50	3.531 ± 0.010
$\psi'(2S)$	3.70	3.633 ± 0.002

Table 2.2: Charmonium masses (in GeV) from Cornell potential.

where

$$N_{il}(\beta) = \beta^{\frac{3}{2}} \left[\frac{2(i-1)!}{\Gamma(i+l+1/2)} \right]^{\frac{1}{2}} . \tag{2.53}$$

Here, β is now just an arbitrary scale parameter. A twenty-five term solution, written in the form

$$\chi^m_{n_r L}(\mathbf{r}) = \sum_i a_i^{n_r Lm} \Omega^m_{iL}(\beta, \mathbf{r}) , \tag{2.54}$$

is found with the coefficients given in Appendix B. The resulting charmonium masses are shown in Table 2.2. We see that this has reproduced the observed masses rather well. The ratio of the wavefunctions at the origin is found to be $|\Psi_{2S}(0)|^2/|\Psi_{1S}(0)|^2 = 0.73$, which is in much better agreement with the observed leptonic width the that predicted in the harmonic oscillator model. However, we find the momentum expectation value for the ground state to be $< p^2/m^2 > \approx 0.26$. Thus, this system is much less non-relativistic than the harmonic oscillator.

In the following chapters, we shall consider both illustrative and realistic models to study deconfinement effects on heavy quark bound states. For the former, we shall employ the harmonic oscillator model. This will yield relatively transparent calculations while providing a rough estimation of the charmonium system. We shall then use the solutions of the Cornell potential for our more critical analyses.

2.4 Extension to Nuclear Collisions

The simplest approach for a QCD description of nucleus-nucleus collisions would be to consider the nuclei as systems of non-interacting nucleons, each of which collide with all of the nucleons of the target nucleus. We would then simply replace the nucleon structure functions (for parton species i) with [32]

$$f_{i/A}(x) = Zf_{i/p}(x) + Nf_{i/n}(x) \tag{2.55}$$

where Z(N) is the number of protons (neutrons) in nucleus A. However, it is becoming apparent from recent experiments that Equation 2.55 does not accurately describe the observed nuclear structure functions. A review of this is given in References [33] and [36]. In particular, the parton densities may be "shadowed" at low x. Also, elastic scattering, prior to the hard inelastic scattering that produces the J/ψ, may significantly widen parton p_T distributions beyond their primordial form [9, 10, 11]. The hadronic environment immediately following the collision must also be considered. It may be dense enough to absorb a sizable fraction of the produced J/ψ's [5, 6, 7]. Finally, there is the possibility of quark gluon plasma formation. In this section, we briefly discuss these effects (excluding QGP formation) and their importance in our later discussion of color screening phenomenology.

There now exists a fair amount of data concerning the A dependence of J/ψ production in nuclear collisions [37, 38]. It has been observed that p-A collisions become less efficient at producing J/ψ's with increasing A, i.e., the ratio $R_{A/p} \equiv \sigma_{pA}/(A\sigma_{pp})$ decreases with increasing A. This ratio has been parametrized in the form [39]

$$R_{A/p} = 1 + a \ln x_2 \ln A \,, \tag{2.56}$$

with $x_2 = 1/2(\sqrt{4M^2/s + x_F^2} - x_F)$. The combined data sets yield the parameter $a = 0.021 \pm 0.001$. In Reference [39], the J/ψ cross sections were shown to be dominated by gluon fusion. This is consistent with the recent observation [40] that the $p\pi \rightarrow J/\psi$ and $\bar{p}\pi \rightarrow J/\psi$ cross sections are nearly equal. Assuming

that the hadronization mechanism (which is represented by the wavefunction at the origin in the color singlet model) is unaffected by mass number, this ratio is simply the ratio of the gluon structure functions, i. e.

$$R_{A/p} \equiv \frac{g_p(x_1)g_A(x_2)}{g_p(x_1)g_p(x_2)} = \frac{g_A(x_2)}{g_p(x_2)} \,. \tag{2.57}$$

In this case, the depletion of J/ψ's per nucleon with increasing A implies a decrease, or "shadowing" of the gluon structure function in nuclei for small x [39].

The p_T distributions in pA collisions show a widening with respect to pp collisions for both J/ψ production [37] and the Drell-Yan process [41]. Elastic scattering of the light quarks in the nuclei before the hard QCD process seemed to explain the A-dependence of the Drell-Yan data [42]. Investigations of the analogous elastic gluon scattering effect on J/ψ production in pA and AA collisions were performed in References [9, 10, 11] and more recently in [43, 44]. It was shown that much of the momentum dependence in the NA 38 results could be explained by initial state effects. We shall discuss this again in Chapter 5 and its effects regarding the observed J/ψ suppression.

Finally, we must consider processes that occur after the $c\bar{c}$ pair is formed. These final state effects include color screening due to quark gluon plasma formation and hadronic absorption of the J/ψ. The first is the subject of the rest of this paper. The second involves the destruction of J/ψ's through processes of the form

$$J/\psi + h \rightarrow D + \bar{D} + X \tag{2.58}$$

while passing through the post-collision hadronic environment. Several specific models [5, 6, 7] have been proposed to explain the observed J/ψ suppression based on this idea. As stated before, these have a weak p_T dependence and require the addition of initial state scattering to replicate the observed p_T dependence of the suppression. We refer the reader to Reference [45] for a review of the various hadronic absorption models.

2.5 Discussion

In this chapter, we have discussed the production of charmonium bound states within the context of color singlet final states. We have seen that the primary production processes occur via ${\alpha_s}^3$ direct J/ψ production and intermediate χ_c production at orders ${\alpha_s}^2$ and ${\alpha_s}^3$. The unifying feature in each of these cases has been the assumption that the QCD process produced a narrow $c\bar{c}$ wavepacket with respect to a wide final bound state. It is the evolution of this initial wavepacket that we will study when examining J/ψ suppression in a quantum mechanical framework.

In Reference [16], it was assumed that the low p_T J/ψ production is dominated by the ${\alpha_s}^2$ intermediate χ_c decay process. This is based on the assumption that low p_T J/ψ production is truly in the perturbative regime. At higher p_T, they find that about half of the J/ψ's are produced directly and half result from χ_c decay. However, the total fraction of the J/ψ's resulting from intermediate χ_c's at $\sqrt{s} \sim 20 - 25$ GeV has been measured at only $\sim 30 - 40\%$ [46, 47]. There does, however, exist one older measurement of this fraction at $70 \pm 28\%$ [48].

In our later discussions of J/ψ suppression, we will be interested in the relative fraction of directly produced J/ψ's to those produced through χ_c decay as a function of p_T. The apparent discrepancy between predictions based on the color singlet approach and experiment indicate that this is still an open question. We will therefore simply consider several generic p_T-distributions and examine the results.

We have also discussed effects observed in making the transition from NN to NA collisions. In this paper, we investigate quark gluon plasma formation as the relevant final state effect. We will first examine what requirements are needed to explain the observed J/ψ suppression purely in terms of this effect. We then examine how these requirements are relaxed when initial state effects are taken

into account.

CHAPTER 3

SEMI-CLASSICAL MODEL OF J/ψ COLLISIONS

Having discussed the production of heavy quark resonances in the previous chapter, we now discuss modifications due to the presence of a deconfining quark gluon plasma. However, we first provide, in Section 3.1, a brief review of the suppression observed by the NA 38 Collaboration. Then we will model this based on semiclassical concepts. In Section 3.2, we describe the formation time argument introduced by Karsch and Petronzio [8] and reviewed in [49]. Then, based on the work of Blaizot and Ollitrault [50], we incorporate this into a hydrodynamical model for the plasma region in Section 3.3. In Section 3.4, we examine the inclusion of J/ψ's produced by χ_c decays and discuss the results in Section 3.5.

3.1 Brief Review of NA 38 Results

The NA 38 Collaboration at CERN has studied the production of dimuons in 200 GeV/nucleon proton-, oxygen-, and sulfur-uranium collisions [4, 51, 52, 53, 54, 55]. The invariant mass and transverse momentum of each dimuon event was measured. The J/ψ resonance appears, through the decay $J/\psi \rightarrow \mu^+\mu^-$, in the invariant mass spectrum at $\sim$ 3.1 GeV. Also measured was the total neutral transverse energy of each collision.

The transverse energy is an indication of the violence of the collision. Therefore, if J/ψ production is impeded due to quark gluon plasma formation, one would expect this to occur at higher E_T. The data was divided into six E_T^0

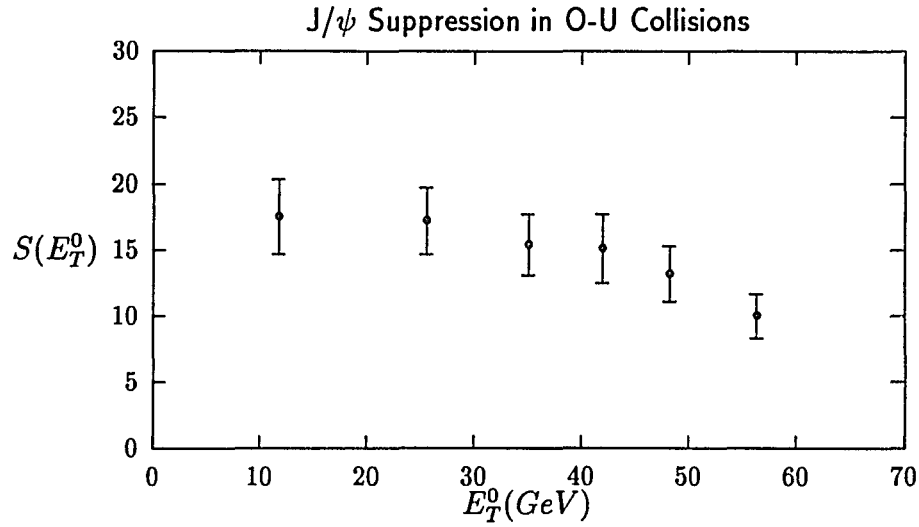

Figure 3.9: $S \equiv N_\psi/N_c$ versus E_T^0 for O-U collisions [54].

bins. The number of J/ψ events, N_ψ, and continuum events in the J/ψ mass range, N_c, was found for each bin. The ratio, $S \equiv N_\psi/N_c$, is plotted as a function of the mean transverse energy for each bin in Figures 3.9 and 3.10. It is seen that this ratio decreases with increasing E_T^0. In contrast, this ratio remained relatively constant at $S \approx 22 - 23$ in proton-uranium collisions [54]. Though the overall normalization, related to the number of nucleon-nucleon interactions, changed, the shape of the Drell-Yan continuum was seen to be independent of E_T. Since the Drell-Yan pairs should be unaffected by the hadronic medium, one would expect this "suppression" as due to some final state effect such as nuclear absorption or color screening in a quark gluon plasma.

Of interest to us will be the transverse momentum dependence of this suppression. The NA 38 group computed the ratio of the number of J/ψ events (normalized to the continuum) in the highest to that in the lowest E_T^0 bin as a function of transverse momentum. This is shown in Figures 3.11 and 3.12. A relatively strong p_T dependence is seen, with a suppression of $\sim 1/2$ at $p_T = 0$ that disappears at $p_T \approx 3$ GeV.

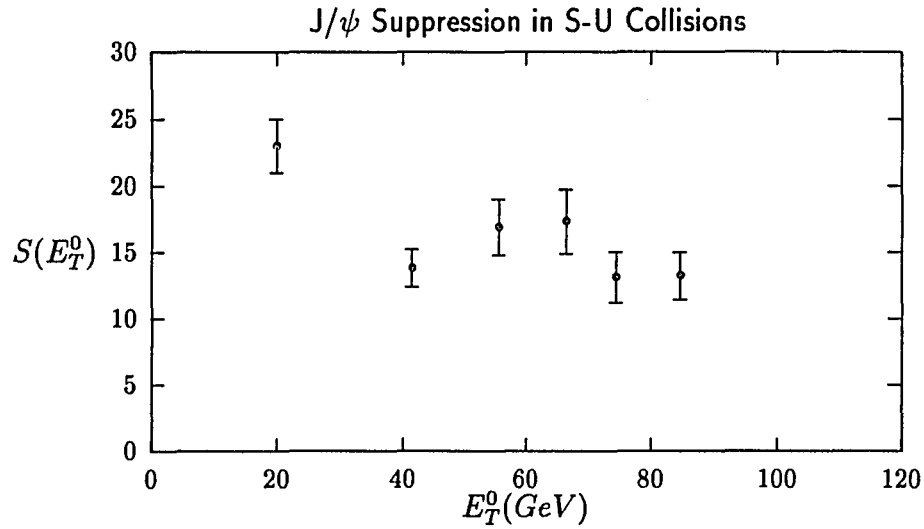

Figure 3.10: $S \equiv N_\psi/N_c$ versus E_T^0 for S-U collisions [54].

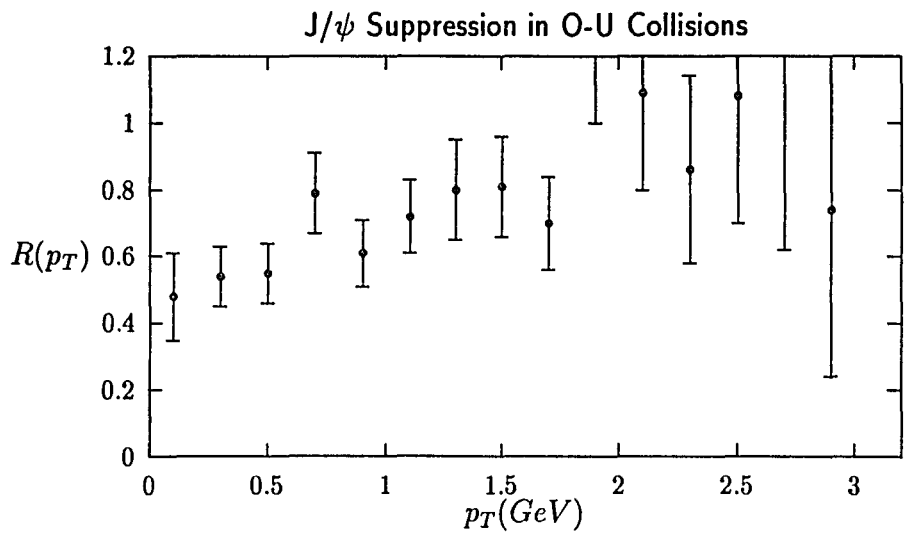

Figure 3.11: Ratio of number of high E_T^0 events (>52 GeV) vs. low $E_T{}^0$ events (<20 GeV), $R(p_T)$, as a function of momentum for O-U collisions [55].

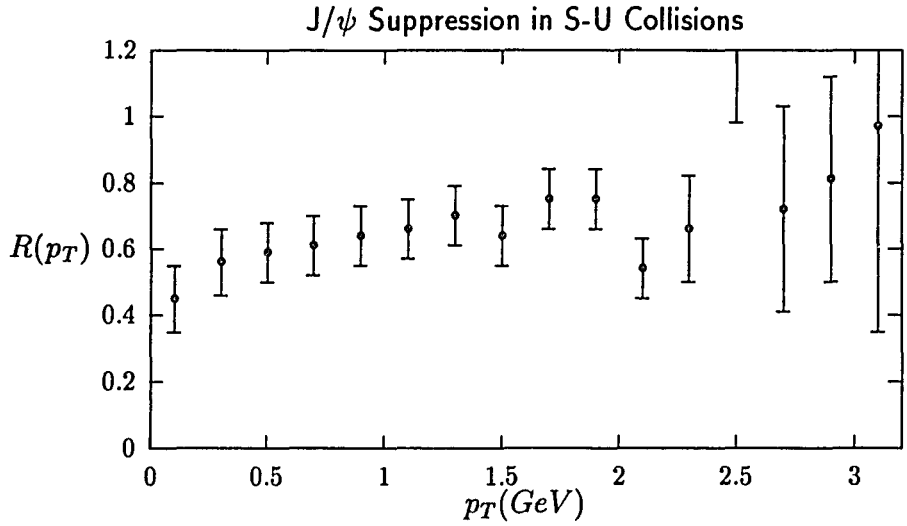

Figure 3.12: Ratio of number of high E_T^0 events (>78 GeV) vs. low $E_T{}^0$ events (<34 GeV), $R(p_T)$, as a function of momentum for S-U collisions [55].

3.2 Formation time argument for J/ψ dissolution

The mechanism responsible for deconfinement in a quark gluon plasma is a Debye-like screening of the color charges [3]. However, unlike normal Debye scattering, color screening in the relativistic energy ranges we are considering becomes stronger with increasing temperature. This screening mechanism in studied using the relatively new techniques of lattice QCD. Though results should still be considered preliminary, it is generally believed that temperatures of $\sim$ 150 – 200 MeV are sufficient to affect charmonium resonances. For now, we shall assume such temperatures are achieved in heavy ion collisions and defer the question of whether this is really true or not until Section 3.5.

We assume that the $c\bar{c}$-pair that eventually forms a J/ψ is created by a hard QCD process in a space-time interval on the order of $1/M_\psi$=0.06 fm. There then exists some characteristic time, t_f^ψ, for the pair to separate to 1/2 fm, the J/ψ radius. If the pair remains in the deconfining region longer than t_f^ψ, they will

have separated too far to form the resonance. We therefore write the probability of resonance formation in the simple form

$$\begin{aligned} P(t) &= 1 \quad t < t_f^R \\ &= 0 \quad t > t_f^R, \end{aligned} \tag{3.59}$$

where t is the time the pair is immersed in the plasma.

The momentum dependence enters in two ways. First, assuming a finite plasma region, a fast moving pair will have a greater chance of escaping the plasma. Also, there will be a time dilation of the J/ψ formation time in the lab frame of the $c\bar{c}$-pair, requiring us to modify Equation 3.59 to

$$\begin{aligned} P(t) &= 1 \quad t < \gamma t_f^R \\ &= 0 \quad t > \gamma t_f^R, \end{aligned} \tag{3.60}$$

where t is measured in the rest frame of the *plasma.* Over the momentum range of interest ($0 < p_\psi < M_\psi$), γ does change considerable ($1 < \gamma < \sqrt{2}$).

There have been some different values used for the resonance formation time. One is the time needed for the quarks to complete one Bohr orbit [56]. However, we choose to follow [8] and define t_f^R as

$$t_f^R = r_R/(p_R/m_q), \tag{3.61}$$

the time it takes for the pair to separate to the characteristic resonance binding radius. The resonance parameters, r_R and p_R, are found by calculating the root mean square radii and momenta from charmonium spectroscopy models described in Chapter 2. The results for various heavy quark resonances, as calculated in references [57, 58], are given in Table 3.3.

We should point out two important results from Table 3.3 that will be important in our later discussions regarding the J/ψ and χ_c resonances. First, the J/ψ is more tightly bound with a smaller r_{rms} than the χ_c which is closer to the

Resonance	r[fm]	p[GeV]	t_f^R
J/ψ	0.453	0.672	0.89
Ψ'	0.875	0.768	1.50
χ_c	0.696	0.456	2.01
Υ	0.226	1.408	0.76
Υ'	0.509	1.271	1.90
χ_b	0.408	0.744	2.60

Table 3.3: Bound state parameters for various quarkonium resonances. From [57].

size of ordinary hadrons (~1 fm). Therefore, dissolution of the J/ψ should require a smaller screening length, and hence, a higher temperature environment, than the χ_c. It is estimated [49, 59] that, while the χ_c should be dissolved at $T \sim T_c$, dissolution of the J/ψ would require $T \sim (1.2 - 1.3)T_c$. However, we also notice that the χ_c has a much larger formation time, thus it can survive in a longer lived plasma. It is important to note that these effects work against each other.

3.3 Plasma Model for Semiclassical J/ψ Suppression

We must now consider a model for the plasma region that is assumed to form in the central rapidity region of a heavy ion collision. We follow the work of Blaizot and Ollitrault [50], which is based on the hydrodynamical picture of Bjorken [60]. This assumes that the transverse expansion of the plasma may be ignored for $t_m/R_0 \ll 1$, where t_m is the lifetime of the hot plasma region and R_0 is the transverse size of the plasma (taken to be the radius of the projectile nucleus). The evolution of a cylindrical plasma is dominated by longitudinal expansion and is governed by entropy conservation,

$$t\, s(r,t) = t_0\, s(r,t_0). \tag{3.62}$$

The parameter, t_0, is the initial equilibration time of the plasma.

We assume the initial entropy profile may be written in the form

$$s(r,t_0) = s_0 \left[1 - \frac{r^2}{R_0^2}\right]^a, \tag{3.63}$$

where a is a free parameter characterizing the collision. As an example, the value, $a = 1/2$, corresponds to the assumption of a central symmetric (A=B) collision and that the entropy scales like the number of participants. Using Equation 3.62, we find

$$s(r,t) = \frac{t_0}{t} s(r,t_0) = \frac{t_0 s_0}{t} \left[1 - \frac{r^2}{R_0^2}\right]^a = s(0,t) \left[1 - \frac{r^2}{R_0^2}\right]^a. \tag{3.64}$$

Therefore, the functional form of the radial profile remains the same with its central value governed by $t\, s(0,t) = t_0\, s_0$. Since we will speak mostly in terms of temperature, we rewrite Equation 3.64 as

$$T(r,t) = T(0,t) \left[1 - \frac{r^2}{R_0^2}\right]^{\frac{a}{3}}, \tag{3.65}$$

where we have assumed that the plasma behaves like a relativistic ideal gas with $s \sim T^3$.

We will be interested in regions above a certain critical temperature. Therefore, we use Equation 3.65 to define isotherms as

$$R^T(t) = R_0 \left[1 - \left(\frac{T}{T(0,t)}\right)^{\frac{3}{a}}\right]^{\frac{1}{2}}. \tag{3.66}$$

Then, defining t_m^T as the time a particular isotherm reaches $r = 0$, the central temperature evolves according to $t_m^T\, T^3(0,t_m^T) = t\, T^3(0,t)$. Identifying $T \equiv T(0,t_m^T)$, we find the evolution of the isotherm to be

$$R^T(t) = R_0 \left[1 - \left(\frac{t}{t_m^T}\right)^{\frac{1}{a}}\right]^{\frac{1}{2}}, \tag{3.67}$$

i.e., it is governed by the single parameter t_m^T. Furthermore, we find that the evolution of all of the isotherms is related through $t_m^{T_1}\, T_1^3 = t_m^{T_2}\, T_2^3$. We plot in Figure 3.13 the isotherms for various temperatures.

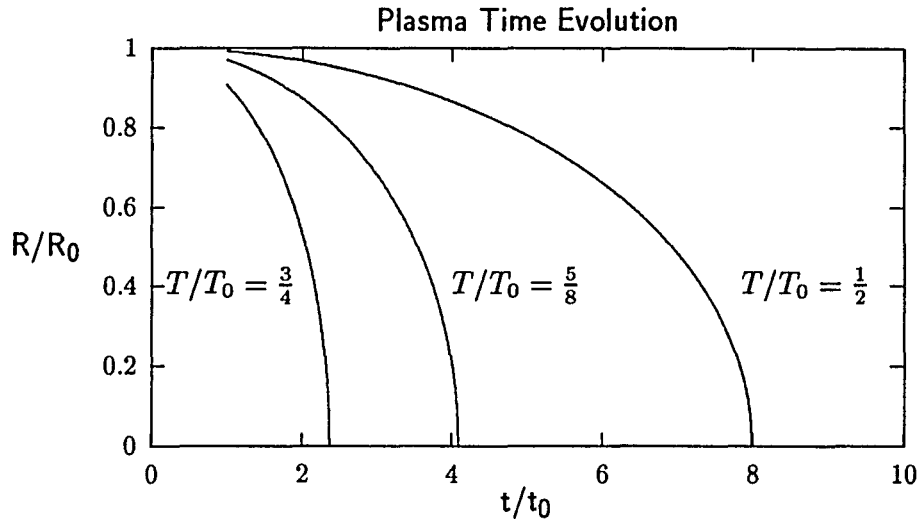

Figure 3.13: Evolution of various isotherms for $a = 1/2$. Isotherms are labeled in units of the initial central temperature.

We are now prepared to discuss a model for J/ψ suppression in a quark gluon plasma. We assume the binding forces for a $c\bar{c}$-pair disappear for the time the pair is in a region of plasma with a temperature greater than some T_ψ. The probability of forming a J/ψ is then given by Equation 3.60, which we average over all initial velocities and production probabilities. For simplicity, we consider only J/ψ's with p_L of zero. The ratio of J/ψ production with and without plasma formation is the written as

$$S(p_T) = \frac{\int_0^{R_0}\int_0^{\pi} r dr d\vartheta \rho(r)\theta[\tau_\psi - t(r,v,\vartheta)]}{\int_0^{R_0}\int_0^{\pi} r dr d\vartheta \rho(r)}. \tag{3.68}$$

Note that we have rewritten Equation 3.60 using the θ-function with $t(r,v,\vartheta)$ as the time spent in the hot region by a J/ψ with velocity v in the direction ϑ created at point r. We have also defined $\tau_\psi = \gamma t_f^\psi$. The production probability, $\rho(r)$, will be taken to be of the form

$$\rho(r) = C\left[1 - \left(\frac{r}{R_0}\right)^2\right]^b. \tag{3.69}$$

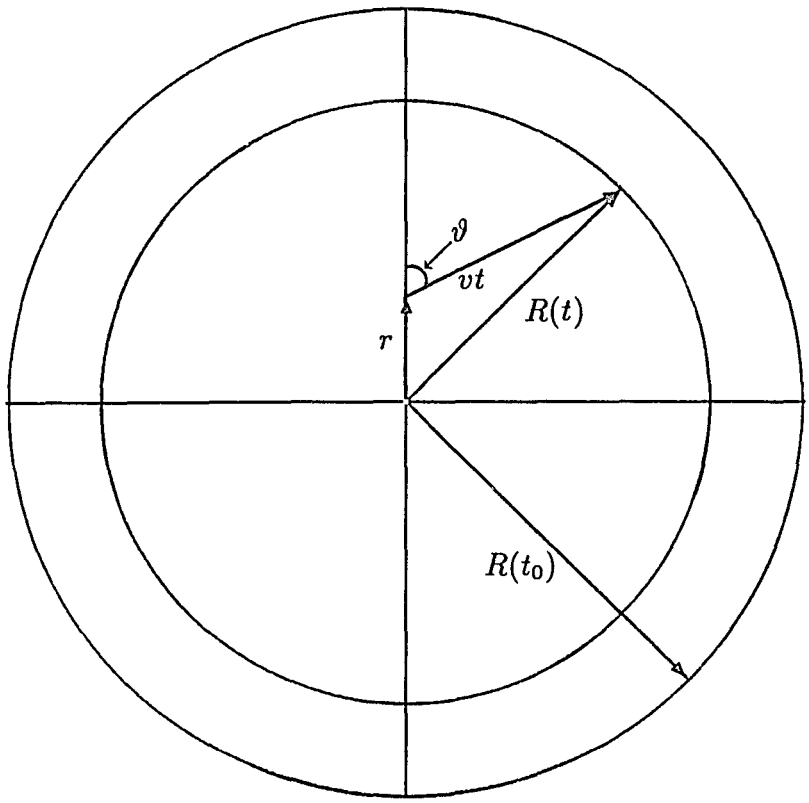

Figure 3.14: Geometry at time, t, when the $c\bar{c}$-pair escapes the deconfining plasma region.

To find the time spent in the hot region, we examine Figure 3.14 and note

$$(r + vt\cos\vartheta)^2 + (vt\sin\vartheta)^2 = R^2(t). \tag{3.70}$$

Performing the square in the first term and using Equation 3.67, we rewrite this as

$$x^2 + 2yx\mu\eta + y^2\eta^2 = (1 - \eta^{\frac{1}{a}}), \tag{3.71}$$

where $x \equiv r/R_0$, $y \equiv vt/R_0$, $\mu \equiv \cos\vartheta$, and $\eta \equiv t/t_m$. Solving this for η yields $t(r, v, \vartheta)$.

A particularly simple approximation is to consider the limit $y \to 0$. This is consistent with our previous assumption that $t_m/R_0 \ll 1$ which justified neglecting any transverse expansion of the plasma. In this limit, $\eta = (1 - x^2)^a$, so the

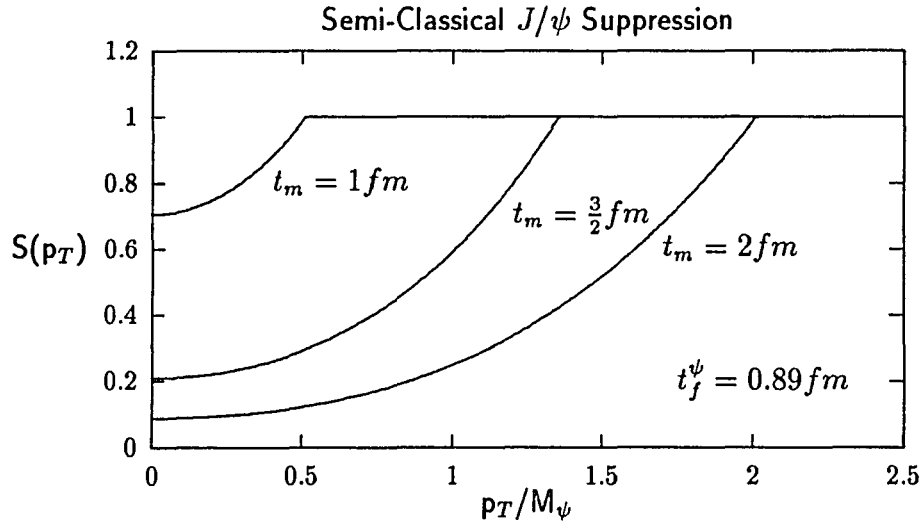

Figure 3.15: J/ψ suppression ratio for various t_m's in the limit $vt_m/R_0 \to 0$.

θ-function requires $\tau_\psi \geq t_m(1-x^2)^a$ or $x \geq (1-(\tau_\psi/t_m)^{1/a})^{1/2} \equiv R(\tau_\psi)/R_0$. Therefore, in Equation 3.68, we simply integrate over all $c\bar{c}$-pairs created outside the critical radius defined by $R(\tau_\psi)$. This yields

$$S(p_T) = \frac{\int_{R(\tau_\psi)}^{R_0} rdr\,(1-r^2/R_0^2)^b}{\int_0^{R_0} rdr\,(1-r^2/R_0^2)^b} = \left[\frac{\gamma t_f^\psi}{t_m}\right]^{\frac{b+1}{a}}, \tag{3.72}$$

where we have used Equation 3.67. Fixing $a = b = 1/2$, we plot this in Figure 3.15 for various values of t_m.

We see that the qualitative features of the NA 38 data are accommodated in this model. However, we have neglected one subtlety, namely, that t_f^ψ must obviously be greater than t_0. Though t_0 is usually taken to be of order a fermi, its exact value is a somewhat free parameter. We will simply assume $t_0 < t_f^\psi$.

3.4 Inclusion of χ_c Contributions

Since, as discussed in Chapter 2, a significant fraction of the J/ψ's are produced from the decay, $\chi_c \rightarrow J/\psi + \gamma$, any realistic model of J/ψ suppression must also include χ_c suppression. This was first examined in [57] where the disappearance of the suppression effect at $p_T \sim M_\psi$ was used to impose restrictions on the lifetimes of different temperature regions in the plasma. We will simply extend the model of the previous section to include χ_c-resonances.

The radiative decay of the χ_c to a J/ψ takes place on a time scale much longer than a fermi, the strong interaction time scale. Therefore, we assume that the J/ψ is formed long after the plasma has disappeared. The effect of this production mechanism on J/ψ suppression is then examined by simply calculating the analogous effect on the χ_c resonance. We generalize Equation 3.68 to

$$S(p_T) = f^\chi(p_T)S^\chi(p_T) + f^\psi(p_T)S^\psi(p_T), \tag{3.73}$$

where $f^{\chi,\psi}(p_T)$ is the fraction of J/ψ's that come from either χ_c-decays or direct J/ψ production. Note that we allow this to vary with p_T, in accordance with the discussion of Chapter 2.

Employing the approximation used in Equation 3.72, we rewrite the above equation as

$$S(p_T) = f^\chi(p_T)\left[\frac{\gamma t_f^\chi}{t_m^\chi}\right]^{\frac{b+1}{a}} + f^\psi(p_T)\left[\frac{\gamma t_f^\psi}{t_m^\psi}\right]^{\frac{b+1}{a}}. \tag{3.74}$$

We then examine Table 3.3 and make two observations:

1. t_f^χ=2.01 fm is much larger than t_f^ψ=0.89 fm,
2. the dimensions of the χ_c are much bigger than for the J/ψ.

We assume from the second statement that less screening, hence a lower temperature should be required to dissolve the χ_c-resonance. We shall assume $T_\psi/T_\chi \sim$

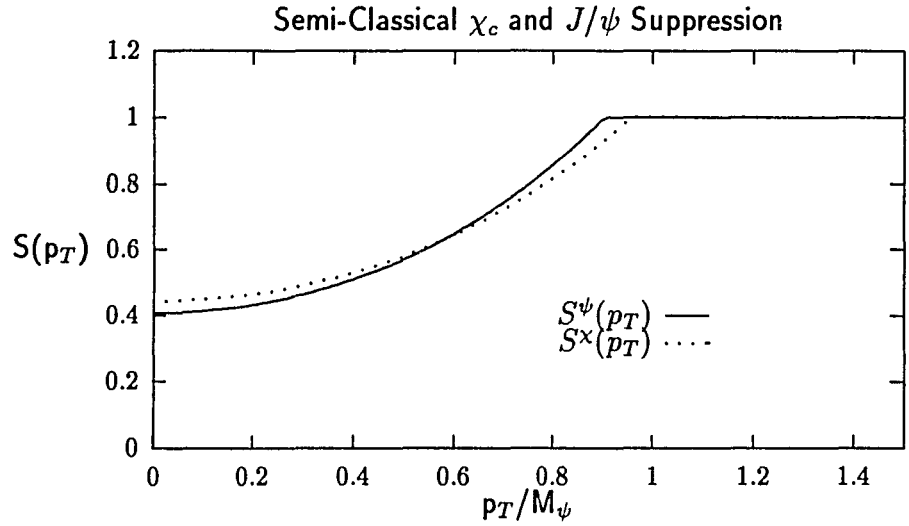

Figure 3.16: Semiclassical suppression as given by Equation 3.74 with $f^{\psi}(p_T)$=1 and $f^{\chi}(p_T)$=1.

$1.2 - 1.3$, as indicated by the previously mentioned estimates. This implies

$$\frac{(t_f^{\chi}/t_m^{\chi})}{(t_f^{\psi}/t_m^{\psi})} = \left(\frac{t_f^{\chi}}{t_f^{\psi}}\right)\left(\frac{T_{\chi}}{T_{\psi}}\right)^3 \sim 0.8 - 1.0 \tag{3.75}$$

and therefore, $S^{\chi}(p_T)$ and $S^{\psi}(p_T)$ should behave very similarly. This is demonstrated in Figure 3.16 where we have used $T_{\psi}/T_{\chi} = 1.3$. We have chosen $t_m^{\psi} = 1.2\,fm$, which gives a suppression of about $1/2$ at $p_T = 0$. The slightly weaker momentum dependence in the χ_c case is due to its slightly higher mass. This should not be given any significance since we have ignored any momentum variation due to the final radiative decay. In a more nonrelativistic system (binding energy $\ll$ mass) these would be truly negligible. We also show the evolution of the two critical isotherms in Figure 3.17. The dotted lines correspond to $t < t_f^R$ and do not affect $S(p_T)$. Note that for an oxygen projectile ($R_0 \approx 3fm$), the approximation $t_m^{\chi} \ll R_0$ is somewhat questionable.

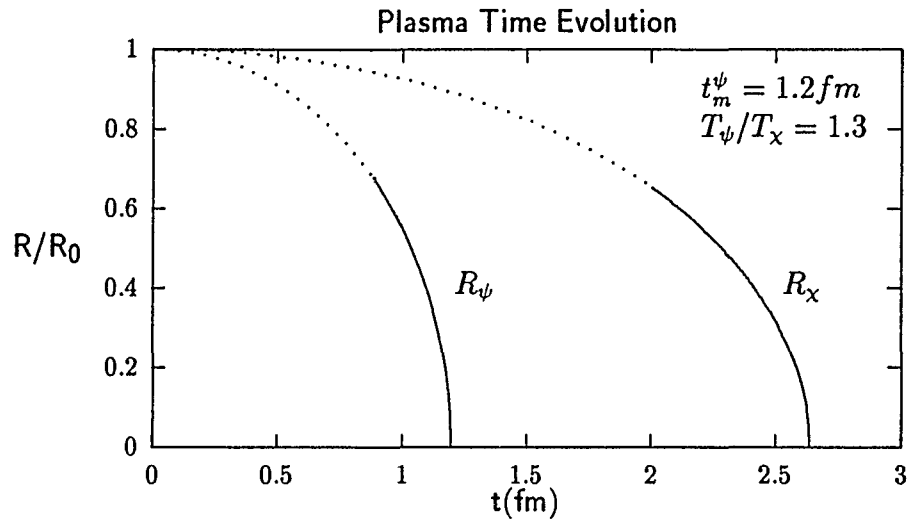

Figure 3.17: Critical isotherm radii as a function of time . Solid lines represent physically relevant regions ($t > t_f^R$).

3.5 Discussion

To replicate the qualitative features of the observed J/ψ suppression's momentum dependence, we required the existence of a plasma region with temperatures of $T_0 \geq T_c$ that persist for 2-3 fm. We may estimate the energy density as the total observed transverse energy per unit rapidity divided by the interaction volume as [60]

$$\epsilon \equiv \frac{< E_T >}{\Delta\eta\, V_0} = \frac{3 < E_T^0 >}{\Delta\eta\, t_0\, (\pi r_0^2 A^{2/3})}\,, \tag{3.76}$$

where $r_0 = 1.2\,fm$ and t_0 is the plasma formation time. Note that we have assumed a central collision and that the total transverse energy is three times the neutral transverse energy. The NA38 group measured $< E_T^0 >= 56.4\,GeV$ and $< E_T^0 >= 84.6\,GeV$ for O-U and S-U collisions respectively [54]. Measured over 2.4 units of rapidity, this yields energy densities of $2.3 - 2.5\,GeV/fm^3$, which corresponds to temperatures of order $T_0 \sim 180 - 190\,MeV$.

Lattice studies predict the critical temperature for quark gluon plasma

formation to be of order $T_c \sim 150 - 200\,MeV$ [61], which correspond to energy densities of $1 - 3\,GeV/fm^3$. We see that the energy densities produced in the NA38 experiments may have been sufficient to create a quark gluon plasma. We may estimate the lifetime of the plasma region as

$$t_m^{\chi} = t_0(T_0/T_{\chi})^3 \approx t_0(T_0/T_c)^3 \sim (0-2)\,t_0\,. \tag{3.77}$$

Since t_0 is of order a fermi, we see that, if $T_c \sim 150\,MeV$, the parameters required to describe the observed suppression in terms of deconfinement are consistent with the NA38 data.

CHAPTER 4

QUANTUM MECHANICAL SUPPRESSION IN ONE DIMENSION

In the previous chapter we presented a model to explain the J/ψ suppression based on the idea of a "resonance formation time". Though we were able to model the NA 38 results somewhat successfully, it was pointed out in Reference [12, 13] that this formation time concept might not have a precise meaning. It was argued that the formation and suppression of heavy quark resonances is a quantum mechanical problem.

In this chapter we will try to determine the best approach to constructing a quantum mechanical suppression model by examining some simple one dimensional examples. We will consider the same physical situation as before. The $c\bar{c}$-pair is first created by a hard QCD process in a small spacetime region of order $1/2m_c$. The pair then encounters a deconfining environment that is above some critical temperature and evolve as free particles for some length of time. When the interquark potential reappears, either by the medium cooling or the $c\bar{c}$-pair escaping the region, we calculate the probability of bound state formation. In the current discussion, we will employ the relatively straightforward rules of quantum mechanics to do this.

In Section 4.1 we will examine the evolution of a narrow wavepacket in relative coordinate space and the resulting bound state suppression. In Section 4.2 we consider a two-particle formalism to see if this will produce any different results. We extend this discussion with a relativistic analysis in Section 4.3 and discuss the best approach for a more realistic model in Section 4.4.

4.1 Relative Wavefunction Analysis

We first examine the quantum mechanical evolution of the heavy quark pair in the center of mass frame. This will be analogous to the work of References [14, 15]. We assume that the result of the hard QCD process is to produce an initial relative wavefunction with $\Delta x \sim 1/2m_c$ where x is the relative coordinate of the two heavy quarks. To model this, we assume the Gaussian form given by

$$\phi(x,0) = C \exp\left[-\frac{1}{2}\left(\frac{x}{a}\right)^2\right], \tag{4.78}$$

where a is determined by imposing the condition $\Delta x \equiv x_{rms} = a/\sqrt{2} = 1/2m_c$. Assuming no plasma formation, we would determine the probability amplitude for producing a particular quarkonium state by projecting the appropriate bound state onto the initial state wavefunction, i.e.

$$A_n(0) = < \chi_n | \phi(0) >, \tag{4.79}$$

where $\chi_n(x)$ is the bound state wavefunction. We will follow the example of Reference [14] and consider a harmonic oscillator form, $V(x) = 1/2\,\mu\,\omega_\psi^2\,x^2$, for the quarkonium potential. The ground state, which we will use to represent the J/ψ, is written as

$$\chi_\psi(x) = N \exp\left[-\frac{1}{2}\left(\frac{x}{r_\psi}\right)^2\right] \tag{4.80}$$

where $r_\psi = 0.5\,fm$ is related to ω_ψ by $\omega_\psi = 1/\mu r_\psi^2$. This, along with the choice $m_c = 2\mu = 1.5\ GeV$, produces a J/ψ mass of 3.1 GeV.

To simulate the effects of the plasma formation, we assume that above some critical temperature, the confining potential disappears and the quarks are allowed to evolve as free particles. After some time, t, the confining potential reappears and we calculate the modified J/ψ formation probability amplitude as

$$A_\psi(t) = < \chi_\psi | \phi(t) > , \tag{4.81}$$

where $\phi(t)$ is the heavy quark wavefunction after it has evolved as a free particle for some time t. The evaluation of Equation 4.81 is most easily performed in momentum space as

$$< \chi_\psi | \phi(t) >= \frac{1}{(2\pi)} \int_{-\infty}^{\infty} \tilde{\chi}^*_\psi(k) \tilde{\phi}(k) \exp[-i\omega_k t] dk \ . \tag{4.82}$$

where the Fourier transforms of the initial and bound states are given by

$$\begin{aligned} \tilde{\phi}(k) &= \tilde{C} \exp\left[-\frac{1}{2}a^2k^2\right] \\ &\text{and} \\ \tilde{\chi}_\psi(k) &= \tilde{N} \exp\left[-\frac{1}{2}r_\psi^2 k^2\right] \end{aligned} \tag{4.83}$$

(see Appendix A for Fourier transform conventions). For now, we will consider the nonrelativistic propagation frequency $\omega_k = k^2/2\mu = k^2/m$. The probability amplitude is then written as

$$A_\psi(t) = \frac{1}{(2\pi)} \int_{-\infty}^{\infty} \left\{ \tilde{N} \exp\left[-\frac{1}{2}r_\psi^2 k^2\right] \right\} \left\{ \tilde{C} \exp\left[-\frac{1}{2}a^2k^2\right] \right\} \exp[-i(t/m)k^2] \, dk \ , \tag{4.84}$$

which becomes

$$A_\psi(t) = \frac{[\tilde{N}\tilde{C}/(\sqrt{2\pi}r_\psi)]}{[(1 + a^2/r_\psi^2) + i\omega_\psi t]^{\frac{1}{2}}} \equiv \frac{D}{[(1 + a^2/r_\psi^2) + i\omega_\psi t]^{\frac{1}{2}}} \ , \tag{4.85}$$

where we have used $\omega_\psi = 1/(\mu r_\psi^2)$.

The survival probability, or the probability of resonance formation normalized to the "no plasma" case, is written as

$$P_s(t) = \frac{|A_\psi(t)|^2}{|A_\psi(0)|^2} = \frac{1}{[1 + \omega_\psi^2 t^2/(1 + a^2/r_\psi^2)^2]^{\frac{1}{2}}} \ . \tag{4.86}$$

We see that this is very different from the classical form,

$$\begin{aligned} P_s(t) &= 1 \quad t < t_f^R \\ &= 0 \quad t > t_f^R, \end{aligned} \tag{4.87}$$

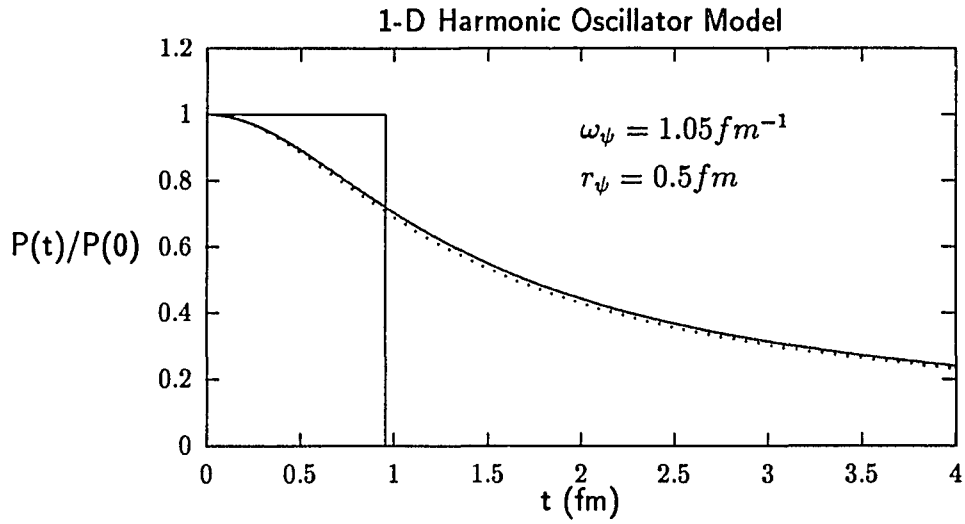

Figure 4.18: Classical vs. quantum mechanical suppression in one dimension. The sharp cutoff in the classical case is at $t_f = 1/\omega_\psi \approx 0.95 fm$. The solid line in the quantum mechanical case is with $a/r_\psi = 1/5$ and the dotted line is with $a/r_\psi = 0$.

given in the previous chapter. For the harmonic oscillator model, the natural choice for the classical formation time is $t_f^R = 1/\omega_\psi$ [14]. A comparison of the two approaches is given in Figure 4.18. We also include the case where $a/r_\psi = 0$. This is the same limit considered in Chapter 2 when discussing different charmonium formation mechanisms. We will see in the next chapter that the smooth behavior in the quantum mechanical model will have a strong effect on the p_T dependence of the J/ψ suppression.

4.2 Two-Particle Wavefunction Analysis

The role of quantum mechanics in explaining the suppression of the J/ψ resonance was first introduced in Reference [12]. The model presented considered separate wavefunctions for the quark and antiquark. Though this two particle formalism is more complicated and requires some additional assumptions, it is possible that it might result in a different survival probability than in the last section. For this

reason, we now examine the two particle formalism in more detail.

We consider a pair of narrow Gaussian wavepackets, each with the form

$$\phi_i(x_i,0) = C\,\exp\left[-\frac{1}{2}\,\frac{x_i^2}{b^2}\right]\,\exp[i\,p_i\,x_i], \tag{4.88}$$

where each wavepacket has some average momentum, p_i. We write the two particle wavefunction in terms of relative ($r \equiv x_1 - x_2$) and center of mass ($R \equiv \frac{1}{2}(x_1 + x_2)$) coordinates as

$$\begin{aligned}\phi(r,R,0) &= \phi_1(x_1,0)\,\phi_2(x_2,0) \\ &= C^2\exp\left[-\frac{R^2}{b^2} - \frac{1}{4}\frac{r^2}{b^2}\right]\,\exp[i(q\,r + s\,R)]\end{aligned} \tag{4.89}$$

where $s \equiv p_1 + p_2$ and $q \equiv \frac{1}{2}(p_1 - p_2)$. We impose the same requirement as before, namely that the relative wavefunction has the property $\Delta r \sim 1/2\,m_c$. This is accomplished by choosing the parameter b such that $\Delta r \equiv r_{rms} = b = 1/2\,m_c$.

We write the final quarkonium wavefunction in the form

$$\psi_f(r,R,0) \equiv \Gamma_p(R)\,\chi_n(r), \tag{4.90}$$

where $\Gamma_p(R) = \exp[i\,p\,R]$ is the free particle wavefunction of the center of mass and $\chi_n(r)$ is the appropriate bound state wavefunction. The probability amplitude, $A(t) \equiv < \psi_f|\phi(t) >$, is then written in momentum space (with $K \equiv k_1 + k_2$ and $k \equiv \frac{1}{2}(k_1 - k_2)$) as

$$\begin{aligned}A(t) &= \frac{1}{(2\pi)^2}\int_{-\infty}^{\infty}\int_{-\infty}^{\infty} dk\,dK\,\tilde{\Gamma}_p^*(K)\,\tilde{\chi}_n^*(k)\,\tilde{\phi}(k,K) \\ &\times \exp\left[-i(\frac{k^2}{2\mu} + \frac{K^2}{2M})\,t\right]\end{aligned} \tag{4.91}$$

where

$$\tilde{\phi}(k,K) = \tilde{C}^2\,\exp\left[-\frac{1}{4}b^2(K-s)^2\right]\,\exp[-b^2(k-q)^2] \tag{4.92}$$

is the Fourier transform of the initial state and

$$\tilde{\Gamma}_p(K)\,\tilde{\chi}_n(k) = (2\pi)\,\delta(p-K)\,\tilde{\chi}_n(k) \tag{4.93}$$

is the Fourier transform of the final quarkonium state. Here, we have used $M = 2m$ and $\mu = m/2$. We introduce the notation

$$A(t) \equiv g(s,p)\, h(q,t) \exp\left[-i\,\frac{p^2}{2M}\,t\right], \tag{4.94}$$

with

$$h(q,t) = \frac{1}{2\pi}\int_{-\infty}^{\infty} dk\, \tilde{\chi}_n^*(k) \exp\left[-b^2(k-q)^2 - i\,\frac{k^2}{2\mu}\,t\right] \tag{4.95}$$

and

$$g(s,p) = \tilde{C}^2 \exp\left[-\frac{1}{4}b^2(p-s)^2\right], \tag{4.96}$$

where we have performed the trivial K integration. Note that we have explicitly separated the overall phase and written $g(s,p)$ independent of t. The interesting time dependence is contained in the function $h(q,t)$.

We shall continue to model the J/ψ as the ground state of a harmonic oscillator with the Fourier transform

$$\tilde{\chi}_\psi(k) = \tilde{N} \exp\left[-\frac{1}{2}\,r_\psi^2\,k^2\right]. \tag{4.97}$$

Inserting this into Equation 4.95 yields the expression

$$\begin{aligned} h(q,t) &= \frac{\tilde{N}/(\sqrt{2\pi}\,r_\psi)}{[(1+2b^2/r_\psi^2) + i\omega_\psi\, t]^{\frac{1}{2}}} \\ &\times \exp\left[-b^2q^2\left\{1 - \left(\frac{2b^2}{r_\psi^2}\right)\frac{[(1+2b^2/r_\psi^2) - i\omega_\psi\, t]}{[(1+2b^2/r_\psi^2)^2 + \omega_\psi^2 t^2]}\right\}\right] \end{aligned} \tag{4.98}$$

where we have again used $\omega_\psi = 1/(\mu r_\psi^2)$. The resulting probability density becomes

$$\begin{aligned} P(p_1,p_2,p,t) &= |g(s,p)|^2 \frac{|\tilde{N}|^2/(2\pi\, r_\psi^2)}{[(1+2b^2/r_\psi^2)^2 + {\omega_\psi}^2 t^2]^{\frac{1}{2}}} \\ &\times \exp\left[-2b^2q^2\left\{1 - \frac{(2b^2/r_\psi^2)}{(1+2b^2/r_\psi^2)}[(1+2b^2/r_\psi^2)^2 + \omega_\psi^2 t^2]\right\}\right]. \end{aligned} \tag{4.99}$$

The two particle formalism has introduced an additional time dependence contained in the exponential that is absent in the relative wavefunction method.

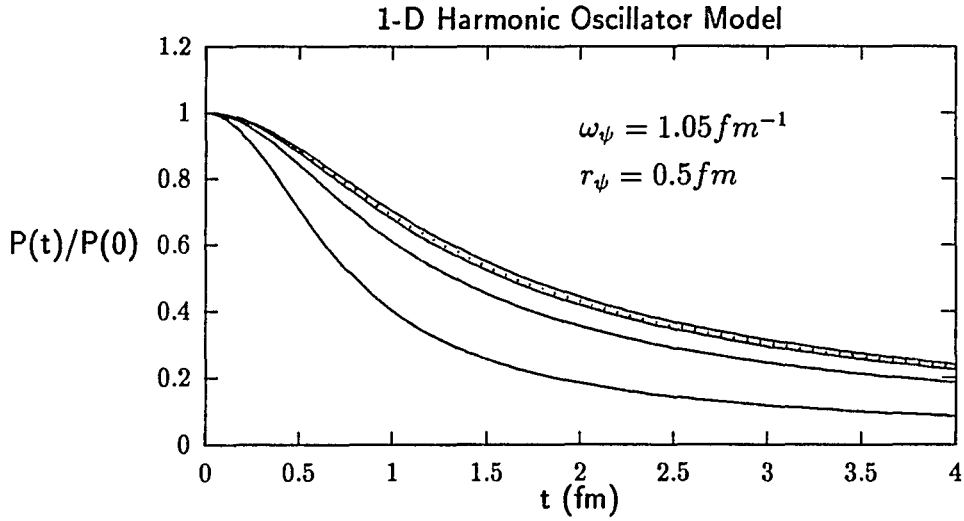

Figure 4.19: Survival probability using two particle wavefunction analysis as given by Equation 4.100. The solid lines from top to bottom are for $q/m = 0, 2, 4$, and 8. We also show for comparison the result from the previous section for a relative wavefunction of vanishing width.

We must now decide how to define the survival probability. The straightforward definition, $P_s(t) \equiv |A(t)|^2/|A(0)|^2$, previously used yields

$$P_s(t) = \frac{\exp\left[-2b^2q^2(2b^2/r_\psi^2)/(1+2b^2/r_\psi^2)^3\left\{\omega_\psi^2 t^2/(1+\omega_\psi^2 t^2/(1+2b^2/r_\psi^2)^2)\right\}\right]}{[1+\omega_\psi^2 t^2/(1+2b^2/r_\psi^2)^2]^{\frac{1}{2}}} \tag{4.100}$$

and is plotted in Figure 4.19. We see that, for large q^2, the survival probability can be significantly different than in the relative wavefunction analysis. However, this simple definition only considers a $c\bar{c}$-pair with a *particular* q^2.

To correctly model the observed J/ψ suppression, we must take into account all possible momenta of the $c\bar{c}$-pairs resulting from the QCD process. Defining $f(p_1, p_2)$ as this momentum distribution, we define the *effective* survival probability as

$$P_s^{eff}(t) = \frac{\int_{-\infty}^{\infty}\int_{-\infty}^{\infty} dp_1\, dp_2\, f(p_1,p_2)\, P(p_1,p_2,p,t)}{\int_{-\infty}^{\infty}\int_{-\infty}^{\infty} dp_1\, dp_2\, f(p_1,p_2)\, P(p_1,p_2,p,0)} . \tag{4.101}$$

To examine the effect of this momentum averaging, we consider a sample distribution of the form $f(p_1, p_2) = constant$. This loosely models a smooth distribution about $p_1, p_2 = 0$. The survival probability becomes

$$\begin{aligned} P_s^{eff}(t) &= \frac{\int_{-\infty}^{\infty}\int_{-\infty}^{\infty} ds\, dq\, |g(s,p)|^2\, |h(q,t)|^2}{\int_{-\infty}^{\infty}\int_{-\infty}^{\infty} ds\, dq\, |g(s,p)|^2\, |h(q,0)|^2} \\ &= \frac{\int_{-\infty}^{\infty} dq\, |h(q,t)|^2}{\int_{-\infty}^{\infty} dq\, |h(q,0)|^2} . \end{aligned} \tag{4.102}$$

Looking at the exponential factor in Equation 4.100, we define

$$g(t) = \left[1 - \left(\frac{2b^2}{r_\psi^2}\right)^2 \frac{(1 + 2b^2/r_\psi^2)}{[(1 + 2b^2/r_\psi^2)^2 + \omega_\psi^2 t^2]}\right] \tag{4.103}$$

to write

$$\begin{aligned} P_s^{eff}(t) &= \frac{1}{[1 + \omega_\psi^2 t^2/(1 + (2b^2/r_\psi^2)^2]^{\frac{1}{2}}} \frac{\int_{-\infty}^{\infty} \exp[-2b^2\, g(t)\, q^2]\, dq}{\int_{-\infty}^{\infty} \exp[-2b^2\, g(0)\, q^2]\, dq} \\ &= \frac{1}{[1 + \omega_\psi^2 t^2/(1 + (2b^2/r_\psi^2)^2]^{\frac{1}{2}}} \left[\frac{g(0)}{g(t)}\right]^{\frac{1}{2}} . \end{aligned} \tag{4.104}$$

We plot this in Figure 4.20 along with the results of the previous section for vanishing initial relative wavefunction width. We see that, for the reasonable parameters chosen, the relative wavefunction method and the momentum averaged two particle wavefunction method produce almost identical results. This is due to the fact that the exponential in Equation 4.100 strongly weights $q \approx 0$, for which

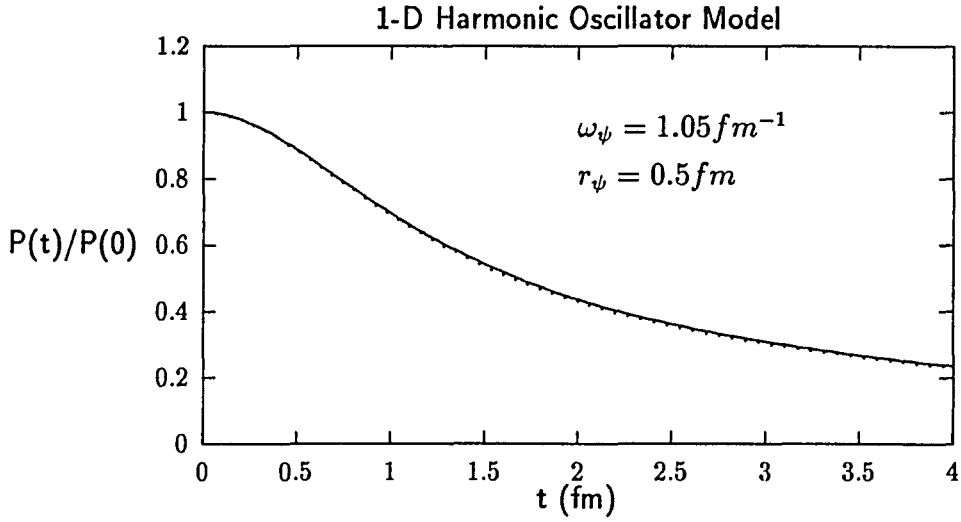

Figure 4.20: Comparison of two particle effective survival probability with relative wavefunction method with $a/r_\psi = 0$.

the survival probability is similar to that derived using the relative wavefunction method. Though the momentum distribution used is unrealistic, any distribution that decreases with q^2 will only enhance this result.

4.3 Relativistic Treatment

The hard QCD interaction forming a $c\bar{c}$-pair is a very local process that takes place in a space-time interval of order $\sim 1/2m_c$. Therefore, any quantum mechanical analysis of this must be able to handle an initial wavefunction with momentum components of order $\sim m_c$. This necessitates a relativistic treatment [62], which we provide in this chapter. Though a complete relativistic analysis would employ quantum field theory to account for particle production, we shall follow the example of Reference [62] and extend the single particle relativistic quantum mechanics formalism as far as possible. In doing so, we will ignore any particle production beyond that which originally created the heavy quark pair. For our purposes, the

relativistic single particle formalism works rather well since we are assuming that the $c\bar{c}$-pair evolve as free particles during the plasma phase. In Section 4.3.1, we review the Klein-Gordon formalism of relativistic quantum mechanics and relate this to ordinary Schrödinger wavefunction analysis in Section 4.3.2. We use this in Section 4.3.3 to formulate a simple one-dimensional suppression model. In Section 4.3.4 we examine the limiting case where the bound state is described by a nonrelativistic wavefunction and discuss the results.

4.3.1 Relativistic Wave Packets

We would like to repeat the two-particle analysis of the last section using relativistic quantum mechanics. To do this, we must first decide what sort of wavepacket to use to represent the initial quark or antiquark of momentum, p. For simplicity, we will consider spin-0 wavefunctions that obey the Klein-Gordon equation [21],

$$(\Box + m^2)\,\phi(x) = 0\,, \tag{4.105}$$

with solutions of the form

$$\phi(x,t) = \frac{1}{2\pi}\int_{-\infty}^{\infty}\frac{dk}{2\omega_{\rm k}}\left\{a(k)\,\exp[-ik\cdot x] + b(k)\,\exp[ik\cdot x]\right\}\,. \tag{4.106}$$

Note that we now use the relativistic expression, $k_0 = \omega_{\rm k} = (k^2+m^2)^{\frac{1}{2}}$. Following the example of [63], we will examine the evolution and transformation of a specific wavefunction defined by

$$\begin{aligned}\phi(x,0) &= \frac{N}{2\pi}\int_{-\infty}^{\infty}\exp[-a\omega_{\rm k}]\,\exp[ikx]\frac{dk}{2\omega_{\rm k}} \\ &= \frac{N}{2\pi}K_0[m\sqrt{x^2+a^2}]\,,\end{aligned} \tag{4.107}$$

where $K_0(x)$ is the modified Bessel function of the second kind of order zero. Since this wavepacket consists purely of positive frequencies, we will interpret

$$P(x,t) = \frac{1}{2}\left[\phi^*\left(i\overleftrightarrow{\partial_t}\right)\phi\right] \tag{4.108}$$

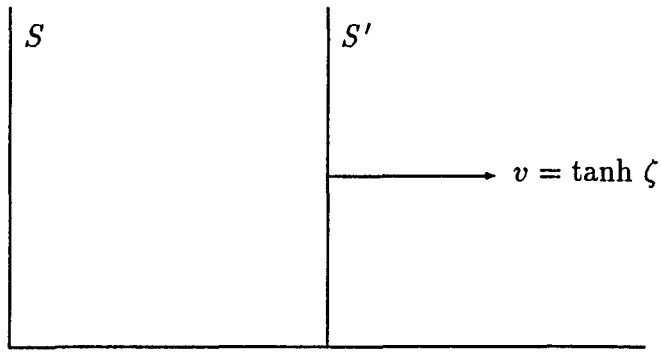

Figure 4.21: Lorentz frame S' moving with velocity, v, with respect to frame S. The Lorentz angle, ζ, is defined by $v = \tanh\zeta$.

as a probability density.

To generate a wavepacket of non-zero momentum, we consider the two Lorentz frames shown in Figure 4.21, where the wavepacket defined by Equation 4.107 is at rest in S'. Between these two frames, four vectors[1] transform as [21]

$$x'_\mu = \Lambda^\nu_\mu x_\nu \ , \tag{4.109}$$

where

$$\Lambda^\nu_\mu \equiv \begin{pmatrix} \cosh\zeta & -\sinh\zeta \\ -\sinh\zeta & \cosh\zeta \end{pmatrix} . \tag{4.110}$$

In particular, the four vector, $k_\mu \equiv (\omega_k, k)$, transforms as $\omega_{k'} = c\omega_k - sk$ and $k' = ck - s\omega_k$, where we have used the shorthand notation $c(s) \equiv \cosh(\sinh)\zeta$. With this, we see that the wavefunction that is a rest in S' becomes

$$\begin{aligned} \phi(x,t) &= \int_{-\infty}^{\infty} \exp[-a\omega_{k'}] \exp[-ik'\cdot x'] \frac{dk'}{2\omega_{k'}} \\ &= \int_{-\infty}^{\infty} \exp[-a(c\omega_k - sk)] \exp[-ik\cdot x] \frac{dk}{2\omega_k} \\ &= \frac{N}{2\pi} K_0[m\sqrt{(x-isa)^2 + (ca+it)^2}] \end{aligned} \tag{4.111}$$

[1]In one spatial dimension, these would really be "two vectors". We will continue to use the standard terminology, "four vector" with the understanding that it has spacial dimensions + 1 components.

in the frame S. Here, we have used the fact that $k \cdot x$ and $dk/\omega_{\mathbf{k}}$ are invariant quantities.

The wavefunction moves with velocity v and evolves in free space according to relativistic quantum mechanics. We will employ a pair of these wavepackets in the same fashion that we used tha Gaussian packets in the previous section.

4.3.2 Relationship to Schrödinger-like Wavefunctions

We would like to project out a particular final state in a manner similar to that used in Section 4.2. Since the charmonium bound states are defined using a non-relativistic Schrödinger wavefunction, we must relate the Klein-Gordon wavefunction to its Schrödinger counterpart. We will accomplish this by employing the Feshbach-Villars formalism and using a transformation similar to the Foldy-Wouthuysen transformation [64, 65].

We want to rewrite the Klein-Gordon wavefunction in such a way that we can write the probability density in the form $P \sim |\psi|^2$. We begin by defining the two component wavefunction

$$\mathbf{\Phi} \equiv \begin{bmatrix} \theta \\ \chi \end{bmatrix} \equiv \frac{1}{2} \begin{bmatrix} \phi + i/m\, \dot{\phi} \\ \phi - i/m\, \dot{\phi} \end{bmatrix} \tag{4.112}$$

governed by the equation

$$i\partial_t \mathbf{\Phi} = \mathbf{H_0}\, \mathbf{\Phi} \tag{4.113}$$

where the free particle Hamiltonian is

$$\mathbf{H_o} = - \begin{bmatrix} 1 & 1 \\ -1 & -1 \end{bmatrix} \frac{\nabla^2}{2m} + \begin{bmatrix} 1 & 0 \\ 0 & -1 \end{bmatrix} m\,. \tag{4.114}$$

Here have we essentially rewritten the Klein-Gordon equation given in Equation 4.105, which is second order in time, as the *two* first order equations shown

in Equation 4.113. In this notation, Equation 4.108 becomes

$$P(x,t) = m\,\Phi^{\dagger}\begin{bmatrix} 1 & 0 \\ 0 & -1 \end{bmatrix}\Phi = m[\theta^{*}\,\theta - \chi^{*}\,\chi] \tag{4.115}$$

where[2] $\Phi^{\dagger} \equiv (\theta^{*}, \chi^{*})$. Though this appears closer to the form we are interested in, positive and negative frequencies are still mixed in both θ and χ. This is easily seen by examining the explicit form,

$$\begin{aligned} \frac{\theta}{\chi} &= \frac{1}{2}\frac{1}{2\pi}\int_{-\infty}^{\infty}\left\{a(k)\left(1 \pm \frac{\omega_{\mathrm{k}}}{m}\right)\exp[-ik\cdot x]\right. \\ &+ \left. b(k)\left(1 \mp \frac{\omega_{\mathrm{k}}}{m}\right)\exp[ik\cdot x]\right\}\frac{dk}{2\omega_{\mathrm{k}}}\,, \end{aligned} \tag{4.116}$$

found by inserting Equation 4.106 into Equation 4.112.

We use a transformation, $\Phi' = e^{iS}\,\Phi$, similar to the Foldy-Wouthuysen transformation [65] of the form

$$S = \begin{bmatrix} 0 & 1 \\ 1 & 0 \end{bmatrix}\Theta(p) \tag{4.117}$$

where

$$\tanh[2i\,\Theta(p)] = \frac{p^{2}}{2m^{2}+p^{2}}\,, \tag{4.118}$$

to completely separate the positive and negative energy components. The explicit form is

$$e^{iS} = \begin{bmatrix} \cos\Theta(p) & i\,\sin\Theta(p) \\ i\,\sin\Theta(p) & \cos\Theta(p) \end{bmatrix} \tag{4.119}$$

where

$$\frac{\cos}{i\,\sin}\Theta(p) = \frac{1}{\sqrt{4mE}}(E \pm m)\,. \tag{4.120}$$

The transformed wave equation,

$$i\partial_{t}\,\Theta' = \mathbf{H}_{0}'\Theta' \tag{4.121}$$

[2]This is *not* the notation of Reference[64].

where

$$\mathbf{H}_0' = \begin{bmatrix} 1 & 0 \\ 0 & -1 \end{bmatrix} , \tag{4.122}$$

now acts on the wavefunction written as

$$\Theta'(x,t) = \frac{1}{2\sqrt{m}}\frac{1}{2\pi}\begin{bmatrix} \int_{-\infty}^{\infty} a(k)\,\exp[-ik\cdot x]\,dk/\sqrt{\omega_k} \\ \int_{-\infty}^{\infty} b(k)\,\exp[ik\cdot x]\,dk/\sqrt{\omega_k} \end{bmatrix} . \tag{4.123}$$

We then write

$$\begin{aligned} P(x,t) &= m\Theta'^{*}\begin{bmatrix} 1 & 0 \\ 0 & -1 \end{bmatrix}\Theta' \\ &= \frac{1}{4}\frac{1}{(2\pi)^2}\int_{-\infty}^{\infty}\int_{-\infty}^{\infty}[a^*(k)\,a(k')\,\exp[-i(k'-k)\cdot x] \\ &+ [b^*(k)\,b(k')\,\exp[i(k'-k)\cdot x]\frac{dk}{\sqrt{\omega_k}}\frac{dk'}{\sqrt{\omega_{k'}}} \end{aligned} \tag{4.124}$$

for the probability density.

From this analysis, we see that for a Klein-Gordon wavepacket of purely positive frequencies,

$$\phi(x,t) \sim \int_{-\infty}^{\infty} a(k)\,\exp[-ik\cdot x]\frac{dk}{2\omega_k} , \tag{4.125}$$

an equivalent "Schrödinger-like" wavefunction may be written in the form

$$\phi_S(x,t) \sim \int_{-\infty}^{\infty} a(k)\exp[-ik\cdot x]\frac{dk}{\sqrt{\omega_k}} , \tag{4.126}$$

with a probability density $P(x,t) \sim |\phi_S(x,t)|^2$. This is essentially what was used in Reference [62]. There, Schrödinger wavefunctions were used with the modification that the non-relativistic free space eigenvalues, $\omega_k^{nr} = k^2/2m$, were replaced by the relativistic ones, $\omega_k^{rel} = (k^2+m^2)^{\frac{1}{2}}$.

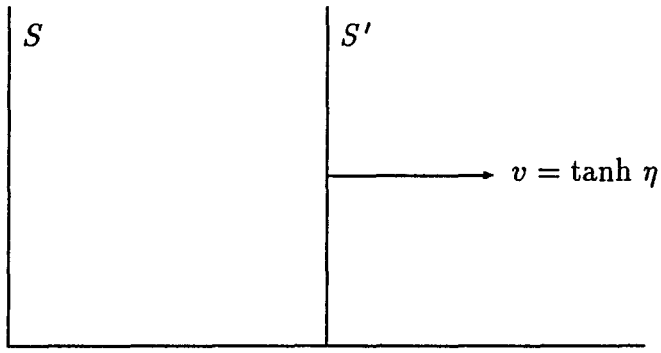

Figure 4.22: J/ψ rest frame, S, and lab frame, S'.

4.3.3 Bound State Formation and Suppression

We are now in a position to model the charmonium formation and suppression. We consider the same model as before, namely, a pair of narrow wavepackets is formed and allowed to evolve in free space for some time, t. Then the appropriate bound state is projected onto the evolved wavefunction pair.

Since the charmonium bound states are described by non-relativistic quantum mechanics, it makes most sense to work in the center of mass frame of the $c\bar{c}$-pair. We therefore consider the two frames shown if Figure 4.22. We take S to be the rest frame of the J/ψ ($c\bar{c}$ center of mass) and S' to be the lab frame moving with velocity , $v = \tanh\eta$, with respect to the J/ψ. Remembering that Lorentz angles add, the "Schrödinger" wavefunction for an initial quark of momentum $p_i \equiv m\sinh\zeta_i$ in the lab frame becomes

$$\phi_{p_i}(x,t) = \frac{N}{2\pi}\int_{-\infty}^{\infty}\exp[-a(c_{\zeta_i+\eta}\omega_k - s_{\zeta_i+\eta}k)]\exp[-ik\cdot x]\frac{dk}{\sqrt{\omega_k}} \qquad (4.127)$$

in frame S. We shall consider $a \approx 0.67/m$, which yields $\Delta k \equiv < k^2 >^{\frac{1}{2}} = m$. The final state wavefunction is defined in the $c\bar{c}$ center of mass frame as $\lim_{p\to 0} e^{ipR}\chi_n(r)$ where r and R are defined as before. We shall therefore calculate the probability

amplitude, $A(p,t)$, and then consider the limit $p \to 0$. This becomes

$$\begin{aligned} A_\psi(p,t) &= \int_{-\infty}^{\infty}\int_{-\infty}^{\infty} dr\, dR\, \{\exp[-ipR]\, \chi_\psi^*(r)\} \\ &\times \frac{N^2}{(2\pi)^2}\int_{-\infty}^{\infty}\int_{-\infty}^{\infty} \exp[i(kr+KR)]\, \exp[-i(\omega_{k_1}+\omega_{k_2})t]\frac{dk\, dK}{\sqrt{\omega_{k_1}\omega_{k_2}}} \\ &\times \exp[-a(c_{\zeta_1+\eta}\omega_{k_1} - s_{\zeta_1+\eta}k_1)]\, \exp[-a(c_{\zeta_2+\eta}\omega_{k_2} - s_{\zeta_2+\eta}k_2)]\,, \end{aligned} \tag{4.128}$$

where we have again changed the variables of integration to $k = \frac{1}{2}(k_1 - k_2)$ and $K = k_1 + k_2$. Performing the R and K integrations yields

$$\begin{aligned} A_\psi(p,t) &= \frac{N^2}{(2\pi)}\int_{-\infty}^{\infty} [\exp[-a(c_{\zeta_1+\eta}\omega_+ - s_{\zeta_1+\eta}k_+)]\, \exp[-a(c_{\zeta_2+\eta}\omega_- - s_{\zeta_2+\eta}k_-)] \\ &\times \exp[-i(\omega_+ + \omega_-)t]\, \tilde{\chi}_\psi^*(k)\, \frac{dk}{\sqrt{\omega_+\omega_-}}\,, \end{aligned} \tag{4.129}$$

where we have defined $k_\pm = \frac{1}{2}p \pm k$ and $\tilde{\chi}_\psi(k)$ is the Fourier transform of the bound state as before. We therefore find

$$\begin{aligned} A_\psi(p,t) &= \lim_{p\to 0} A(p,t) \\ &= \frac{N^2}{(2\pi)}\int_{-\infty}^{\infty} \exp[-a(c_{\zeta_1+\eta} + c_{\zeta_2+\eta})\omega_k]\, \exp[a(s_{\zeta_1+\eta} - s_{\zeta_2+\eta})k] \\ &\times \tilde{\chi}_\psi^*(k)\, \exp[-i(2\omega_k)t]\, \frac{dk}{\omega_k} \end{aligned} \tag{4.130}$$

for the probability amplitude of forming a J/ψ in its own rest frame.

We shall define the J/ψ wavefunction in terms of the momentum space function, $\tilde{\chi}(k) = C\exp[-\beta(\omega_k/m)]$, where we assume $\beta \gg 1$. In coordinate space, this becomes

$$\begin{aligned} \chi_\psi(r) &= \frac{C}{2\pi}\int_{-\infty}^{\infty} \exp\left[-\beta\frac{\omega_k}{m}\right] \exp[ikr]\, dk \\ &= \frac{C\beta}{\pi m}\frac{K_1[\sqrt{\beta^2 + (rm)^2}]}{\sqrt{\beta^2 + (rm^2}} \\ &\underset{\beta\gg 1}{\longrightarrow} \frac{C\beta}{\pi m}\frac{\exp[-\sqrt{\beta^2+(rm)^2}]}{[2\pi\sqrt{\beta^2+(rm)^2}]^{\frac{1}{2}}} \\ &\approx A\exp\left[-\frac{1}{2\beta}(rm)^2\right]\,. \end{aligned} \tag{4.131}$$

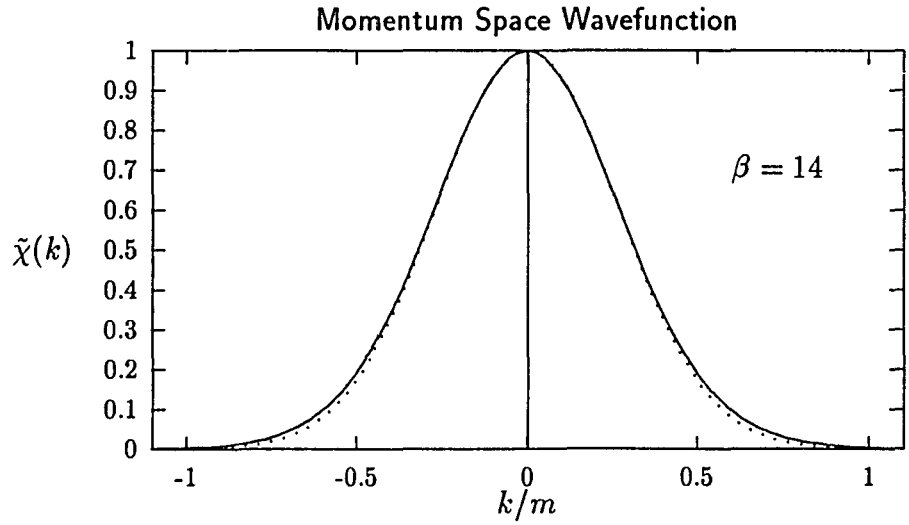

Figure 4.23: Comparison of $\tilde{\chi}_\psi(k) = C\ \exp[-\beta(\omega_k/m)]$ (solid) and harmonic oscillator form, $\tilde{\chi}(k) = A\ \exp[-(\beta/2)(k^2/m^2)]$ (dotted).

We see that, for β sufficiently large, this closely resembles a harmonic oscillator. In this limit, we may relate β to the previously defined r_ψ as $\beta \equiv r_\psi^2 m^2$. Choosing the parameters $r_\psi = 0.5\,fm$ and $m = 1.5\,GeV$, implies $\beta \approx 14 \gg 1$. Comparing this form for $\tilde{\chi}_\psi(k)$ and the harmonic oscillator in Figure 4.23, we see that, with $\beta \approx 14$, $\tilde{\chi}_\psi(k)$ closely represents the harmonic oscillator used in our non-relativistic analysis.

Though we may now insert Equation 4.131 into Equation 4.130 to write the probability amplitude analytically as

$$A(t) = \frac{CN^2}{2\pi} K_0[m\sqrt{[a(c_{\zeta_1+\eta} + c_{\zeta_2+\eta}) + (\beta/m) + 2it]^2 - a^2(s_{\zeta_1+\eta} - s_{\zeta_2+\eta})^2}]\,, \tag{4.132}$$

it is instructive to examine the following approximation. The non-relativistic character of the bound state weights the momentum integral in Equation 4.130 such that the major contributions come from the region $|k| \ll m$. Therefore, we consider the approximation where we evaluate the integral with $\omega_k \equiv (k^2 + m^2)^{\frac{1}{2}} \approx k^2/2m$. In this approximation, the leading term in Equation 4.130 becomes the simple

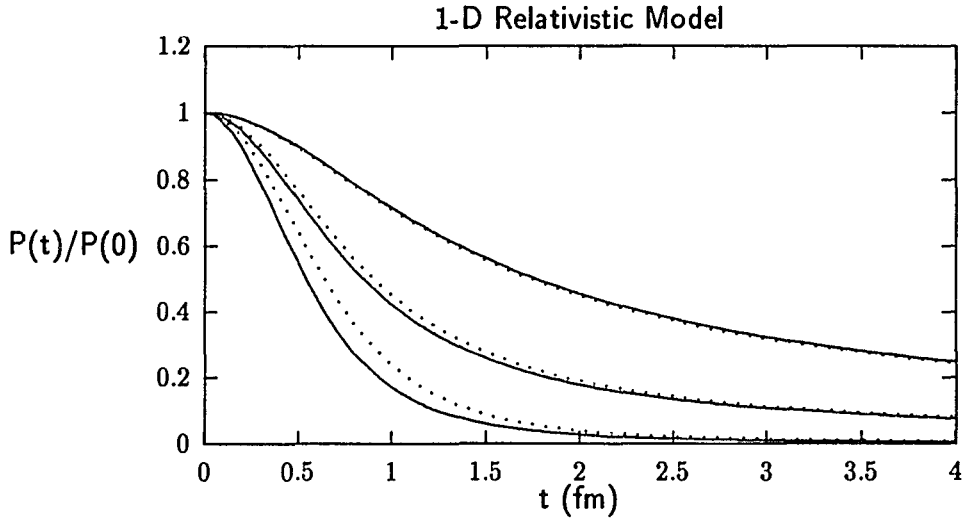

Figure 4.24: Exact (solid) versus non-relativistic approximation (dotted) survival probabilities for $q/m = 0, 4$, and 8. We have set $ma = 0.67$.

Gaussian integral

$$\begin{aligned} A(t) &\approx \frac{CN^2}{2\pi} \exp[-m\{a(c_{\zeta_1+\eta} + c_{\zeta_2+\eta}) + \beta/m + 2it\}] \\ &\times \int_{-\infty}^{\infty} \exp\left[-\{a(c_{\zeta_1+\eta} + c_{\zeta_2+\eta}) + \beta/m + 2it\}\frac{k^2}{2m} + a(s_{\zeta_1+\eta} - s_{\zeta 2+\eta})k\right] dk \\ &= \frac{CN^2}{\sqrt{2\pi}} \exp[-m\{a(c_{\zeta_1+\eta} + c_{\zeta_2+\eta}) + \beta/m + 2it\}] \end{aligned}$$

$$\times \exp\left[\frac{m^2a^2(s_{\zeta_1+\eta} - s_{\zeta_2+\eta})^2}{2m\{a(c_{\zeta_1+\eta} + c_{\zeta_2+\eta}) + \beta/m + 2it\}}\right] \frac{1}{[m\{a(c_{\zeta_1+\eta} + c_{\zeta_2+\eta}) + \beta/m + 2it\}]^{\frac{1}{2}}}. \quad (4.133)$$

The resulting survival probability and that from the exact solution given by Equation 4.132 are plotted in Figure 4.24 for different $q = \frac{1}{2}(p_1 - p_2)$, where we have fixed $p_1 = -p_2$ and $\eta = 0$. We see that including only non-relativistic propagation frequencies when calculating the survival probabilities works rather well, at least for small q.

Previously, we noted that to correctly model the J/ψ survival probability, we must average over all initial momenta. We numerically evaluate the *effective*

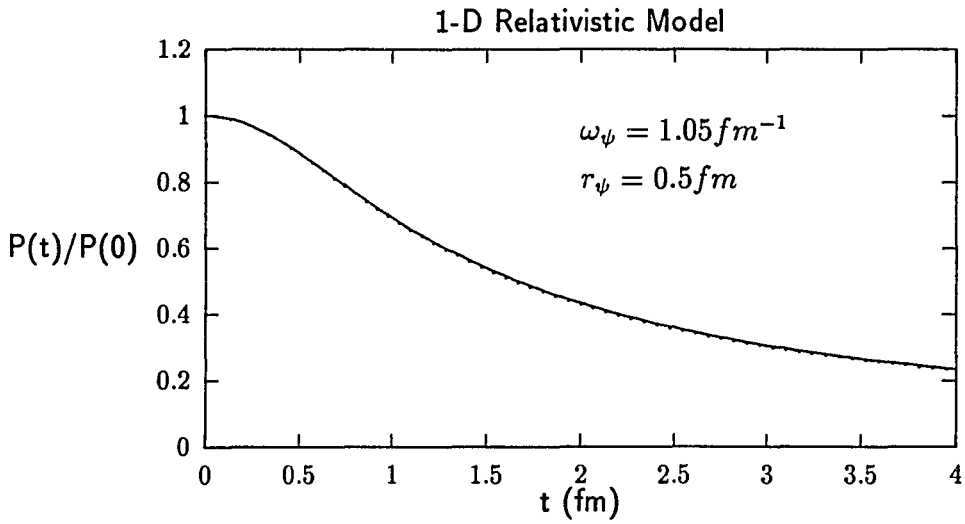

Figure 4.25: Comparison of two particle relativistic effective survival probability (solid line) with non-relativistic relative wavefunction method with $a/r_\psi = 0$ (dotted line).

survival probability defined in Equation 4.101 using the relativistic amplitude given by Equation 4.132 and show the results in Figure 4.25. Here, we have again used $f(p_1, p_2) = constant$. On the same graph, we have also plotted the survival probability calculated using a non-relativistic relative wavefunction of vanishing width. We note that the results are almost identical. We also point out that, if the non-relativistic approximation given by Equation 4.133 was used instead of Equation 4.132, a plot identical to Figure 4.25 would be produced.

4.4 Discussion

In this chapter, we have examined various one-dimensional examples to help gain some intuitive understanding for building a quantum mechanical model of the J/ψ suppression. We examined a non-relativistic suppression model employing a single relative initial wavefunction and then considered two-particle non-relativistic and relativistic initial wavefunctions. We found that the wide nature of the J/ψ bound

state in relation to an initial wavefunction resulted in the fact that form of the *final* state tended to dominate the behavior of the survival probability. In fact, we found that, when using either a relative initial wavefunction or a non-relativistic two particle initial wavefunction with small relative momentum, we obtained similar results for the survival probability. The results did differ somewhat for the two particle model when we considered large relative momenta. However, when we averaged over all initial momenta to calculate an effective survival probability, contributions from high relative momenta were minimal, resulting in almost identical results for the two models. We also noted that a relativistic formalism was required to correctly describe the evolution for the narrow wavepackets under consideration. However, we found that the wide J/ψ bound state (and hence, narrow in momentum space) tended to damp out any relativistic contributions to the production amplitude. Differences in the resulting survival probability due to considering only non-relativistic frequencies were again found only for large initial momenta, which did not have much effect on the resulting effective survival probability. To conclude, we found that the two particle formalisms, both relativistic and non-relativistic, produced identical results as the simple non-relativistic relative wavefunction method. This is the method that we will employ in constructing a more realistic three dimensional suppression model in the next chapter.

CHAPTER 5

QUANTUM MECHANICAL MODEL OF SUPPRESSION

We examined a fully relativistic quantum mechanical suppression model in the previous chapter. We found that, for loosely bound final states, that we could treat the problem in a nonrelativistic fashion. With this in mind, we develop a three-dimensional suppression model in Section 5.1. We will consider harmonic oscillator final states and present some illustrative results in Section 5.2. In Section 5.3, we will perform the same analysis employing more realistic final states. We then discuss our results in Section 5.4

5.1 Three-dimensional Description of Survival Probability

In Chapter 2, we found that the matrix elements for producing heavy quark resonances was proportional to either the wavefunction at the origin of the bound state or its derivative. This was due to the assumption of the nonrelativistic nature of the bound state. In this section we will examine modifications to this matrix element due to a deconfining quark gluon plasma. We shall *assume* some generic initial relative wavefunction with dimension $\sim 1/M_\psi$ representing the hard QCD process. We then allow it to evolve in a deconfined environment before projecting it onto some loosely bound final state. The modifications due to the quark gluon plasma are contained solely in this matrix element. In the approximations that we consider, the only kinematical factor that enters is the J/ψ's final momentum. Therefore, we may write the suppression ratio simply in terms of this matrix element.

We consider a Gaussian-like initial relative wavefunction written as

$$\phi(\mathbf{r},0) = A\exp\left[-\frac{1}{2}\left(\frac{r}{a}\right)^2\right] + B_m r\exp\left[-\frac{1}{2}\left(\frac{r}{b}\right)^2\right] Y_{1m}(\Omega) \tag{5.134}$$

with $a, b \sim 1/2m_c$. This form is chosen so as to be capable of producing both J/ψ ($l = 0$) and χ_c ($l = 1$) states. Also, the limits $a, b \to 0$ allow us to examine the effects of expanding the wavefunction in momentum space, as was done in Chapter 2. We write the final state wavefunctions in the general form

$$\chi_{nlm}(\mathbf{r}) \;=\; R_{nl}(r)Y_{lm}(\Omega). \tag{5.135}$$

We again use a harmonic oscillator potential to represent the confining interquark force. The J/ψ and χ_c radial wavefunction are given as

$$R_{J/\psi}(r) \;=\; \frac{2}{\pi^{\frac{1}{4}}}\frac{1}{r_\psi^{\frac{3}{2}}}\exp\left[-\frac{1}{2}\left(\frac{r}{r_\psi}\right)^2\right] \tag{5.136}$$

$$\text{and} \qquad R_\chi(r) \;=\; \frac{2}{\pi^{\frac{1}{4}}}\left(\frac{2}{3}\right)^{\frac{1}{2}}\frac{1}{r_\psi^{\frac{5}{2}}} r\exp\left[-\frac{1}{2}\left(\frac{r}{r_\psi}\right)^2\right].$$

The parameter, r_ψ, is related to the defining harmonic oscillator potential by $r_\psi = 1/\sqrt{\mu\omega_\psi}$ where we assume $r_\psi \sim 1/2fm \gg a, b$. We note that $R_\psi(0) \propto 1/r_\psi{}^{\frac{3}{2}}$ and $R'_\chi(0) \propto 1/r_\psi{}^{\frac{5}{2}}$.

We simulate the effects of plasma formation in the same manner as in Chapter 4. We assume that immediately after the initial wavefunction is created it is immersed into a totally deconfining environment. This wavefunction is allowed to propagate freely for some time, t, the time the center of mass of the J/ψ system is within a region above some critical temperature. After this time, the confining potential reappears and we project its various bound states onto the modified initial wavefunction. The calculation is performed in momentum space where the final probability amplitude is written as

$$< \chi_{nlm}|\phi(t) >= \frac{1}{(2\pi)^3}\int \tilde{\chi}^*_{nlm}(\mathbf{k})\tilde{\phi}(\mathbf{k})\exp[-i\omega_{\mathbf{k}}t]d^3\mathbf{k}\,, \tag{5.137}$$

where $\omega_{\mathbf{k}}$ is the propagating frequency for a free particle and $\tilde{\chi}_{nlm}(\mathbf{k})$ and $\tilde{\phi}(\mathbf{k})$ are the Fourier transforms of the initial and final states respectively. Adhering to the definitions in Appendix A, the initial state Fourier transform is written as

$$\tilde{\phi}(\mathbf{k}) = a(k) + b_m(k)Y_{1m}(\Omega_{\mathbf{k}}) \tag{5.138}$$

$$\text{with} \qquad a(k) = C\exp\left[-\frac{1}{2}(ak)^2\right]$$

$$\text{and} \qquad b_m(k) = D_m k\exp\left[-\frac{1}{2}(bk)^2\right].$$

The bound state Fourier transforms are similarly written as

$$\tilde{\chi}_{nlm}(\mathbf{k}) = \tilde{R}_{nl}(k)Y_{lm}(\Omega_{\mathbf{k}}) \tag{5.139}$$

$$\text{with} \qquad \tilde{R}_{\psi}(k) = (2\pi)^{\frac{3}{2}}\frac{2}{\pi^{\frac{1}{4}}}r_{\psi}^{\frac{3}{2}}\exp\left[-\frac{1}{2}(r_{\psi}k)^2\right]$$

$$\text{and} \qquad \tilde{R}_{\chi}(k) = -i(2\pi)^{\frac{3}{2}}\frac{2}{\pi^{\frac{1}{4}}}\left(\frac{2}{3}\right)^{\frac{1}{2}}r_{\psi}^{\frac{5}{2}}k\exp\left[-\frac{1}{2}(r_{\psi}k)^2\right].$$

The orthogonality of the spherical harmonics allows us to write Equation 5.137 in the form

$$< \chi_{nlm}|\phi(t) >= \delta_{l0}\delta_{m0}A_n(t) + \delta_{l1}B_{nm}(t), \tag{5.140}$$

where

$$A_{\psi}(t) = \frac{1}{(2\pi)^3}\int_0^{\infty}\tilde{R}_{\psi}^*(k)a(k)\exp[-i\omega_{\mathbf{k}}t]k^2dk \tag{5.141}$$

and

$$B_{\chi}^m(t) = \frac{1}{(2\pi)^3}\int_0^{\infty}\tilde{R}_{\chi}^*(k)b_m(k)\exp[-i\omega_{\mathbf{k}}t]k^2dk \tag{5.142}$$

are the probability amplitudes for producing a J/ψ or χ_c.

We examine Equation 5.138 and note that the initial wavefunction contains momentum components of order m_c. This would indicate that we should use a relativistic expression for $\omega_{\mathbf{k}}$. However, in accordance with the discussion in the

previous chapter, we assume that the radial bound state wavefunctions damp out any contributions from $k > 1/r_\psi \ll m_c$. We are therefore justified in writing ω_k completely in the relative coordinate frame as $\omega_k \approx k^2/2\mu = k^2/m_c$. We may therefore perform the integrals to get

$$A_\psi(t) = \left[\left(\frac{r_\psi}{2\pi}\right)^{\frac{2}{3}} \pi^{\frac{1}{4}}\sqrt{2}C\right] \frac{1}{\left[r_\psi^2 + a^2 + 2it/m_c\right]^{\frac{3}{2}}} = \frac{C' R_\psi(0)}{\left[\left(1 + a^2/r_\psi^2\right) + i\omega_\psi t\right]^{\frac{3}{2}}} \quad (5.143)$$

and

$$B_\chi^m(t) = \left[\frac{r_\psi^{\frac{5}{2}}}{(2\pi)^{\frac{2}{3}}} \frac{2\pi^{\frac{1}{4}} D_m}{\sqrt{3}}\right] \frac{1}{\left[r_\psi^2 + b^2 + 2it/m_c\right]^{\frac{5}{2}}} = \frac{D'_m R'_\chi(0)}{\left[\left(1 + b^2/r_\psi^2\right) + i\omega_\psi t\right]^{\frac{5}{2}}} \quad (5.144)$$

where we have used $\omega_\psi = 2/r_\psi^2 m_c$. We note that for, $t = 0$ (no plasma formation) and the limits $a^2/r_\psi^2, b^2/r_\psi^2 \to 0$, we find that the J/ψ and χ_c production probability amplitudes are proportional to the resonance wavefunction at the origin and its derivative. This is the same limit considered in Chapter 2.

We are interested in the ratio of resonance production with and without plasma formation. Therefore, we define the survival probability as

$$P(t) = \frac{|<\chi_{nlm}|\phi(t)>|^2}{|<\chi_{nlm}|\phi(0)>|^2} \quad (5.145)$$

which, for the J/ψ and χ_c resonances, becomes

$$P_\psi(t) = \frac{1}{\left[1 + \omega_\psi^2 t^2/(1 + a^2/r_\psi^2)^2\right]^{\frac{3}{2}}} \quad (5.146)$$

and

$$P_\chi(t) = \frac{1}{\left[1 + \omega_\psi^2 t^2/(1 + b^2/r_\psi^2)^2\right]^{\frac{5}{2}}} \quad (5.147)$$

We plot this in Figure 5.26 for $\omega_\psi = 1.05\, fm^{-1}$ ($r_\psi = 0.5 fm$ and $m_c = 1.5 GeV$). We note that the $l = 1$ χ_c-state is dissolved much more quickly that the $l = 0$ J/ψ.

We also examine the dependence of the survival probability on the width of the initial wavefunction. Examining the limit, $a^2/r_\psi^2, b^2/r_\psi^2 \to 0$, which corresponds to the analysis of Reference [14], we see from Figure 5.26 that there is

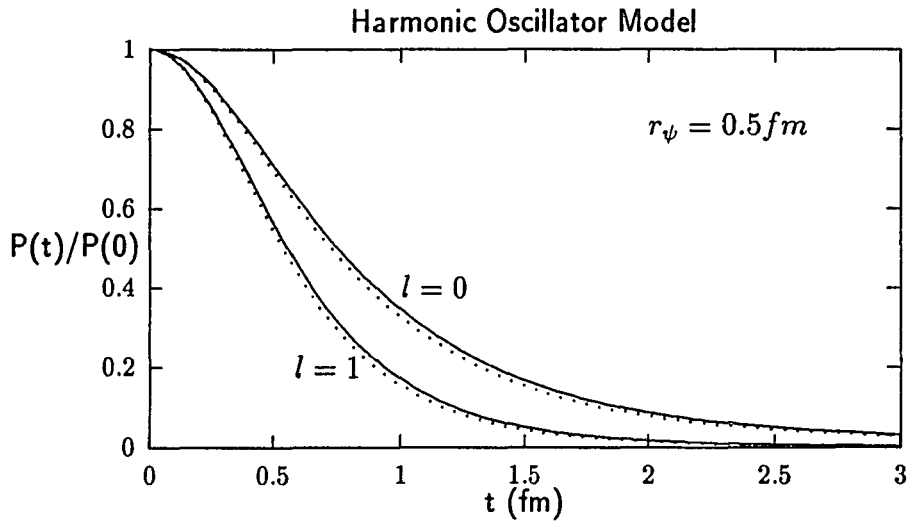

Figure 5.26: Survival probability for harmonic oscillator model-dotted line is with $a/r_\psi = 1/5$ and full line is with $a/r_\psi = 0$.

very little effect on the survival probability. This is consistent with the analysis in Appendix A of Reference [15] where it was shown that, with the initial wavefunction width much less than the final bound state width, the survival probability is relatively independent of the initial wavefunction *form*. It is the final wavefunction that dominates the suppression behavior.

5.2 Resonance Suppression in the Harmonic Oscillator Model

In the last section we noted that, in the harmonic oscillator model, the χ_c-state was dissolved much more quickly than the J/ψ. This is in direct contrast to the semiclassical result where the χ_c had a much longer formation time. This will have an important effect when introduced into a model for the deconfining environment. In the semiclassical model, the longer formation time tended to offset the fact that the χ_c was dissolved at a lower temperature. This produced a suppression effect not much different than that of the J/ψ. However, in the quantum mechanical

case, we see that these two effects are additive, resulting in a suppression much stronger than that of the J/ψ.

We will employ the same hydrodynamical picture that was used in Chapter 3 to model the plasma. However, the suppression must now be rewritten an

$$S(p_T) = \frac{\int_0^{R_0}\int_0^{\pi} r dr d\vartheta \rho(r) P[\tau(r,v,\vartheta)]}{\int_0^{R_0}\int_0^{\pi} r dr d\vartheta \rho(r)}. \tag{5.148}$$

where we have replaced the θ-function in Equation 3.68 with the quantum mechanical survival probability. Note that $\tau(r,v,\vartheta) = t(r)/\gamma$ is the time that the center of mass of the bound state system (as measured in its *own* rest frame) remains in the deconfining region. This time is determined by both the hydrodynamical evolution of the plasma and the motion of the resonance.

The plasma model used in Chapter 3 provides no information regarding the plasma region for times less than t_0, the "formation" time of the plasma. This was not a problem as long as we required that this be less than the resonance formation time, i.e. $t_f^R > t_0$. However, in Equation 5.148, $R(\tau)$ is a constantly varying function of deconfinement time, therefore we must make some assumptions regarding $t < t_0$. We shall assume that, though the plasma region is not in complete equilibrium, local conditions should still be hot enough to provide a color screening environment. To approximate this, we follow the example in [15, 66] and consider the temperature profile for $t < t_0$ to be *equal* to that at t_0, i.e.

$$R^T(t) = R_0[1 - (t_0/t_m^T)^{\frac{1}{a}}]^{\frac{1}{2}} \tag{5.149}$$

for $t < t_0$.

As stated in Section 5.1, we assume that the environment becomes *totally* deconfined above some critical temperature. We take this to be the temperature for which the screening radius becomes significantly less than the rms radius of a particular resonance. For the present analysis, only T_ψ/T_χ is critical, which we

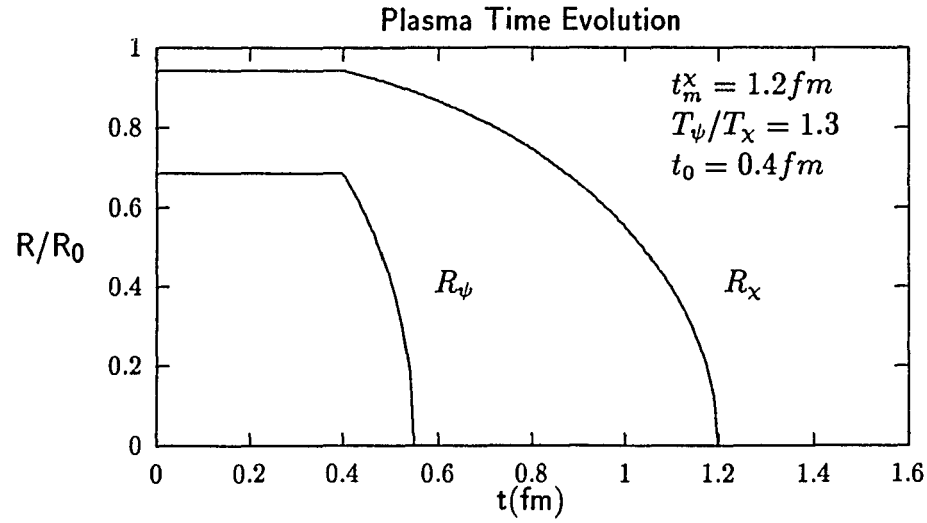

Figure 5.27: Critical isotherm radii as a function of time

take to be about 1.2-1.3 as before. Fixing t_m for a particular temperature and t_0, Equation 3.67 determines the evolution of all critical isotherms. This is shown in Figure 5.27 for the J/ψ and χ_c deconfinement regions.

We see from Figure 5.27 that there is a region beyond which there is no deconfinement effect. Using $t_0 T_0^3 = t_m^R T_R{}^3$, we find this to be

$$R_c^R \equiv R^{T_R}(0) = R_0[1 - (T_R/T_0)^{\frac{3}{a}}]^{\frac{1}{2}} \tag{5.150}$$

where T_0 is the initial central temperature of the cylindrical plasma. Equation 5.148 may then be separated to reflect this and be written as

$$\begin{aligned} S(p_T) &= \frac{\int_0^{R_c}\int_0^{\pi} r dr d\vartheta \rho(r) P[\tau(r,v,\vartheta)] + \int_0^{R_c}\int_0^{\pi} r dr d\vartheta \rho(r)}{\int_0^{R_0}\int_0^{\pi} r dr d\vartheta \rho(r)} \\ &= \frac{2(b+1)}{\pi {R_0}^2}\int_0^{R_c}\int_0^{\pi} r dr d\vartheta \frac{(1-r^2/R_0^2)^b}{[1+\omega_\psi^2\tau^2(r,v,\vartheta)]^{\frac{n}{2}}} + (1 - R_c^2/R_0^2)^{b+1} \end{aligned} \tag{5.151}$$

where $n = 3(5)$ for $l = 0(1)$ suppression. Note that we have explicitly inserted the form $\rho(r) \sim (1 - r^2/R_0^2)^b$ from Chapter 3 and the suppression probability from the previous section.

As in Chapter 3, we examine the limit $y \equiv vt_m/R_0 \rightarrow 0$. With this, Equation 3.71 yields $t/t_m \approx (1 - r^2/{R_0}^2)^a$ and Equation 5.151 may be written in the form

$$S(p_T) = 2(b+1)I(n,a,b,(\omega_\psi t_m/\gamma)^2, R_c/R_0) \quad (5.152)$$

$$+(1 - R_c^2/{R_0}^2)^{b+1}$$

$$\text{with} \qquad I(n,a,b,\alpha,\beta) = \int_0^\beta \frac{x dx (1-x^2)^b}{[1+\alpha(1-x^2)^{2a}]^{\frac{n}{2}}}$$

$$= \frac{1}{2a}\int_0^{(1-\beta^2)^a} \frac{dy y^{\frac{(b-a)+1}{a}}}{[1+\alpha y^2]^{\frac{n}{2}}}.$$

To compare with the semiclassical model, we consider the specific case $a = b = \frac{1}{2}$. The relevant integrals in Equation 5.152 are [28]

$$I(5,\frac{1}{2},\frac{1}{2},\alpha,\beta) = \frac{1}{3}\left[\frac{1}{(1+\alpha)^{\frac{3}{2}}} - \frac{(1-\beta^2)^{\frac{3}{2}}}{[1+\alpha(1-\beta^2)]^{\frac{3}{2}}}\right]$$

$$I(3,\frac{1}{2},\frac{1}{2},\alpha,\beta) = \frac{1}{\alpha^{\frac{3}{2}}}\ln\left[\frac{\sqrt{\alpha}+\sqrt{1+\alpha}}{\sqrt{\alpha(1-\beta^2)}+\sqrt{1+\alpha(1-\beta^2)}}\right]$$

$$-\frac{1}{\alpha}\left[\frac{1}{\sqrt{1+\alpha}} - \frac{\sqrt{1-\beta^2}}{\sqrt{1+\alpha(1-\beta^2)}}\right].$$

In Figures 5.28 and 5.29 we show the suppression as given by Equation 5.152 for the J/ψ and χ_c resonances. Here, we have assumed $\beta \approx 1$ (i.e. $T_R \ll T_0$). Note that the momentum dependence in this quantum mechanical model is much weaker than in the semiclassical model.

We combine the effects of direct J/ψ and intermediate χ_c suppression to write the total J/ψ suppression in the form

$$S(p_T) = f^\chi(p_T)S^\chi(p_T) + f^\psi(p_T)S^\psi(p_T), \quad (5.153)$$

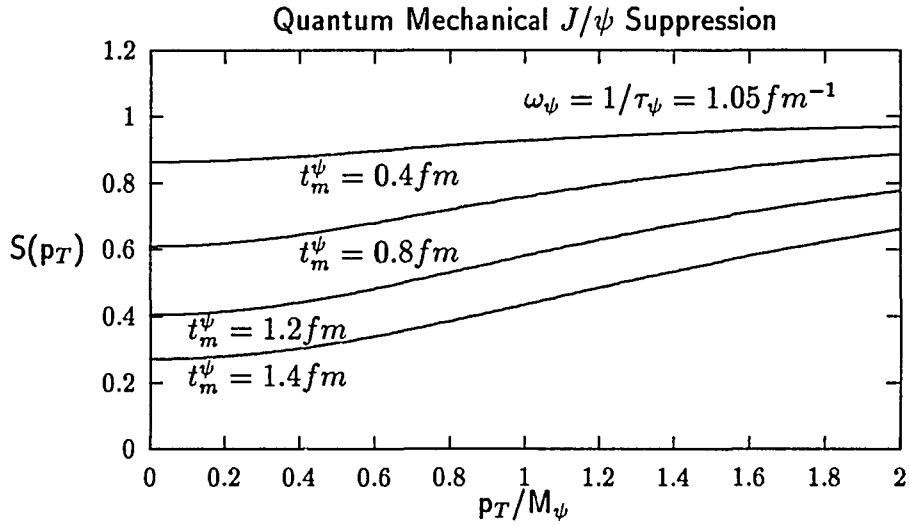

Figure 5.28: J/ψ suppression as given by Equation 5.152 with $T_R/T_0 \ll 1$.

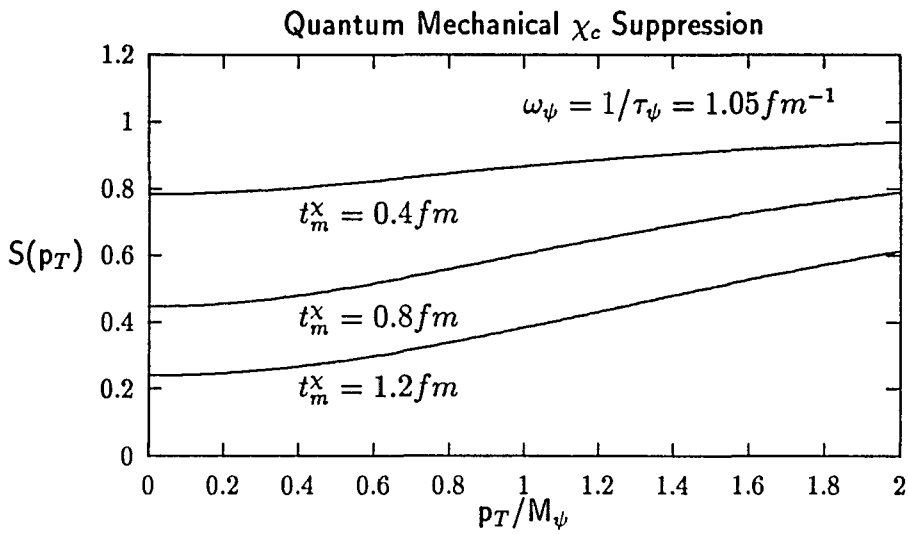

Figure 5.29: χ_c suppression as given by Equation 5.152 with $T_R/T_0 \ll 1$.

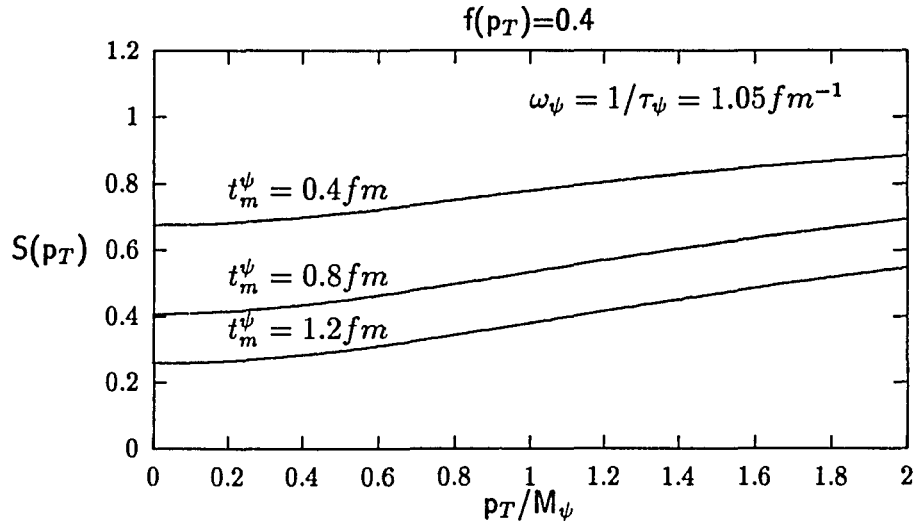

Figure 5.30: J/ψ suppression with 40% of the J/ψ's coming from χ_c-decays. Here we have taken $T_\psi/T_\chi = 1.3$.

as was done in Chapter 3. Making the standard assumption, $f^\chi(p_T) \approx 0.4 \equiv$ constant (and still keeping $T_R \ll T_0$), produces the suppression shown in Figure 5.30. We note that the only effect that this has produces is to strengthen the suppression with respect to direct J/ψ suppression. The momentum dependence is still very weak. However, in Chapter 2, we noted that naive arguments regarding the order of the hard QCD production process implied that production in the low p_T region should be dominated by the χ_c-decay contribution, which is also more highly suppressed. This could result in a stronger p_T-dependence of the total suppression factor.

To fully examine the suppression in the quantum mechanical model, we must first note that an extra parameter has been introduced. Along with the lifetime of the hot region, t_m, we must also consider the initial temperature of the center of the plasma, T_0. These two parameters may be chosen (but are not uniquely determined) by the suppression at $p_T = 0$. Assuming that this region

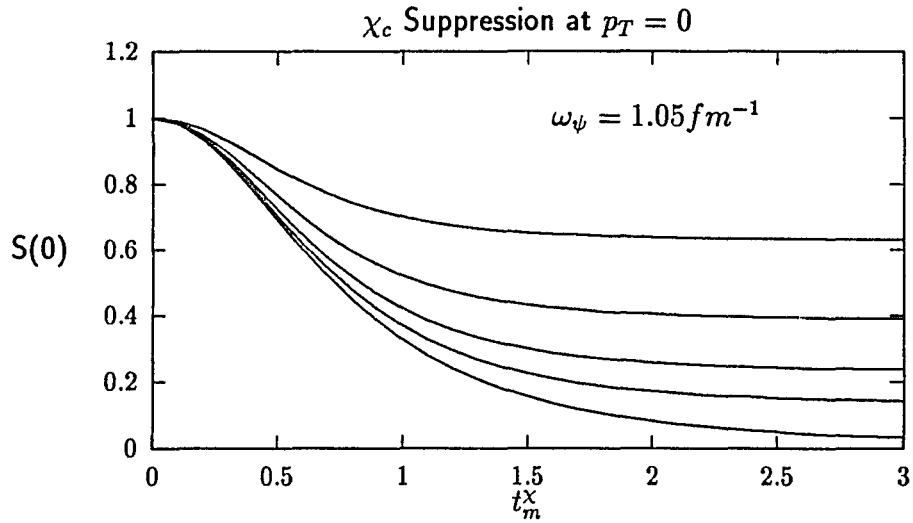

Figure 5.31: χ_c suppression at $p_T = 0$ versus t_m for varying T_χ/T_0. From top to bottom, the curves represent $T_\chi/T_0 = 0.95, 0.9, 0.85, 0.8$, and 0.6. The $T_\chi/T_0 = 0.6$ case is also representative of $T_\chi/T_0 \approx 0$.

is dominated by χ_c-decay contributions ($f^\chi(p_T = 0) = 1$), we examine the suppression at $p_T = 0$ for different plasma lifetimes and temperatures in Figure 5.31. We see that imposing the restriction, $S(0) \approx \frac{1}{2}$, still leaves considerable freedom in choosing the parameters t_m^χ and T_χ/T_0. Therefore, we also examine Figure 5.32 in which we show the fraction of resonances that are affected by plasma screening versus plasma temperature. We note that the choice of T_χ/T_0 strongly affects whether any direct J/ψ suppression will occur or not.

We are interested in situation that produces a strong momentum dependence in the overall suppression. Therefore, we will consider the case where $T_\psi/T_\chi = 1.3$ and examine two situations; one that includes direct J/ψ suppression and one that does not. Looking at Figure 5.32, we choose the temperatures to be $T_\chi/T_0 = 0.6$ and $T_\chi/T_0 = 0.8$ (note that in our notation *lower* T_χ/T_0 implies a *higher* plasma temperature). From Figure 5.31 we see that in both situations, a suppression ratio of about $40 \sim 50\%$ is achieved with $t_m^\chi \approx 0.8 fm$. We plot these

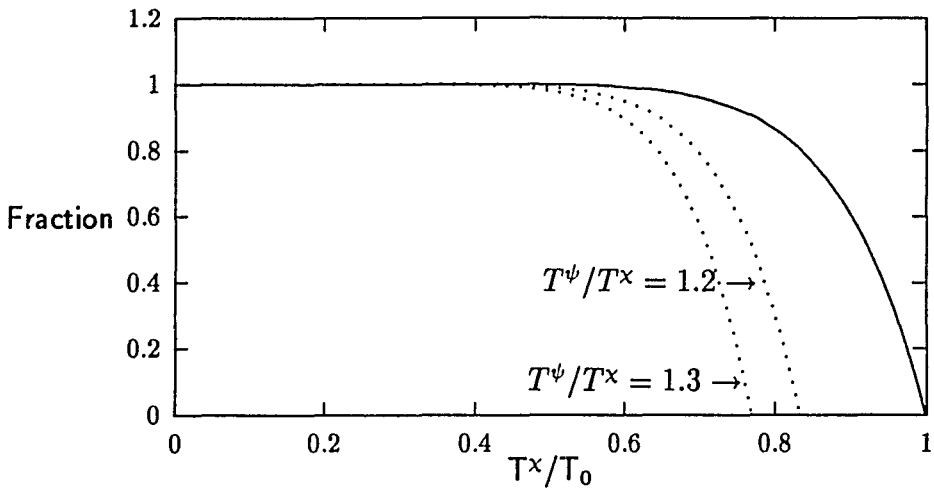

Figure 5.32: Fraction of resonances affected by screening mechanism ($a = b = \frac{1}{2}$). Solid line corresponds to χ_c resonances and dotted lines correspond to J/ψ resonances.

two situations in Figures 5.33 and 5.34 for different J/ψ distributions. The choice of exponentials is meant only to qualitatively reflect a decreasing χ_c-dominance with p_T. The important point to note is the increased momentum dependence of the suppression over the χ_c-dominated ($f = 1$) case and the direct J/ψ case (Figure 5.28).

5.3 Realistic Final States

To discuss the suppression of realistic charmonium states, we recall from Chapter 2 that the charmonium wavefunctions may be written in the form

$$\chi_{nlm}(\mathbf{r}) = \sum_i a_i^{nlm} \Omega_{il}^m(\beta, \mathbf{r}) \,, \tag{5.154}$$

where

$$\Omega_{il}^m(\beta, \mathbf{r}) = N_{il}(\beta) \exp\left[-\frac{\beta^2 r^2}{2}\right] L_{i-1}^{l+1/2}(\beta^2 r^2)\,(\beta r)^l\, Y_{lm}(\Omega) \tag{5.155}$$

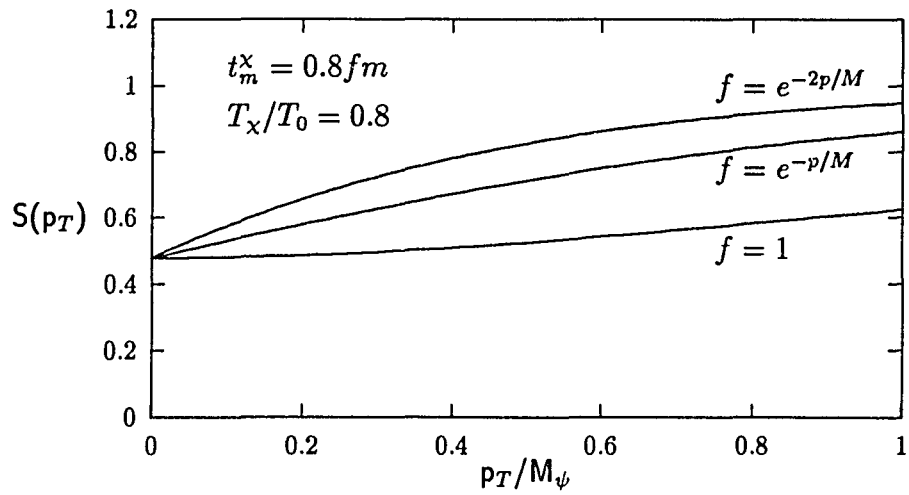

Figure 5.33: Suppression for different $f^x(p_T)$'s. Plasma temperature is such that that no direct J/ψ suppression occurs.

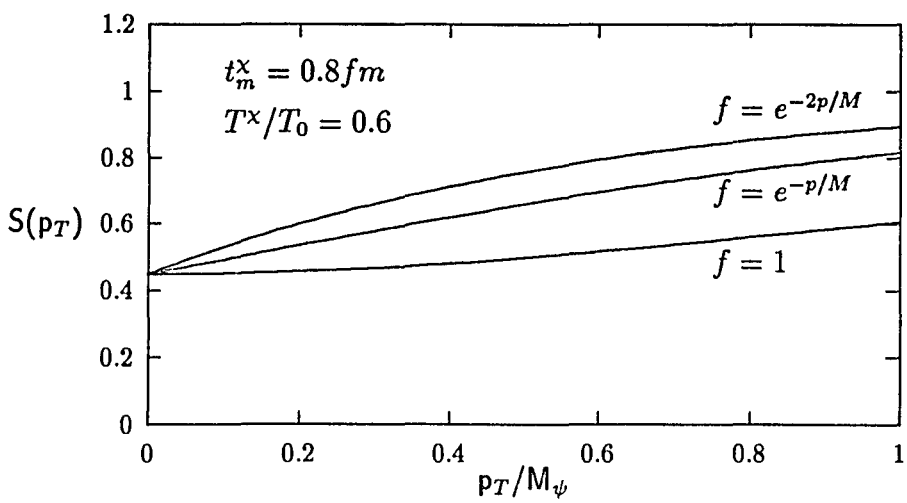

Figure 5.34: Suppression for different $f^x(p_T)$'s. Plasma temperature is such that $\sim 90\%$ of the direct J/ψ's are affected by the screening process.

with

$$N_{il}(\beta) = \beta^{\frac{3}{2}} \left[\frac{2(i-1)!}{\Gamma(i+l+1/2)} \right]^{\frac{1}{2}} . \tag{5.156}$$

Also, recall the Fourier transform relation,

$$\tilde{\Omega}^m_{il}(\beta, \mathrm{k}) = (2\pi)^{3/2}(-1)^{i+l-1} i^l \Omega^m_{il}(\beta^{-1}, \mathrm{k}) . \tag{5.157}$$

The final probability amplitude, Equation 5.137, is then written as

$$< \chi_{nlm} | \phi(t) >= \sum_i a_i^{nlm} \frac{1}{(2\pi)^3} \int d^3k \tilde{\Omega}^{m*}_{nl}(\beta, \mathrm{k}) \tilde{\phi}(k) \exp[-i\omega_{\mathrm{k}} t] . \tag{5.158}$$

Using the same initial wavefunction as before (given by Equation 5.134), we find the probability amplitude (given in Equation 5.140) for producing a J/ψ or χ_c to be

$$A_\psi(t) = \frac{C}{(2\pi)^{3/2}} \sum_i a_i^\psi (-1)^{i-1} N_{i0}(\beta^{-1}) \, I_{i0}(a, \beta, t/\mu) \tag{5.159}$$

and

$$B^m_\chi(t) = \frac{-iD_m}{(2\pi)^{3/2}} \sum_i a_i^{\chi m} (-1)^i N_{i1}(\beta^{-1}) \, I_{i1}(b, \beta, t/\mu) \tag{5.160}$$

where

$$\begin{aligned} I_{il}(a, \beta, \tau) &\equiv \int_{-\infty}^{\infty} \exp\left[-\frac{1}{2} k^2 (a^2 + \frac{1}{\beta^2} + i\tau) \right] L^{l+1/2}_{i-1}(k^2/\beta^2) \left(\frac{k}{\beta} \right)^l k^{l+2} dk \\ &= \frac{\beta^{l+3}}{2} \frac{\Gamma(i+l+1/2)}{(i-1)!} \left[\frac{2}{1 + a^2\beta^2 + i\beta^2\tau} \right]^{l+\frac{3}{2}} \left[1 - \frac{2}{1 + a^2\beta^2 + i\beta^2\tau} \right]^{(i-1)} \end{aligned} \tag{5.161}$$

Note that we still have the overall suppression factor, $2/(1 + a^2\beta^2 + i\beta^2\tau)^{l+3/2}$ that increases with l.

We show the resulting survival probabilities for the J/ψ and χ_c states in Figure 5.35. Here, we have fixed a and b such that $< r^2 >^{1/2} = \sqrt{3/2}a(b) = 1/2m_c = 0.075fm$. We also examine the limit $a, b \to 0$ in Figures 5.36 and 5.37. We see that the $l = 0$ and $l = 1$ survival probabilities are very similar. This is a result of the larger size of the χ_c tending to cancel the higher l suppression. We also note that it is this larger size of the χ_c that makes the $a, b \to 0$ approximation work better than in the J/ψ case.

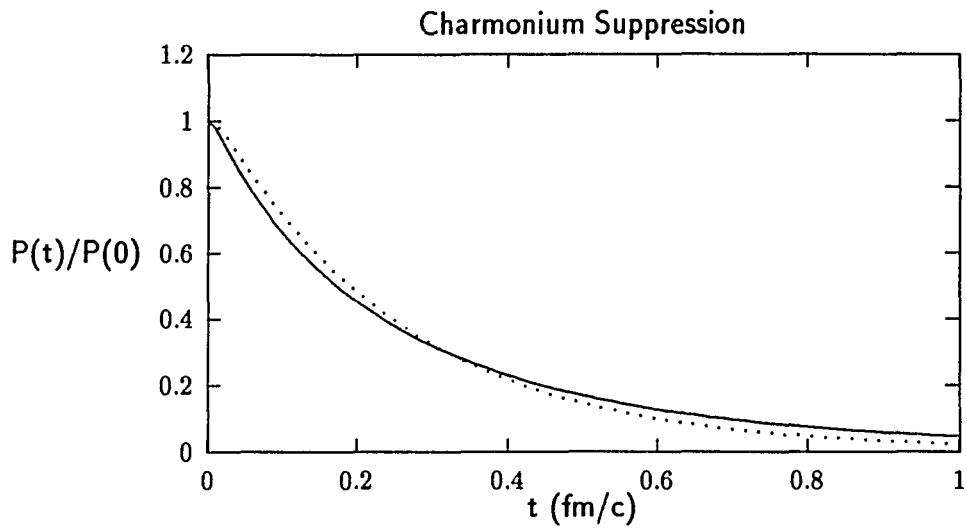

Figure 5.35: J/ψ (solid) and χ_c (dotted) survival probabilities.

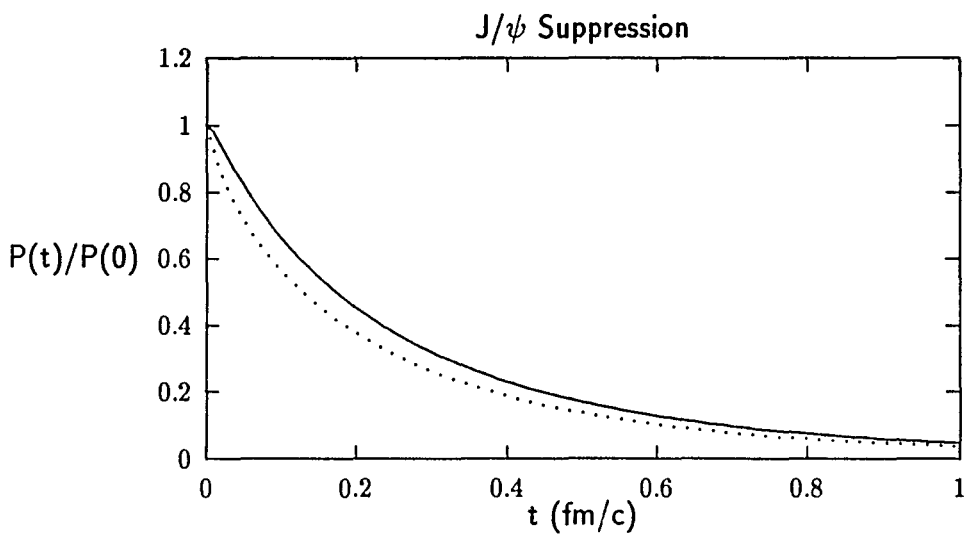

Figure 5.36: J/ψ survival probability with a=0.061 fm (solid) and a=0 (dotted).

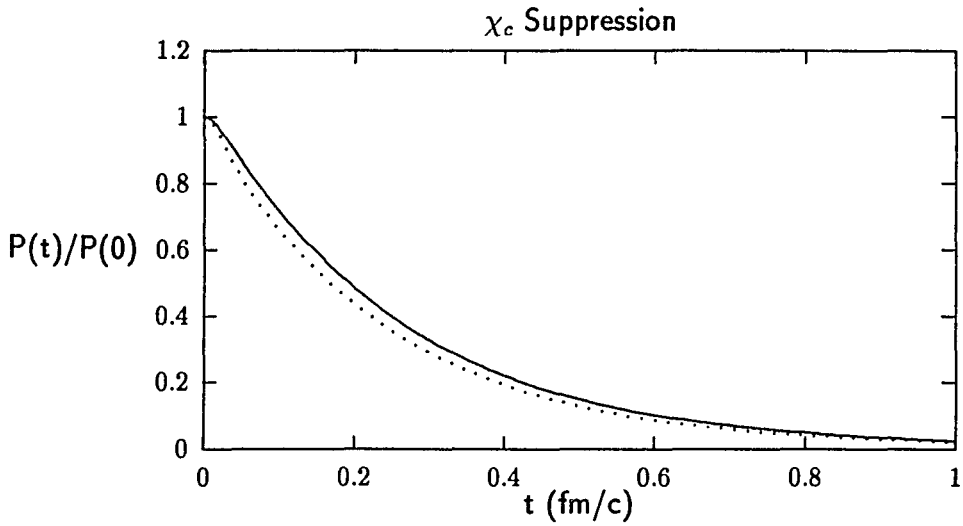

Figure 5.37: χ_c survival probability with a=0.061 fm (solid) and a=0 (dotted).

We next examine the resulting suppression based on Equation 5.148. Employing the same plasma model as before, we plot the momentum dependence of the resonance suppression in Figure 5.38. Here, we have assumed that the plasma initial central temperature, T_0, is much greater than the resonance screening temperature, T_R, resulting in the fact that almost all of the resonances are affected by the screening. The slight decrease of the χ_c survival probability with respect to that of the J/ψ, seen in Figure 5.35, can also be seen in Figure 5.38. We note that the p_T dependence here is even weaker than in the harmonic oscillator model.

We now examine the combined effects of direct J/ψ and intermediate χ_c suppression as defined in Equation 5.153. Again, we are interested in situations that will strengthen the transverse momentum dependence. Since the survival probabilities are similar, we no longer have the additive effect of lower screening temperature *and* faster dissolution for the χ_c. This, combined with the weaker p_T dependence shown in Figure 5.38, indicate that, to replicate the p_T dependence of the NA 38 data, we must consider situations in which little or no direct J/ψ suppression occurs. From Figure 5.32, we see that this requires $T_\chi/T_0 \geq 0.75$

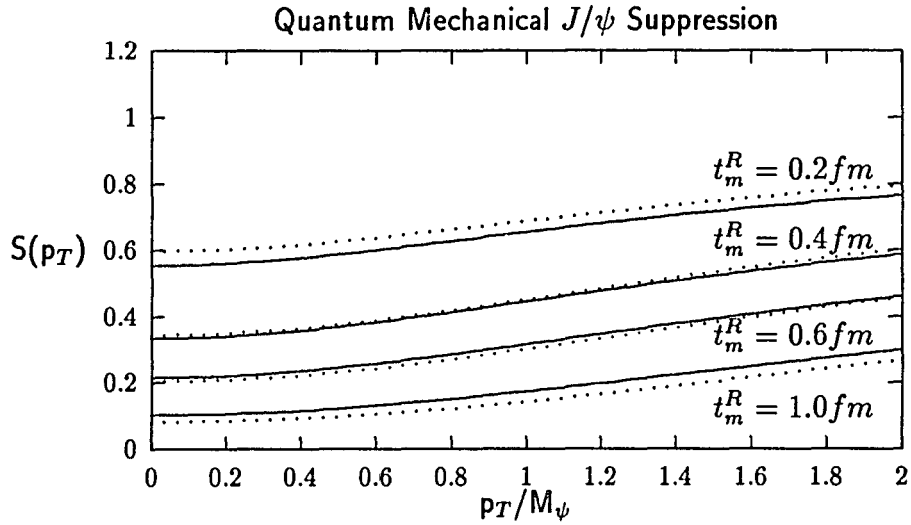

Figure 5.38: J/ψ (solid) and χ_c (dotted) suppression with $T_R/T_0 \ll 1$.

for $T_\psi/T_\chi \sim 1.3$. Examining Figure 5.39, we see that $T_\chi/T_0 \sim 0.9$ gives $S(0) \sim 40 - 50\%$ for $t_m \sim 0.6 - 0.8fm$. We show the transverse momentum dependence of the suppression for $T_\chi/T_0 = 0.9$ in Figures 5.40 and 5.41 for the two plasma lifetimes $t_m{}^\chi = 0.8$ and 0.6. We note that in these cases, the amount of suppression directly reflects the fraction of J/ψ's produced through intermediate χ_c's at a particular p_T. This is evident by examining the $f^\chi = 1$ case. Therefore, to replicate the NA 38 data requires a p_T dependence of this fraction similar to the strong p_T dependence of the observed suppression. For completeness, we show in Figure 5.42 the case with $T_\chi/T_0 = 0.6$, which has $\sim 90\%$ of the direct J/ψ's affected by the screening. We see that the momentum dependence is much weaker than in the corresponding harmonic oscillator case, Figure 5.34, as expected.

In the previous examples, we considered lifetimes for the hot plasma region, t_m^χ, to be of order 0.6 – 0.8 fm. This implied rather short plasma formation times of order $t_0 = (T_\chi/T_0)^3\, t_m^\chi = (0.9)^3\,(0.6 - 0.8)$ fm $\approx 0.45 - 0.6$ fm. The motivation for considering such short lifetimes was to try to maximize the momentum dependence due to dilation. However, we have seen that the primary momentum

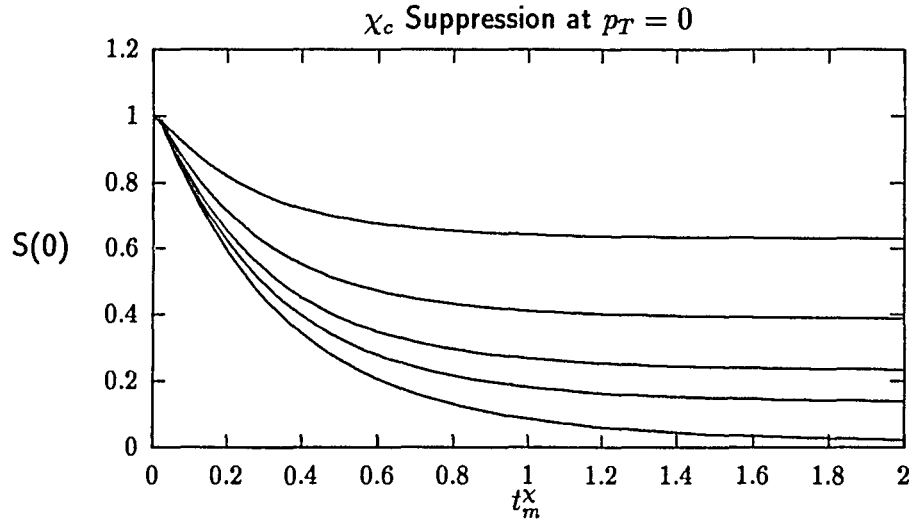

Figure 5.39: χ_c suppression at p_T=0 versus t_m for varying T_χ/T_0. From top to bottom, the curves represent T_χ/T_0 =0.95, 0.9, 0.85, 0.8, and 0.6. The T_χ/T_0 =0.6 curve is also representative of $T_\chi/T_0 \approx 0$.

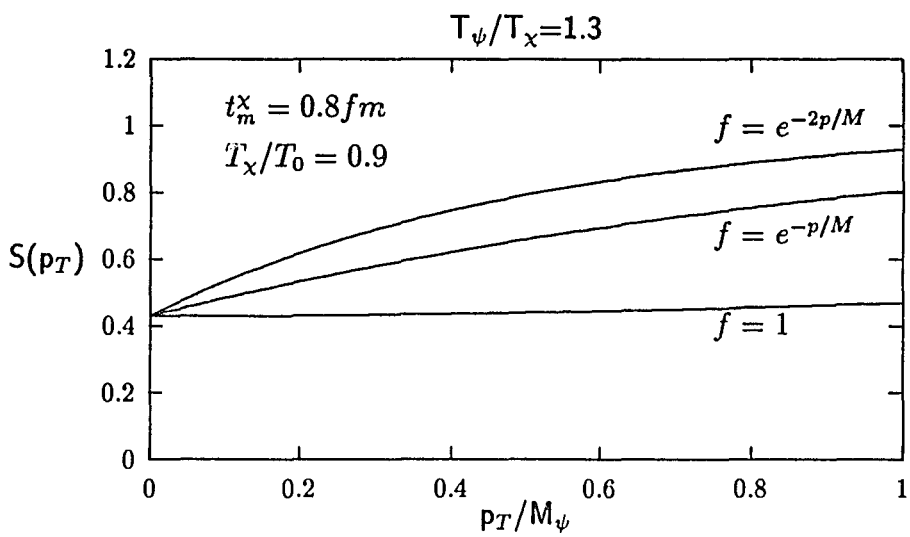

Figure 5.40: Suppression for different $f^\chi(p_T)$'s. Plasma temperature is such that no direct J/ψ suppression occurs.

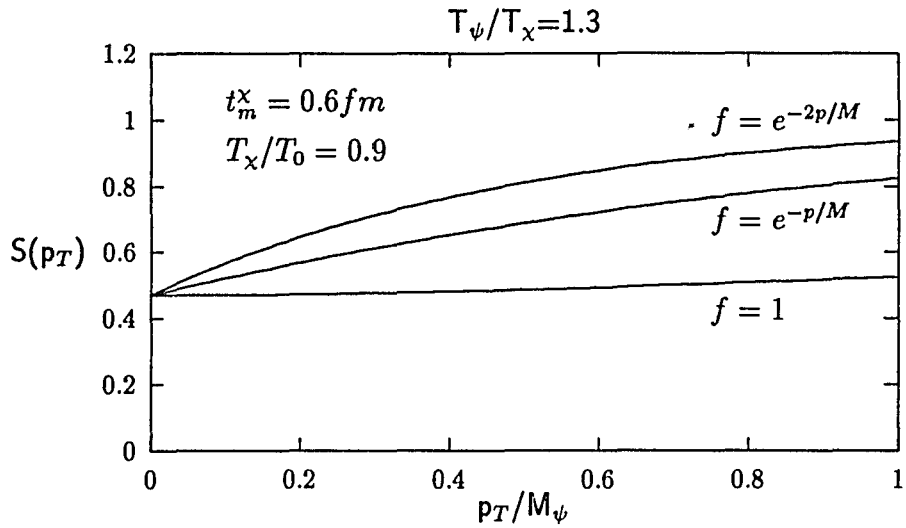

Figure 5.41: Suppression for different $f^\chi(p_T)$'s. Plasma temperature is such that no direct J/ψ suppression occurs.

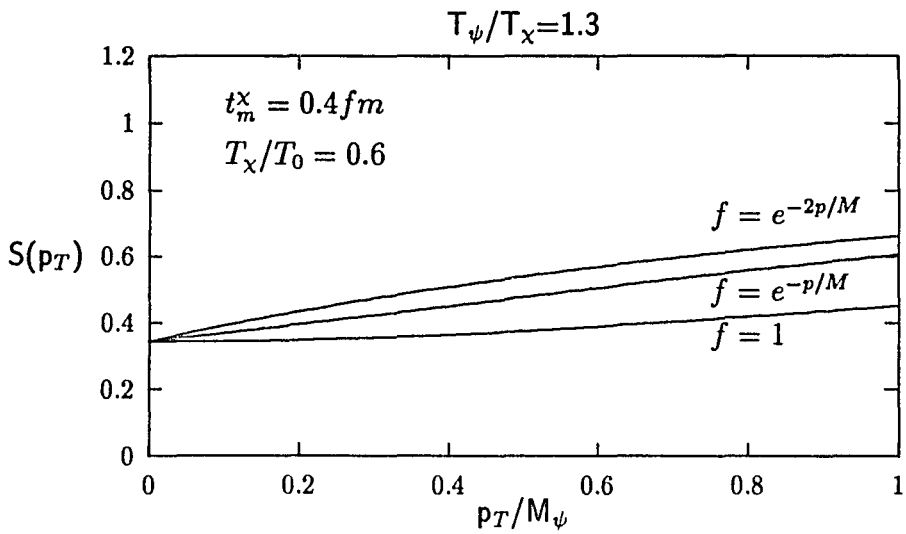

Figure 5.42: Suppression for different $f^\chi(p_T)$'s. Plasma temperature is such that $\sim$ 90% of the directJ/ψ's are affected by the screening process.

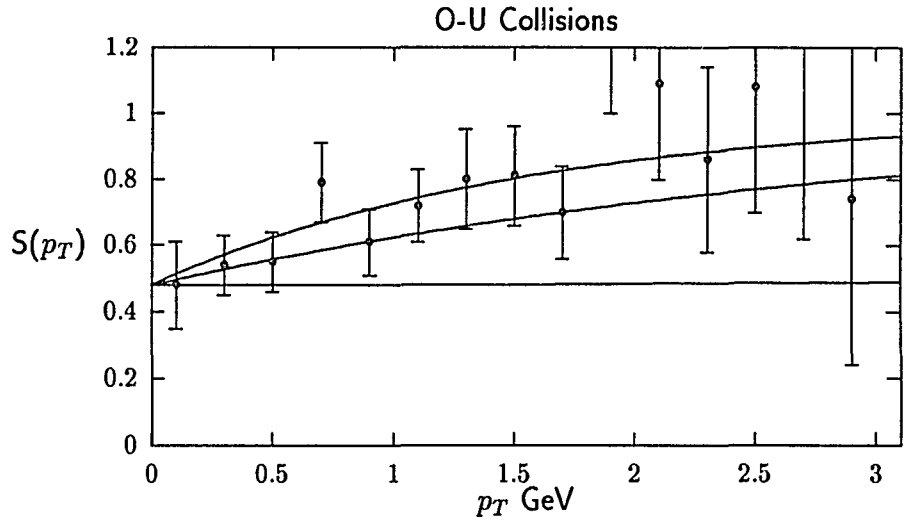

Figure 5.43: Suppression with $T_\chi/T_0 = 0.92$ and $t_m^\chi = 1.3fm$ for the three distributions, (from top to bottom) $f = \exp[-2p_T/M], \exp[-p_T/M]$, and 1. Superimposed is the NA 38 O-U data [55].

dependence in the suppression arises through the momentum dependence of the production mechanism, i.e., whether the J/ψ was produced directly or through χ_c-decay. We are therefore free to consider longer lifetimes.

We shall consider plasma lifetimes such that the plasma formation time is taken to be its canonical value of about a fermi. Examining Figure 5.39, we find that requiring $S(0) \sim 0.45$ requires $T_\chi/T_0 \approx 0.92$ for $t_m^\chi \geq 1.0$ fm. This implies $t_m^\chi = 1.3$ fm. We plot the resulting suppression for our three distributions in Figures 5.43 and 5.44, along with the NA 38 O-U and S-U data. We note that this choice of temperature implies that no direct J/ψ occurs. We see that both the $\exp[-p_T/M]$ and the $\exp[-2p_T/M]$ distributions are consistent with the NA 38 data.

In Section 2.4, we mentioned that initial state parton scattering can increase the width of the J/ψ momentum distributions. This effect is expected to increase with the centrality of the collision. Therefore, some of the momentum

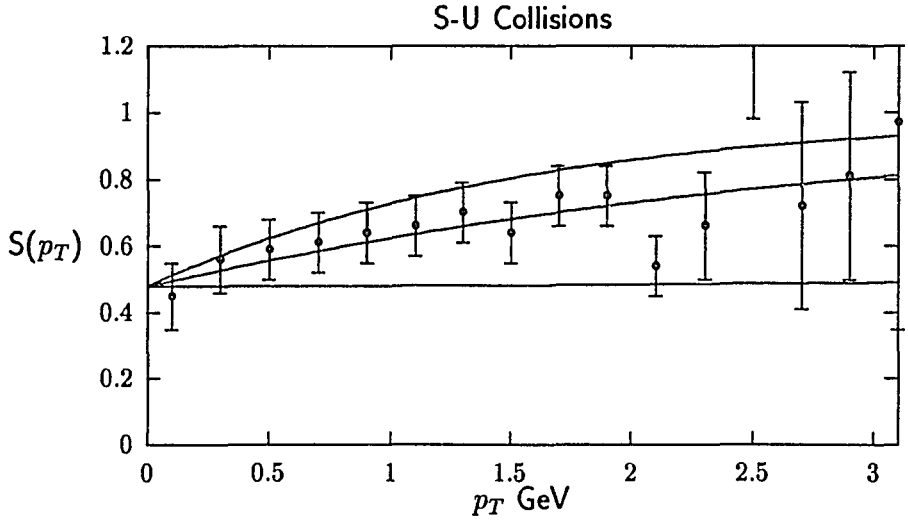

Figure 5.44: Suppression with $T_\chi/T_0 = 0.92$ and $t_m^\chi = 1.3fm$ for the three distributions, (from top to bottom) $f = \exp[-2p_T/M], \exp[-p_T/M]$, and 1. Superimposed is the NA 38 S-U data [55].

dependence in the observed suppression may be due to a depletion of J/ψ's at low p_T for high E_T events. This effect must be removed from the data to properly determine the constraints that the data put on any plasma model. This was done in Reference [44]. We plot, in Figure 5.45, our previous calculation against the "initial state corrected" S-U data of Reference [44]. Though the statistics are rather poor, we see that the calculation shown in Figure 5.46 is more in line with the data. Here, we have considered a hotter and longer lived plasma with $T_\chi/T_0 = 0.77$ and $t_m^\chi = 2.2fm$. More importantly, we have taken the fraction of directly produced J/ψ's to be momentum *independent.*

5.4 Discussion

We have found that the faster dissolution for $l = 1$ states observed in the harmonic oscillator was not seen when realistic charmonium states were used. We also saw that the zero width initial approximation was less reliable than in the harmonic

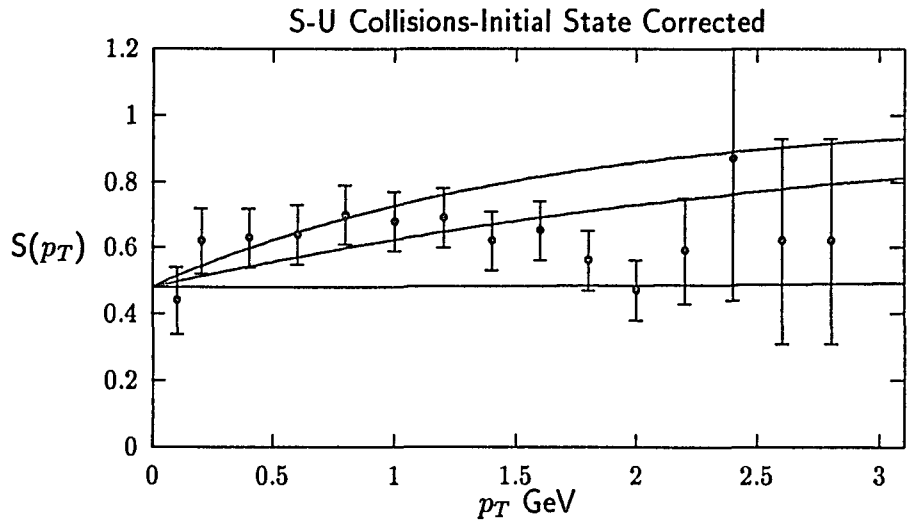

Figure 5.45: Suppression with $T_\chi/T_0 = 0.92$ and $t_m^\chi = 1.3fm$ for the three distributions, (from top to bottom) $f = \exp[-2p_T/M], \exp[-p_T/M]$, and 1. Superimposed is the "initial state corrected" NA 38 S-U data [44].

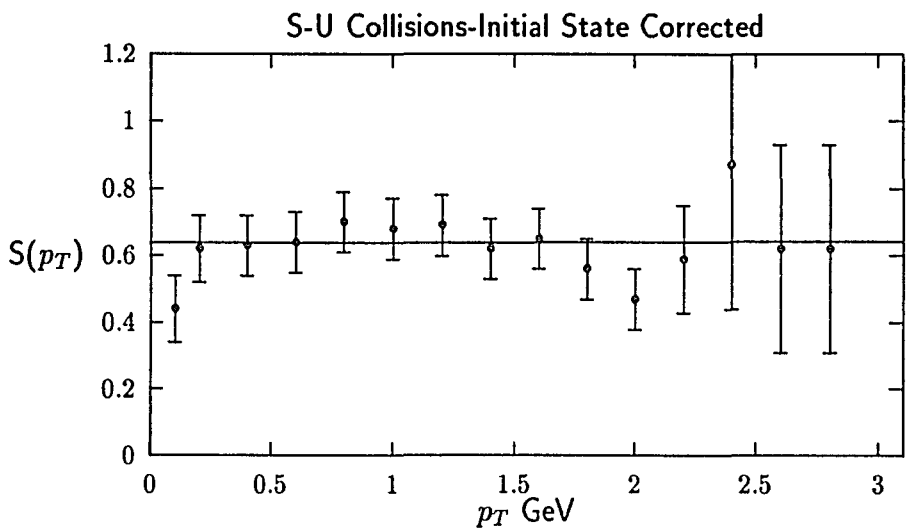

Figure 5.46: Suppression with $T_\chi/T_0 = 0.77$, $t_m^\chi = 2.2fm$, and $f = 0.4$. Superimposed is the "initial state corrected"NA38 S-U data [44].

oscillator case. This was due to the fact that the Fourier transforms of realistic charmonium wavefunctions contained more relativistic components than would be expected of a truly non-relativistic bound state. This also implied that the approximation of using non-relativistic propagation frequencies may be less effective than we had hoped (see for example Reference [67]). Both of these effects should be weaker in the χ_c system due to its larger size. Therefore, one would expect relativistic corrections to affect the J/ψ survival probability more, resulting in a χ_c dissolution slightly faster than that of the J/ψ.

We attempted to model the p_T-dependence of the J/ψ suppression with relatively short plasma lifetimes to maximize the momentum dependence due to time dilation. This required plasma formation times of order $t_0 \sim 0.45 - 0.6 fm$. Though there is some theoretical support for such short formation times [68], one usually considers $t_0 \sim 1 fm$. It was seen that the momentum dependence of the suppression was dominated by the momentum dependence of the production mechanism. Therefore, we considered longer plasma lifetimes, more in accord with estimates in Section 3.5. To replicate the NA 38 data, we required that the plasma temperatures be such that little or no direct J/ψ suppression occurred and that the momentum dependence of the fraction of indirectly produced J/ψ's reflect that of the data. This implied that the fraction of J/ψ's resulting from χ_c-decay must dominate at low p_T and diminish to about $10 - 40\%$ at $p_T \sim M_\psi$. This is a stronger momentum dependence than implied in Reference [16] where it was estimated that at least 50% or more of the high p_T are produced through this mechanism. However, when initial state effects are taken into account, the required momentum dependence is much weaker.

Concerning the relevant time scales of the resonance suppression, we note that plasma lifetimes greater than a fermi or two are sufficient to melt almost all of the resonances created within the hot region. Therefore, calculating the fraction of resonances created within the critical isotherm provides a good estimate of the overall suppression for each resonance. This differs from the semi-classical

analysis where the χ_c formation time is about 2 fm. Therefore, even for the longer plasma lifetimes of order 2-3 fm, one must still consider the significant fraction of resonances that survive the plasma.

CHAPTER 6

CONCLUSION

A semi-classical analysis of the $c\bar{c}$ system yields a formation time for the χ_c of about twice that of the J/ψ. This implies that a $c\bar{c}$ pair that is to create a χ_c can remain emersed in a deconfining medium for a longer time than a pair that is to create a J/ψ. However, the χ_c is a larger system, indicating that a lower temperature is required to melt it. These two effects work against each other resulting, in similar suppression behaviors. Therefore, the observed suppression is relatively independent of whether the J/ψ is formed directly or through the radiative decay of a χ_c.

In this paper, we have examined J/ψ suppression within a quantum mechanical framework. We have shown that, for non-relativistic final states, a non-relativistic treatment is adequate, even though the initial wavepacket contains relativistic components. We observed the general feature that states of higher l tend to dissolve more quickly. This was shown to be true for the specific case of the harmonic oscillator. Thus, the lower screening temperature for the χ_c works in *conjunction* with its faster dissolution. However, the examination of more realistic charmonium states defined by the QCD motivated linear plus Coulomb potential yielded similar survival probabilities for the χ_c and J/ψ. This was a result of the larger size of the χ_c compensating for the higher l suppression. The wider χ_c state was also more effective than the J/ψ in damping the relativistic components of the initial wavefunction. Though the two resonances have similar survival probabilities, they still have two different screening temperatures. Therefore, to model the suppression properly, it is still important to know the origin of the observed

J/ψ in a quantum mechanical analysis.

Another feature of the quantum mechanical suppression model is its very weak transverse momentum dependence. However, perturbative QCD predicts that low p_T J/ψ production is dominated by the intermediate χ_c process. Considering a momentum dependent fraction of J/ψ's that are produced through this process that decreases with p_T can strengthen the suppression momentum dependence somewhat. However, to replicate the transverse momentum dependence observed in the NA38 data required a very steep production process momentum dependence coupled with plasma temperatures that produced only χ_c suppression. This requirement was greatly weakened when initial state effects were taken into account.

It is becoming increasingly clear that the observed features of J/ψ suppression in relativistic heavy ion collisions will not be explained by one simple process. Aside from considering possible quark gluon plasma formation, one must take into account the nuclear effects on the initial parton densities and the absorption of the resonances in dense hadronic matter. We have now seen that, at least for temperatures near $T_\chi \sim T_c$, it is also important to know the origin of the J/ψ.

APPENDIX A

FOURIER TRANSFORMS

We follow reference [21] and define Fourier transform pairs as

$$g(\mathbf{p}) = \int e^{-i\mathbf{p}\cdot\mathbf{r}} f(\mathbf{r})\, d^3r \tag{A.162}$$

and

$$f(\mathbf{r}) = \frac{1}{(2\pi)^3} \int e^{i\mathbf{p}\cdot\mathbf{r}} g(\mathbf{p})\, d^3p \tag{A.163}$$

In particular, this modifies the harmonic oscillator eigenfunctions of reference [31]. The coordinate space eigenfunctions remain

$$\Omega^m_{nl}(\beta, \mathbf{r}) = N_{nl}(\beta)\, e^{-\beta^2 r^2} L^{l+\frac{1}{2}}_{n-l-1}(\beta^2 r^2)\, (\beta r)^l\, Y_{lm}(\theta, \phi) \tag{A.164}$$

where $N_{nl} = \beta^{3/2}(2(n-l-1)!/\Gamma(n+\frac{1}{2}))^{1/2}$, however, the momentum space eigenfunctions contain an extra factor of $(2\pi)^{3/2}$ and are written as

$$\tilde{\Omega}^m_{nl}(\beta, \mathbf{p}) = (2\pi)^{3/2}(-1)^{n-1}\, i^l\, \Omega^m_{nl}(\beta^{-1}, \mathbf{p})\,. \tag{A.165}$$

All other notations follow reference [31].

APPENDIX B

CHARMONIUM WAVEFUNCTIONS

The charmonium wavefunctions used in the text are defined by the solutions to Schrödinger equation,

$$\mathbf{H}\Psi = \left[\frac{\mathbf{P}^2}{2\mu} + \mathbf{V}\right] = E\Psi \ , \tag{B.166}$$

for the potential given in Reference [29]. The coordinate space form of this potential is

$$V(r) = -\frac{k}{r} + ar \ , \tag{B.167}$$

with $k = 0.471$ and $a = 0.192\,GeV^2$. The charmed quark mass is taken to be $1.32\,GeV$. The solutions are found using the Rayleigh-Ritz-Galerkin method [29, 30]. Writing $\mathbf{H}\Psi_\lambda = E_\lambda \Psi_\lambda$, we approximate the solution as

$$\Psi_\lambda^{(N)} = \sum_{i=1}^{(N)} a_i^{\lambda(N)} \hat{\mathbf{e}}_i \ , \tag{B.168}$$

where the $\hat{\mathbf{e}}_i$'s form some complete set of orthonormal which contain some variational parameter. We then diagonalize the Hamiltonian, evaluated in this basis, to determine the expansion coefficients and eigenvalues. Since $\mathbf{H}$ is a self-adjoint operator with positive definite eigenvalues, the approximate eigenvalues will always be greater that the exact ones, i. e. $E_\lambda^{(N)} \geq E_\lambda$. We therefore vary the basis function parameter to minimize $E_\lambda^{(N)}$.

For our basis function, we chose to employ the set of harmonic oscillator eigenfunctions written as [31]

$$\Omega_{il}^m(\beta, \mathbf{r}) = N_{il}(\beta)\, e^{-\beta^2 r^2} L_{i-1}^{l+\frac{1}{2}}(\beta^2 r^2)\, (\beta r)^l\, Y_{lm}(\theta, \phi) \tag{B.169}$$

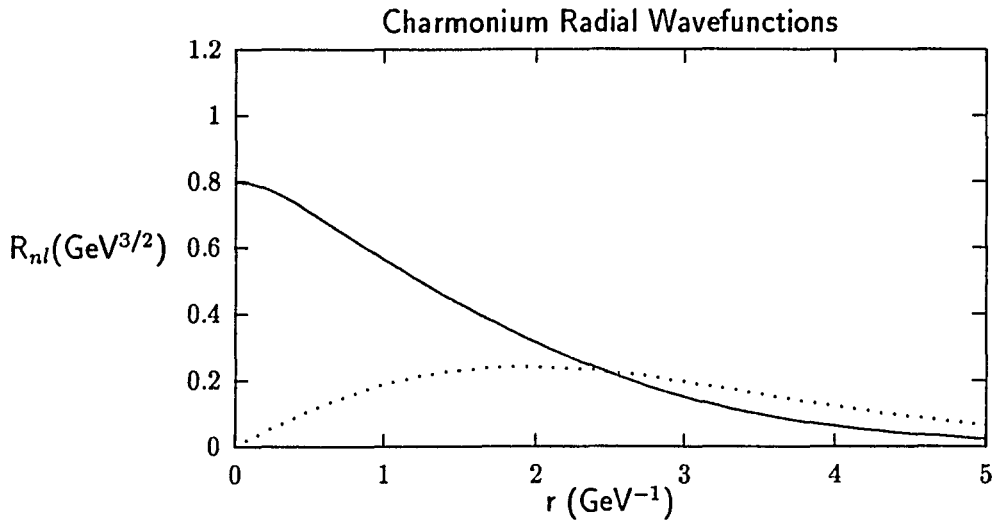

Figure B.47: Radial wavefunctions for $\psi(1S)$ (solid) and $\chi_c(1P)$ (dotted).

where $N_{il} = \beta^{3/2}(2(i-1)!/\Gamma(i+l+\frac{1}{2}))^{1/2}$. Using the Fourier transform relation for the functions given in Appendix A, we may write the Hamiltonian matrix elements as

$$H^l_{ij} = \frac{N_{il}(\beta)N_{jl}(\beta)}{2\beta^2}\int_0^\infty \left[\left(\frac{\beta}{2\mu}\right)(-1)^{i+j}x - \frac{k}{\sqrt{x}} + \left(\frac{a}{\beta^2}\right)\sqrt{x}\right] \times e^{-x}\, L^{l+1/2}_{i-1}(x)\, L^{l+1/2}_{j-1}(x)\, x^{l+1/2}\, dx\,, \tag{B.170}$$

which we evaluate using a Gauss-Laguerre quadrature. The scale parameter, β, is then varied until the eigenvalues are minimized.

The parameters for the 25 term solution that we use to represent the charmonium system are given in Table B.4. The radial wavefunctions for the $\psi(1S)$ and $\chi_c(1P)$ are shown in Figure B.47.

Resonance	$\psi(1S)$	$\chi_c(1P)$	$\psi'(2S)$
β (GeV)	1.056	0.528	1.056
a_1	0.768047	0.973814	0.437621
a_2	-0.460837	-0.200191	0.059299
a_3	0.326681	0.104396	-0.249692
a_4	-0.213637	-0.020591	0.347708
a_5	0.152881	0.016358	-0.361700
a_6	-0.103131	-0.000749	0.350600
a_7	0.075260	0.003840	-0.316099
a_8	-0.051624	0.000973	0.280055
a_9	0.038423	0.001414	-0.239826
a_{10}	-0.026586	0.000778	0.204572
a_{11}	0.020182	0.000718	-0.170835
a_{12}	-0.014003	0.000513	0.142841
a_{13}	0.010848	0.000428	-0.117529
a_{14}	-0.007508	0.000334	0.097038
a_{15}	0.005940	0.000274	-0.078981
a_{16}	-0.004079	0.000220	0.064538
a_{17}	0.003296	0.000179	-0.051952
a_{18}	-0.002231	0.000145	0.041920
a_{19}	0.001834	0.000117	-0.033195
a_{20}	-0.001211	0.000093	0.026197
a_{21}	0.000999	0.000074	-0.020069
a_{22}	-0.000626	0.000056	0.015052
a_{23}	0.000494	0.000043	-0.010578
a_{24}	-0.000263	0.000027	0.006754
a_{25}	0.000155	0.000022	-0.003231
M (GeV)	3.072	3.500	3.700

Table B.4: Charmonium wavefunction parameters.

REFERENCES

[1] R. C. Hwa, ed., *Quark Gluon Plasma-Advanced Series on Directions in High Energy Physics-Vol.6*, (World Scientific, Singapore) 1990

[2] B. Sinha, S. Pal, and S. Raha, eds.,*Quark-Gluon Plasma-Invited Lectures of Winter School, Puri, Orissa, India*, (Springer-Verlag) 1990

[3] T. Matsui and H. Satz, Phys. Lett. **B178**, 416 (1986)

[4] A. Bussiere, et. al., Z. Phys. C.-Particles and Fields **38**, 117 (1988)

[5] J. Ftáčnik, P. Lichard, and J. Pišut, Phys. Lett. **B207**, 194 (1988)

[6] S. Gavin, M. Gyulassy, and A. Jackson, Phys. Lett. **B207**, 257 (1988)

[7] R. Vogt, M. Prakash, P. Koch, and T. H. Hansson, Phys. Lett. **B207**, 263 (1988)

[8] F. Karsch and R. Petronzio, Phys. Lett. **B193**, 105 (1987)

[9] S. Gavin and M. Gyulassy, Phys. Lett. **B214**, 241 (1988)

[10] J. Hüfner, Y. Kurihara, and H. J. Pirner, Phys. Lett. **B215**, 218 (1988)

[11] J. P. Blaizot and J. Y. Ollitraut, Phys. Lett. **B217**, 392 (1988)

[12] J. Cleymans and R. L. Thews, Arizona Preprint AZPH-TH89/7, January 1989

[13] J. Cleymans and R. L. Thews, Z. Phys. C.-Particles and Fields **37**, 391 (1990)

[14] T. Matsui, Ann. Phys. (NY) **196**, 182 (1989)

[15] V. Černý, I. Horváth, R. Lietava, A. Nagová, and J. Pišút, Z. Phys. C.-Particles and Fields **46**, 481 (1990)

[16] R. Baier and R. Rückl, Z. Phys. C.-Particles and Fields **19**, 251 (1983)

[17] C. E. Carson and R. Suaya, Phys. Rev. **D14**, 3115 (1976); **D15**, 1416 (1977)

[18] F. E. Close, *An Introduction to Quarks and Partons* (Academic Press, New York) 1979

[19] F. Halzen and A. D. Martin, *Quarks and Leptons: An Introductory Course in Modern Particle Physics* (John Wiley and Sons, New York) 1984

[20] R. D. Field, *Applications of Perturbative QCD* (Addison-Wesley, New York) 1989

[21] M. D. Scadron, *Advanced Quantum Theory* (Springer- Verlag, New York) 1979

[22] R. V. Gavai and S. Gupta, Z. Phys. C.-Particles and Fields **49**, 663 (1991)

[23] E. Eichten, K. Gottfried, T. Kinoshita, J. Kogut, K. D. Lane, and T. M. Yan, Phys. Rev. Lett. **34**, 369 (1975)

[24] D. Dlamm and F. Schöberl, *Introduction to the Quark Model of Elementary Particles* (Gordon and Breach, New York) 1982

[25] W. Kwong, J. Rosner, and C. Quigg, in *Annual Review of Nuclear and Particle Science Vol. 37* (Annual Reviews, Inc., Palo Alto) 1987

[26] C. Quigg and J. Rosner, Physics Reports **56**, 168 (1979)

[27] P. Morse and H. Feshbach, *Methods of Theoretical Physics* (McGraw-Hill, New York) 1953

[28] I. S. Gradshteyn and I. M. Ryzhik, *Table of Integrals, Series, and Products*, (Academic Press, San Diego) 1980

[29] S. Jacobs, M. G. Olsson, and C. Suchyta III, Phys. Rev. **D33**, 3338, (1986)

[30] C. A. J. Fletcher, *Computational Galerkin Methods* (Springer-Verlag, New York) 1984

[31] E. J. Weniger, J. Math. Phys. **26**, 276 (1985)

[32] V. D. Barger and R. J. N. Phillips, *Collider Physics* (Addison-Wesley, New York) 1987

[33] F. E. Close in *QCD Hard Hadronic Processes*, B. Cox, Ed. (Plenum Press, New York) 1988

[34] B.Humpert, Phys. Lett. **B184**, 105 (1987)

[35] R. Gastmans, W. Troost, and T. T. Wu, Phys. Lett. **B184**, 257 (1987)

[36] F. E. Close in Reference [2]

[37] J. Badier, et. al., Z. Phys. C-Particles and Fields **20**, 101 (1983)

[38] D. M. Alde, et. al., Phys. Rev. Lett **66**, 133 (1991)

[39] S. Gupta and H. Satz, Z. Phys. C- Particles and Fields **55**, 391 (1992)

[40] L. Antoniazzi, et. al, E705 Collaboration, Fermilab-Pub-92/141-E (May 1992)

[41] P. Bordalo, et. al., Phys. Lett. **B193**, 373 (1987)

[42] P. Chiappetta and H. J. Pirner, Nucl. Phys. **B291**, 765 (1987)

[43] H. Satz, Phys. Lett. **B242**, 107 (1990)

[44] S. Gupta and H. Satz, Phys. Lett. **B283**, 439 (1992)

[45] R. A. Salmeron in Reference [2]

[46] Y. Lemoinge, et. al., Phys. Lett. **B113**, 509 (1982)

[47] L. Antoniazzi, et. al., E705 Collaboration, Fermilab-Pub-92/140-E (May 1992)

[48] T. B. W. Kirk, et. al., Phys. Rev. Lett **42**, 619 (1979)

[49] H. Satz, Nucl. Phys. **A488**, 511c (1988)

[50] J. P. Blaizot and J. Y. Ollitrault, Phys. Lett. **B199**, 499 (1987)

[51] C. Baglin, et. al., Phys. Lett. **B220**, 471 (1989)

[52] C. Baglin, et. al., Phys. Lett. **B251**, 465 (1990)

[53] C. Baglin, et. al., Phys. Lett. **B251**, 472 (1990)

[54] C. Baglin, et. al., Phys. Lett. **B255**, 459 (1991)

[55] C. Baglin, et. al., Phys. Lett. **B220**, 362 (1991)

[56] J. Kapusta, Phys. Rev. **D36**, 2857 (1987)

[57] F. Karsch and R. Petronzio, Z. Phys. C.-Particles and Fields **37**, 627 (1988)

[58] F. Karsch, M. T. Mehr, and H. Satz, Z. Phys. C.-Particles and Fields **37**, 617 (1988)

[59] F. Karsch and H. Satz, Z. Phys. C.-Particles and Fields **51**, 209 (1991)

[60] J. D. Bjorken, Phys. Rev. **D27**, 140 (1983)

[61] F. Karsch in Reference [1]

[62] R. L. Thews, Nucl. Phys. **A525**, 685c (1991)

[63] F. Bakke and H. Wergeland, Physica **69**, 5 (1973)

[64] H. Feshbach and F. Villars, Rev. Mod. Phys. **30**, 24 (1958)

[65] J. D. Bjorken and S. D. Drell, *Relativistic Quantum Mechanics*, (McGraw-Hill, New York) 1964

[66] R. Lietava, Z. Phys. C.-Particles and Fields **50**, 107 (1991)

[67] R. Lietava, A. Nagová, and J. Pišút, Z. Phys. C.-Particles and Fields **54**, 449 (1992)

[68] E. V. Shuryak Nucl. Phys. **A525**, 3c (1991)